

VILNIUS GEDIMINAS TECHNICAL UNIVERSITY

Justinas RAČKAUSKAS

MAGNETOMECHANICAL STUDY OF  
OPEN-BORE TWO-RAIL  
ELECTROMAGNETIC LAUNCHER

DOCTORAL DISSERTATION

TECHNOLOGICAL SCIENCES,  
MECHANICAL ENGINEERING (09T)



Vilnius LEIDYKLA TECHNICA 2018

Doctoral dissertation was prepared at Vilnius Gediminas Technical University in 2013–2018.

### **Supervisor**

Prof. Dr Habil. Rimantas KAČIANAUSKAS (Vilnius Gediminas Technical University, Mechanical Engineering – 09T).

The Dissertation Defence Council of Scientific Field of Mechanical Engineering of Vilnius Gediminas Technical University:

### **Chairman**

Prof. Dr Dalius MAŽEIKA (Vilnius Gediminas Technical University, Mechanical Engineering – 09T).

### **Members:**

Prof. Dr Habil. Saulius BALEVIČIUS (Vilnius Gediminas Technical University, Electrical and Electronic Engineering – 01T),

Assoc. Prof. Dr Sergejus BORODINAS (Vilnius Gediminas Technical University, Mechanical Engineering – 09T),

Dr Oliver LIEBFRIED (French-German Research Institute of Saint-Louis, France, Physics – 02P),

Prof. Dr Habil. Minvydas Kazys RAGULSKIS (Kaunas University of Technology, Mechanical Engineering – 09T).

The dissertation will be defended at the public meeting of the Dissertation Defense Council of Mechanical Engineering in the Senate Hall of Vilnius Gediminas Technical University at **2 p. m. on 30 August 2018**.

Address: Saulėtekio al. 11, LT-10223 Vilnius, Lithuania.

Tel.: +370 5 274 4956; fax +370 5 270 0112; e-mail: doktor@vgtu.lt

A notification on the intend defending of the dissertation was send on 27 July 2018. A copy of the doctoral dissertation is available for review at VGTU repository <http://dspace.vgtu.lt> and at the Library of Vilnius Gediminas Technical University (Saulėtekio al. 14, LT-10223 Vilnius, Lithuania).

VGTU leidyklos TECHNIKA 2018-037-M mokslo literatūros knyga

ISBN 978-609-476-121-8

© VGTU leidykla TECHNIKA, 2018

© Justinas Račkauskas, 2018

*justinas.rackauskas@vgtu.lt*

VILNIAUS GEDIMINO TECHNIKOS UNIVERSITETAS

Justinas RAČKAUSKAS

BĖGIŲ TIPO ATVIROJO KANALO  
ELEKTROMAGNETINĖS SVAIDYKLĖS  
MAGNETOMECHANINIO EFEKTO TYRIMAS

DAKTARO DISERTACIJA

TECHNOLOGIJOS MOKSLAI,  
MECHANIKOS INŽINERIJA (09T)



LEIDYKLA  
Vilnius TECHNIKA 2018

Disertacija rengta 2013–2018 metais Vilniaus Gedimino technikos universitete.

### **Vadovas**

prof. habil. dr. Rimantas KAČIANAUSKAS (Vilniaus Gedimino technikos universitetas, mechanikos inžinerija – 09T).

Vilniaus Gedimino technikos universiteto Mechanikos inžinerijos mokslo krypties disertacijos gynimo taryba:

### **Pirmininkas**

prof. dr. Dalius MAŽEIKA (Vilniaus Gedimino technikos universitetas, mechanikos inžinerija – 09T).

### **Nariai:**

prof. habil. dr. Saulius BALEVIČIUS (Vilniaus Gedimino technikos universitetas, elektros ir elektronikos inžinerija – 01T),

doc. dr. Sergejus BORODINAS (Vilniaus Gedimino technikos universitetas, mechanikos inžinerija – 09T),

dr. Oliver LIEBFRIED (Saint-Louiso Prancūzijos-Vokietijos tyrimų institutas, Prancūzija, fizika – 02P),

prof. habil. dr. Minvydas Kazys RAGULSKIS (Kauno technologijos universitetas, mechanikos inžinerija – 09T).

Disertacija bus ginama viešame Mechanikos inžinerijos mokslo krypties disertacijos gynimo tarybos posėdyje **2018 m. rugpjūčio 30 d. 14 val.** Vilniaus Gedimino technikos universiteto senato posėdžių salėje.

Adresas: Saulėtekio al. 11, LT-10223 Vilnius, Lietuva.

Tel.: (8 5) 274 4956; faksas (8 5) 270 0112; el. paštas doktor@vgtu.lt

Pranešimai apie numatomą ginti disertaciją išsiusti 2018 m. liepos 27 d.

Disertaciją galima peržiūrėti VGTU talpykloje <http://dspace.vgtu.lt> ir Vilniaus Gedimino technikos universiteto bibliotekoje (Saulėtekio al. 14, LT-10223 Vilnius, Lietuva).

# Abstract

The dissertation investigates the electromagnetic launcher electromagnetic properties and their influence on mechanical construction. The main object of research is open bore two rail construction electromagnetic launcher. The dissertation aims to investigate the distribution of electromagnetic forces and their influence over the electromagnetic launcher construction volume.

The work presents five tasks such as the electromagnetic and mechanical model application of the numerical model. The first task is formulated to review the literature. The next two tasks are formulated to calculate the distribution of electromagnetic forces throughout the electromagnetic launcher construction volume. The last two tasks investigate the effect of the forces distribution differences over the electromagnetic launcher construction.

The dissertation work consists of an introduction, four chapters, general conclusion, references, a list of publications by the author on the topic of the dissertation, a summary in Lithuanian and five annexes.

The introductory chapter discusses the research problem, relevance of the work, introduces the object of the research, formulates the aim and the tasks of the work, describes the research methodology, scientific novelty of the work, considers the practical significance of the work results and defensive statements. At the end of the introduction, the publications and reports published by the author of the dissertation and the structure of the dissertation are presented.

Chapter 1 is devoted to review the electromagnetic launcher analyses methods in literature. A brief overview of the adaptation and development history of electromagnetic launchers are provided. At the end of the chapter, conclusions are formulated, and the tasks of the dissertation are refined.

Chapter 2 presents the structure and parameters of the electromagnetic launcher. According to this type of launcher, the electromagnetic and mechanical models were developed. The mathematical model of each modeling and boundary conditions are described, and the conclusions are presented.

Chapter 3 and 4 provide the results of electromagnetic and mechanical modeling. The dependence between electromagnetic and mechanical problems are described. Conclusions are presented at the end of both sections.

4 articles have been published on the topic of the dissertation in the scientific journals included in the Clarivate Analytics Web of Science list, one article is in conference materials in the Clarivate Analytics Web of Science Proceedings database, and two is in peer-reviewed international conferencing materials. 4 presentations on the subject of the dissertation have been given in conferences at national and international levels.

# Reziomė

Disertacijoje nagrinėjamos elektromagnetinių svaidyklių elektromagnetinės savybės ir jų poveikis mechaninei konstrukcijai. Pagrindinis tyrimo objektas dviejų bėgių tipo atvirojo kanalo elektromagnetinės svaidyklės. Disertacijos tikslas – iš-tirti elektromagnetinių jėgų pasiskirstymą elektromagnetinės svaidyklės bėgyje ir šių jėgų įtaką elektromagnetinės svaidyklės konstrukcijai.

Darbe sprendžiami penki uždaviniai pateikiantys elektromagnetinės svaidyklės elgseną veikimo metu. Pirmas uždavinys uždavinys apima literatūros apž-valgą. Kiti du uždaviniai suformuluoti siekiant apskaičiuoti elektromagnetinių jėgų pasiskirstymą visame elektromagnetinės svaidyklės bėgio tūryje. Paskutiniai du uždaviniai skirti iš-tirti skirtingai pasiskirsčiusių tūryje jėgų poveikį elektro-magnetinės svaidyklės konstrukcijai.

Disertaciją sudaro įvadas, keturi skyriai, bendrosios išvados, naudotos litera-tūros ir autoriaus publikacijų disertacijos tema sąrašai, santrauka lietuvių kalba ir 5 priedai.

Įvadiniamame skyriuje aptariama tiriamoji problema, darbo aktualumas, prista-tomas tyrimų objektas, formuluojamas darbo tikslas bei uždaviniai, aprašoma ty-rimų metodika, darbo mokslinis naujumas, darbo rezultatų praktinė reikšmė, gi-namieji teiginiai. Įvado pabaigoje pristatomos disertacijos tema autoriaus paskelbtos publikacijos ir pranešimai konferencijose bei disertacijos struktūra.

Pirmasis skyrius skirtas literatūros analizei. Pateikiama trumpa apžvalga apie elektromagnetinių svaidyklių pritaikymą ir vystymo istoriją. Apžvalgoje pristatyti elektromagnetinių svaidyklių tyrimų aspektai ir metodikos. Skyriaus pabaigoje formuluojamos išvados ir tikslinami disertacijos uždaviniai.

Antrajame skyriuje pateikta elektromagnetinės svaidyklės konstrukcija ir pa-rametrai, kurios pagrindu buvo kuriamas elektromagnetinis ir mechaniniai mode-liai. Pristatoma kiekvienos metodikos matematinis modelis ir modelio kraštines sąlygos. Skyriaus pabaigoje pateikiamos skyriaus išvados.

Trečiajame ir ketvirtajame skyriuose pateikiami elektromagnetinio ir mecha-ninio modeliavimo rezultatai. Aprašoma priklausomybė tarp elektromagnetinio ir mechaninio uždavinių. Abiejų skyrių pabaigoje pateikiamos išvados.

Disertacijos tema paskelbtos 7 publikacijos: 4 – mokslo žurnaluose, įtrauk-tuose į Clarivate Analytics Web of Science sąrašą, vienas – konferencijos leidi-nyje, referuotame Clarivate Analytics Web of Science Proceedings duomenų bazėje, du – recenzuojamose tarptautinių konferencijų leidiniuose. Disertacijos tema perskaityti 4 pranešimai Lietuvos bei kitų šalių konferencijose.

---

# Notations

## Symbols

$\nabla$  – the nabla operator;  
 $\mathbf{H}$  – the magnetic field;  
 $\mathbf{E}$  – the electric field;  
 $\mathbf{D}$  – the electric field displacement;  
 $\mathbf{B}$  – the magnetic flux density;  
 $\mathbf{j}$  – the current density;  
 $I$  – electric current;  
 $L$  – inductance gradient;  
 $\vec{j}$  – electric current density;  
 $q$  – electric charge quantity;  
 $\vec{v}$  – the moving velocity of electric charge;  
 $\vec{F}$  – propulsive force;  
 $E_{Kin}$  – kinetic energy;  
 $m$  – the launching mass;  
 $v$  – is the speed of launched mass;  
 $p(t)$  – mechanical pressure on the rail surface;  
 $\rho_e$  – is the volume density of the free electric charge;  
 $\sigma_{ij}$  – is the stress;  
 $f_i$  – is the body force;  
 $\varepsilon_{ij}$  – is the strain;  
 $u$  – is the displacement;  
 $i, j, k = 1, 2, 3$ ;  
 $E$  – is Young's modulus;  
 $\nu$  – is the Poisson's ratio;  
 $\mathbf{u}(t)$  – a vector comprising unknown nodal values of the time-dependent displacement;

$\dot{\mathbf{u}}(t)$  – the vector of nodal velocities;  
 $\ddot{\mathbf{u}}(t)$  – the acceleration vector;  
[ $\mathbf{K}$ ] – the stiffness matrix;  
[ $\mathbf{C}$ ] – the damping matrix;  
[ $\mathbf{M}$ ] – the mass matrix;  
 $\mathbf{F}_N(t)$  – the magnetic pressure in the form of a vector;  
 $\Omega_{lat}$  – the lateral displacement dependent upon time;  
 $t$  – time;  
 $m_{rai}$  – the mass per rail unit length;  
 $I_{in}$  – the moment of inertia of the rail cross-section.

## Abbreviations

EM – Electromagnetic;  
FE – Finite element;  
FEM – Finite element method;  
GRP – Glass reinforced plastic;  
ISL – French-Germany Research Institute of Saint-Louis;  
PDE – Partial differential equations;  
PFU – Pulse forming unit;  
RAFIRA – EM launcher called RApid FIre RAilgun.



---

# Contents

INTRODUCTION .....	1
Problem Formulation.....	1
Relevance of the Thesis.....	2
The Object of Research.....	2
The Aim of the Thesis.....	2
The Tasks of the Thesis.....	2
Research Methodology.....	3
Scientific Novelty of the Thesis .....	3
Practical Values of the Research Findings .....	3
The Defended Statements.....	4
Approval of the Research Findings .....	4
Structure of the Dissertation.....	5
Acknowledgements .....	5
1. THE REVIEW OF NUMERICAL ANALYSIS METHODS OF ELECTROMAGNETIC LAUNCHER.....	7
1.1. History of an Electromagnetic Launcher .....	7
1.2. Principle of Operation .....	9
1.3. Types of Constructions.....	11
1.4. Electromagnetic Launcher Application Areas.....	13
1.5. Finite Element Method.....	14

1.5.1. Finite Element Method in Electromagnetics.....	15
1.5.2. Finite Element Method in Mechanics .....	17
1.6. Applications of Finite Element Method in Electromagnetics .....	18
1.7. Applications of Finite Element Method in Mechanics .....	20
1.8. Coupling Concept.....	21
1.9. Conclusions of Chapter 1 and Formulation of the Objectives of the Thesis.....	22
2. DATA OF THE RAFIRA ELECTROMAGNETIC LAUNCHER.....	25
2.1. The View of RAFIRA Electromagnetic Launcher .....	25
2.2. Parameters of an Electromagnetic Launcher .....	26
2.4. Power Supply.....	28
2.5. Types of Armature.....	30
2.6. Load of the Electromagnetic Launcher.....	32
2.7. Analysis Idea and Algorithm.....	33
2.8. Conclusions of Chapter 2 .....	35
3. ELECTROMAGNETIC ANALYSIS OF THE ELECTROMAGNETIC LAUNCHER.....	37
3.1. Electromagnetic Field Model .....	37
3.2. The Calculation Method for the Electromagnetic Case .....	39
3.3. Models of an Electromagnetic Launcher .....	40
3.4. Boundary Conditions for Electromagnetic Analyses.....	42
3.5. Finite Element Mesh and Their Evaluation .....	42
3.6. Results and Discussion of Electromagnetic Models .....	47
3.6.1. Rail-armature Electromagnetic Model.....	47
3.6.2. Moving Armature vs Static armature.....	48
3.6.3. Local Effect Induced by the Armature.....	50
3.6.4. Types of Armature .....	50
3.6.5. Constructing Bolts Influence for Electromagnetic Calculations .....	52
3.7. Conclusions of Chapter 3 .....	56
4. MECHANICAL ANALYSIS OF THE ELECTROMAGNETIC LAUNCHER.....	59
4.1. The Elastic Foundation of a Mechanical Model .....	59
4.2. A Mechanical Model for Local Effects Investigation.....	60
4.3. Finite Element Model of the Mechanical Model .....	61
4.4. The Mechanical Models With Different Loads .....	62
4.5. Armature Influence on a Mechanical Model .....	64
4.6. Constructing Bolts Effect on a Mechanical Model.....	66
4.7. The Mechanical Models of Dynamic Behaviour .....	67
4.8. Investigation of Two Shoots.....	68
4.9. The Local Effect on the Dynamic Model .....	72
4.10. Conclusions of Chapter 4 .....	73
GENERAL CONCLUSIONS .....	75

REFERENCES .....	77
LIST OF SCIENTIFIC PUBLICATIONS BY THE AUTHOR ON THE TOPIC OF THE DISSERTATION .....	85
SUMMARY IN LITHUANIAN .....	87
ANNEXES <sup>1</sup> .....	101
Annex A. COMSOL Report of Electromagnetic Model .....	102
Annex B. COMSOL Report of Mechanical Model .....	187
Annex C. Declaration of the Dissertation Authority .....	299
Annex D. The Co-authors Agreements to Present Publications for the Dissertation Defense.....	300
Annex E. Copies of Scientific Publications by the Author on the Topic of the Dissertation.....	304

---

<sup>1</sup>The annexes are supplied in the enclosed compact disc.



---

# Introduction

## Problem Formulation

The principle of operation of the device is based on the impulse accumulation of electricity and its surface and irradiation energy. Fields of application include space technology, small space objects, defence technology as a weapon of fire-arms, or a tool for research into substances in the process of rapid deformation in industry and science.

Nowadays the most of scientist investigate EM launcher to increase the mass of payload, projectile velocity, and EM launcher efficiency. The electromagnetic, mechanical and thermal modelling methods have been used for electromagnetic launcher technology. However, there is no common linking to a single mathematical model. Mostly the EM and mechanical investigations are performed separately. The mechanical analysis performed with simplifications for boundary conditions of mechanical models because the values at each construction point are not taken into account.

Using the finite element method, the electromagnetic launcher structure behaviour, which acts by electromagnetic forces, is analyzed. The dissertation is devoted to the investigation of two-rail type electromagnetic launcher by solving coupled electromagnetic and mechanical tasks consistently.

## Relevance of the Thesis

The mechanical behaviour of the electromagnetic launcher during the flare movement in the fire channel, the changes in force or shape of the components in its construction elements depends on the frame design of the structure and the effect of the electromagnetic forces acting on the structure. It is mechanical properties that are less studied in the field of complex multifunctional processes. The dynamic behaviour of electromagnetic transmission and the local effects of electromagnetic forces in the structure is an important scientific and technological problem that solves the research and design of this type of device and improves its performance.

This work uses a coupled two-way electromagnetic and mechanical application solution to investigate the overall behaviour of the EM launcher construction. The calculation method is a composite and performed in a series of steps: solving the electromagnetic problem, introducing integrated force density into the force volumes and the task of the task force in solving mechanical assignments. Such consistency allows solving large-scale problems by saving computing resources.

The task of the 3D modelling of the electromagnetic launcher operation is complex and important, helping to improve the existing equipment and identify the most problematic design issues.

## The Object of Research

The contribution of the 3D magnetic field to the mechanical behaviour of the two-rail open-bore design EM launcher is the object of research.

## The Aim of the Thesis

The evaluation of the contribution of the 3D magnetic field forces to the mechanical behaviour of electromagnetic launcher presents the main goal of the thesis.

## The Tasks of the Thesis

In order to achieve the aim of the thesis, the following tasks have to be performed:

1. To review the literature studies on electromagnetic launcher fields, to analyze existing electromagnetic and mechanical analysis methods.
2. To develop the 3D electromagnetic and structural FE models for the two-rail open-bore RAFIRA EM launcher.

3. To evaluate 3D variation of the magnetic field and magnetic load in the vicinity of the moving armature using developed EM model sequence.
4. To evaluate the difference between the EM load into the EM launcher construction volume and the mechanical load on the EM launcher rail surface.
5. To investigate the influence of electromagnetic load on the mechanical behaviour of the EM construction.

## **Research Methodology**

To investigate the object, the weak coupling research of numerical electromagnetic and structural analysis by the finite element method is chosen.

## **Scientific Novelty of the Thesis**

The following new results were obtained when researching open bore EM launchers construction:

1. An algorithm for local application of the EM force model, for the mechanical analysis of the whole structure, was developed. The solutions of these models allow estimating the influence of structural elements and projectile armature geometrical parameters.
2. Calculated volume forces generated by a magnetic field that estimate the spatial effects of these forces on the mechanical behaviour of the construction.
3. The mechanical behaviour of the structural elements characteristic of an open bore EM launcher has been investigated: acting forces of the constructing bolts and rail surface deformation.

## **Practical Values of the Research Findings**

In this work, an electromagnetic and mechanical model of the electromagnetic launcher is introduced, which can be adapted to each mode of operation of the electromagnetic launcher. The applied computational algorithm allows one to study the distribution of electromagnetic and mechanical gradients in the volume of the electromagnetic launcher design, which can identify the weakest points of the structure and make improvements in order to improve the efficiency of the electromagnetic launcher operation.

The investigations carried out in this work have a functional value and can be very useful in practice, and the proposed idea of a connected task can be applied to the study of other forms of electromagnetic launcher.

## The Defended Statements

The following statements based on the results of the present investigation may serve as the official hypotheses to be defended:

1. Estimation of distributed volume forces reduces localized deformations into EM launcher rail.
2. The volumetric magnetic forces distributed overall rail volume cause an uneven deformation of the rail surface.
3. The magnetic force decreases at the region near EM launcher construction bolts.

## Approval of the Research Findings

The main results of the doctoral dissertation were published in 7 scientific papers: 4 papers in journals indexed in Clarivate Analytics Web of Science (Schneider *et al.* 2013), (Stonkus *et al.* 2015), (Račkauskas *et al.* 2018), (Račkauskas *et al.* 2018) 1 paper in conference proceedings indexed in Clarivate Analytics Web of Science Proceedings (Stonkus *et al.* 2015), and 2 paper in conference proceedings (Račkauskas *et al.* 2015), (Račkauskas *et al.* 2016).

The author has made 4 presentations at 4 scientific conferences at national and international levels:

- International conference “The 17-th Electromagnetic Launch Technology Symposium (EML)”, held on 7–11 July 2014 San Diego, California.
- International conference “Polish Congress of Mechanics and Computer Methods in Mechanics (PCM-CMM 2015)”, held on 8–11 September 2015 in Gdansk, Poland;
- International conference “The 18-th Electromagnetic Launch Technology Symposium (EML)”, held on 24–28 October 2016 Wuhan, China.
- 13-th International conference “Mechatronics Systems and Materials” held on 3–5 July 2017, Vilnius, Lithuania.



## Structure of the Dissertation

The dissertation consists of an introduction, four main chapters, general conclusions, references, a list of publications by the author on the topic of the dissertation and a summary in Lithuanian. The total scope of the thesis is 100 pages, 31 equations, 41 figure and 4 tables. For the present dissertation, references were made to 92 source papers.

## Acknowledgements

Firstly, I want to thank my supervisors Rimantas Kačianauskas that lead and consulting me during my study time.

I also thank my supervisor at ISL Markus Schneider who trained and helped me while I was doing this research. I would like to thank him for his suggestions, advice, especially for interesting and valuable discussions.

My sincere thanks are extended to colleague at ISL: Martin Roch for spending time on exciting conversations and leisure activities during the staying period at ISL.

I want to express my heartfelt gratitude to my family. The support of my wife Ieva and my son Izidorius was priceless. I am grateful to my parents Danguolė and Gintautas for their support during my life and education.



---

## The Review of Numerical Analysis Methods of Electromagnetic Launcher

An EM launcher is a device which converts electric energy into kinetic energy (Liebfried 2011). This chapter provides an overview of the literature on investigation scopes and methods of the EM launcher application.

Parts of this chapter are published in Schneider *et al.* (2013), Stonkus *et al.* (2015) and Račkauskas *et al.* (2018).

### 1.1. History of an Electromagnetic Launcher

The idea of EM launch was suggested in the 19th century. The first efforts to develop an EM launcher were undertaken by Kristian Birkeland in Norway (McNab 1999). In the following World War I further ideas were developed by French scientist Fauchon-Villeplee. He built the EL launcher in about 1916 and submitted a patent application on June 22, 1916. Later, during World War II, the work in Germany was very important for the breadth of its innovation and derailed analyses undertaken. Dr. Joachim Hansler was the focal point for the studies in

railgun application. At the same time, the Japanese program for railgun was undertaken by the 7th Army Technical Research Laboratory and Tokyo Shibana Electric Company (McNab 1999). Over the last century, many experiments have been done to improve the launcher design and to create more powerful devices.

In the last years, scientists and engineers have focused on the development of simulation methods. Simulation provides the potential to obtain information about the main physical parameters such as current density, magnetic flux density, mechanical deformation and thermal distribution during EM launcher operation.

**Table 1.1.** The classification of electromagnetic launchers

Device	Group	Class	EM launcher name
Launcher	Electromagnetic	Armature current provided by the indirect connection	Reconnection
			Collapsing wave
			Linear induction motor
		Armature current provided by direct connection	Conventional railgun
			Series-augmented railgun
			Parallel-augmented railgun
			Muzzle-shunt railgun
			Multi-rail
			Coaxial rail
			Conventional helical
			Voice coil
			High n helical
			Variable gradient helical
			Reluctance
		Synchronous (powered coil)	
		Electro-thermal-chemical: use plasma hydrostatic pressure	SIRENS
			Electron beam electro-thermal
		Magnetic: uses only magnetic field force	Permanent magnet
		Electrostatic: use only electric field force	Contact
			Bombardment
		Hybrid: uses combinations of devices, groups, classes, and types	Externally-augmented railgun
Voice coil (permanent magnet)			
Synchronous (permanent magnet)			
Electrical exploding railgun			
Electro-thermal-railgun			
Gun-railgun			
Railgun-rocket			

Till nowadays a lot of EM launchers concepts were created. The differences of EM launchers and their special types are presented in Table 1.1 (Engel 2017). Also, Table 1.1 represents the classification of EM launchers. It indicates a huge amount of EM launchers concepts and various opportunities for use of this application. The stage of classification is to divide the EM launcher group into six classes. The specific manner in which the EM force is produced serves as the standard to perform this division. All cases can be divided into 27 types of the EM launchers. The EM launcher type classification indicates the refinement of the force generation mechanism. The thesis presents the investigation work based on Conventional railgun type EM launcher from Armature current provided by direct connection class.

## 1.2. Principle of Operation

The EM forces are the result of the Lorentz forces produced by the interaction between the electromagnetic travelling wave and the sleeve. The physics of the Lorentz force  $F$  acting on a charged particle is calculated according to equation (Bengui *et al.* 2011; Hasirci *et al.* 2015):

$$\vec{F} = q(\vec{E} + \vec{v} \times \vec{B}). \quad (1.1)$$

The forces  $\vec{f} = \vec{dF} / \vec{dV}$  per unit volume containing  $N \cdot q$  charges which move with velocity  $\vec{v}$  in a magnetic field, then

$$\vec{f} = q\vec{E} + \vec{j} \times \vec{B}, \quad (1.2)$$

this formula without the electric field ( $q\vec{E}$ ) will be referred as the Lorentz force:

$$F = \int_V \vec{j} \times \vec{B} dV. \quad (1.3)$$

The electromagnetic forces acting on the armature are not only the source loads during the structural analysis but also the basis and connecting link between the magnetic field and the structure. This work deals with rail launcher which operates according to this principle.

The EM rail accelerator is a device consisting of two rails and an armature between them (see Fig. 1.1) (Marshall and Ying 2004). The power supply (e.g., capacitor and pulse forming unit) and the others components (e.g., switches) are required to operate railguns (Keshtkar *et al.* 2008). The pulse forming unit generates pulsed currents which create high (in range of some Tesla) magnetic

fields. The armature is a conducting part of the projectile of a railgun which is capable of moving along the rails because of the Lorentz force acting on the armature due to the interaction between the current flowing in the armature and the magnetic field generated by the rails. The accelerating force  $F$  of the projectile in a shot direction ( $z$ ) can be calculated using following formula (Peterson 1993; Marshall and Ying 2004):

$$F_z = \frac{1}{2} L' I^2, \quad (1.4)$$

here  $L' = dL/dz$  is the inductance gradient of rails in shot direction.

The current flows from the current source along one rail pass through the armature, which is perpendicular to the rails, returns through another rail (see red arrows in Fig. 1.1). The magnetic field is mainly produced in contour between two rails and armature. The rails repel each other and they both, in turn, repel the armature. The rails are fixed. Thus the armature starts to move as a result of electromagnetic means (Murugan and Udayakumar 2005).

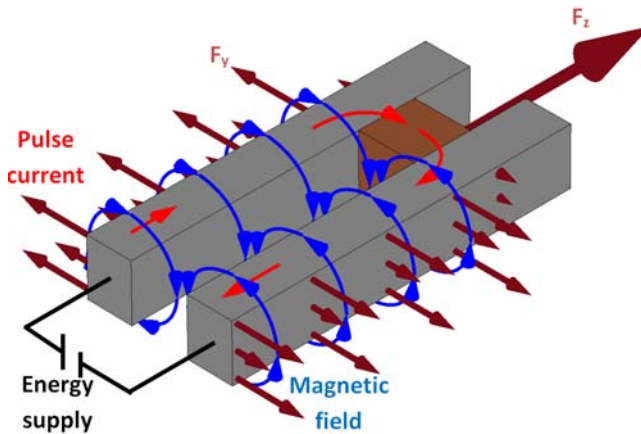


**Fig. 1.1.** Illustration of electromagnetic rail launcher operation principle

Similar as in conventional guns the law of energy conservation exists which state that the total amount of energy is conserved over time. According to this law, the energy can change its as within the system, for instance, magnetic energy can become kinetic energy (Perotoni et al. 2017). According to kinetic energy equation:

$$E_{Kin} = \frac{m \cdot v^2}{2}. \quad (1.5)$$

The variation of launching mass varies the velocity of launching mass (if the mass is increasing the velocity is decreasing, or vice versa). Nowadays, rail-guns can accelerate very large masses (more than 10 kg) up to velocities below 100 m/s and can accelerate small masses (some grams) more than 10 km/s (Marshall and Ying 2004). The main advantage of EM launchers is that launching process can be controlled much more easily than in conventional guns: the different charged energy creates the different speed of launching mass.

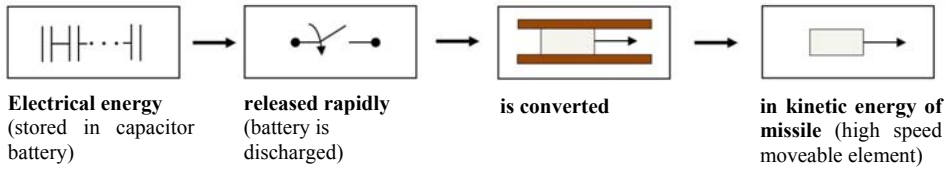


**Fig. 1.2.** Illustration of electromagnetic launcher system (Domin, 2016)

The EM launcher system shown in Fig. 1.1 can be presented by block diagram (see Fig. 1.2) which indicates the energy changing form during four stages. The first stage is to accumulate electric energy into capacitor battery. The capacitors keep the accumulated energy for discharge. The second stage is electric pulse forming stage, where during this stage the capacitor is discharged, and the energy in the capacitor is converted into an electric pulse. The electric pulse current flow through the EM launcher and converts the electric energy into mechanical energy during the third stage. The mechanical energy can be estimated according to equations (1.1) and (1.4). The last stage energy in the launched mass can be estimated according to Eq. 1.5.

### 1.3. Types of Constructions

The three types of constructions are presented in Figure 1.3, which are under investigation nowadays. A simple railgun employs two parallel rails on both sides of an armature. The conventional railgun constructions also investigated with different rail shapes. Most popular EM rail launchers are with rectangle rail in cross-section. Moreover, the primary focus is to find the optimal operation mode for this type EM launcher. However, other forms of rails are under investigation to find the optimal rails considering the efficiency. The EM launcher constructions with circular rails are discussed in these papers (Fahrenthold *et al.* 1989; Peterson 1993; Bayati and Keshtkar 2015). The second type is the coil gun EML system, which propels the projectile by an electromagnetic force caused by the electric current that energizes electromagnetic solenoid coils (Musolino and Rizzo 2011; Abdo *et al.* 2017).

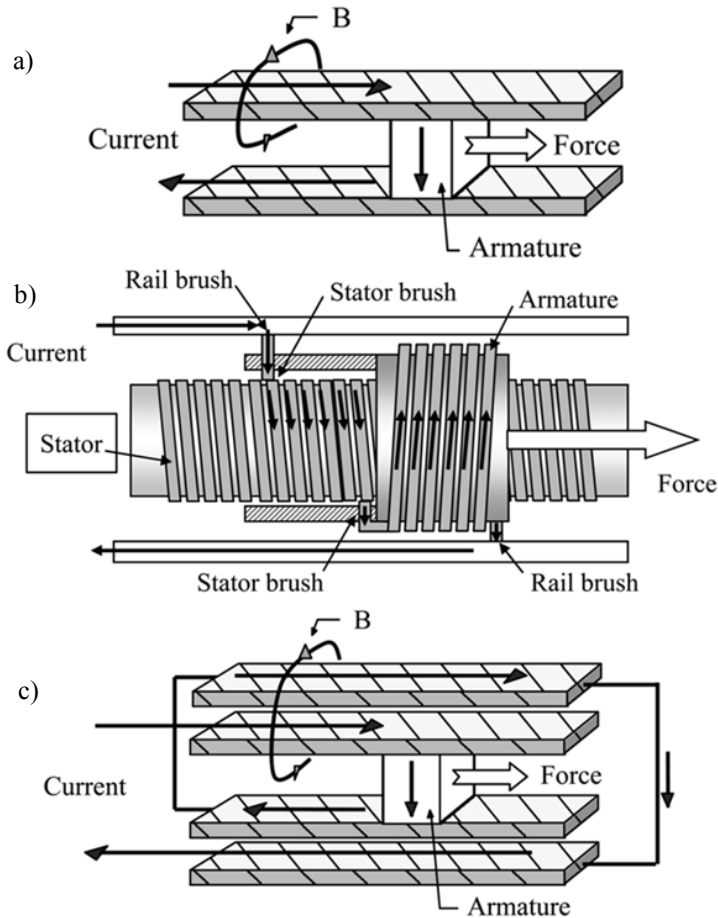


**Fig. 1.3.** Three types of railgun presented: a) conventional railgun; b) coilgun; c) augmented railgun (Engel, Neri and Veracka, 2008)

The third type of the EM launcher (see Fig. 1.3) system that is accessible is the augmented railgun. This type of EM launcher is based on parallel rails construction with additional coils for the magnetic field augmentation. Using the magnetic field augmentation, it is possible to reduce the current through the armature by applying an external magnetic field, which supports the magnetic field that is produced by the electrical current in the rails (Roch *et al.* 2014).

Also, not only the shape of rails are investigated. The study is performed by increasing the number of rails such as the hexagonal segmented railgun, the so-called SR\3-60 s in ISL (Vincent and Hundertmark 2012). Alternatively, new electromagnetic launcher, with sextupole rails, which the toroidal magnetic field



interacts with the orthogonal toroidal current to generate axial acceleration force (Xue *et al.* 2017).

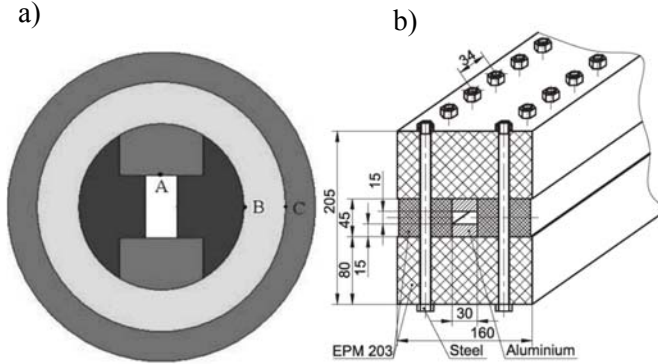


**Fig. 1.4.** Closed bore electromagnetic launchers: a) closed bore type cross section; b) open bore type cross section

Regarding the mechanical construction, two types of EM launchers exist. One type is called closed structure, which is based on rail placed in the tube or particular composite overlap (Fig. 1.4a). The system consists copper rails, fibreglass sidewalls, an inner ceramic or fibre epoxy cylinder, and a steel outer cylinder (Daneshjoo *et al.* 2007; Tzeng and Schmidt 2011). The other type could be called open bore structure when the rails are connected with discrete bolts, and in the particular cases the rail is not closed (Fig. 1.4b). The housing is constructed from a combination of bars made of a glass fibre reinforced plastic material and symmetrically located steel bolts (Tumonis *et al.* 2011).

## 1.4. Electromagnetic Launcher Application Areas

One of the main areas for the EM launchers to be considered is the defence objectives. Naval applications of railguns include ship defence, direct fire, and long-range indirect fire to support troops ashore. EM launchers will exceed the operating parameters of conventional guns and will also be able to replace traditional weapons for various missions (Thomas 2014). The main advantage of EM launcher is a significantly higher firing speed (2–3 km/s), which exceeds the standard propellant speed (McNab *et al.* 2005). For this reason, the propagation time to the target and the radius of the impact of the flight are shorter. The EM launcher to not use the chemical propulsion which is highly flammable and explosive (McNab and Beach 2007).

When modern railgun research began in the 1970s, it was believed that EM launcher will be able to achieve up to 50 km/s, because similar velocities had been observed when arcs alone had been studied (McNab 2013). However, by the mid of 1980s, a velocity ceiling was 6 km/s, and nowadays the experiments with solid payloads reach 11 km/s. One of the essential assets of such an EM launcher is the launch fee, which should not exceed \$ 600 / kg, while Space Shuttle space cost is more than \$ 20,000 / kg (McNab 2009, 2015).

Also, the application of EM launchers is in nuclear physics (Keshtkar *et al.* 2008) and other technology fields such as ultra-high pressure investigations space industry, or hypervelocity research (Hively and Condit 1991; Kolm *et al.* 2017).

From the very first flight to space, engineers began to develop materials for the outer shell of satellites, which would protect their electronic equipment from both harsh space conditions and harmful cosmic dust. The assessment of damage to these collisions is important for the space industry. Physical tests, when the protective material is directly exposed in orbit, is expensive and takes a long time, so for reach this range of speed for the experiment the EM launcher is used. They are used to investigate the effects of micrometre shock protection when the target is struck from  $10^{-4}$  to  $10^{-7}$  g particles accelerated up to 11 km/s (Upshaw and Kajs 1991).

The future of EM launcher applications is the managing nanostructured fusion is the hope of future energy. The cyclic transport of hydrogen isotope bottoms to magnetically isolated plasma in these studies is a widely accepted measure. It makes it possible to support the constant thermonuclear fusion efficiently. EMC is also used for this purpose. With the help of the shooters, fusion plasma is shot at a speed of 10 km/s, and the repetition rate is more than 10 Hz (Tompkins *et al.* 1995).

Research in this direction is further developed. In the future, these devices will be used in the aforementioned areas and many other fields of science and industry.

## 1.5. Finite Element Method

FEM is one of the most widely used related calculation methods for solving the problems of mechanical, thermal, hydraulic, electromagnetic, efficiency and other physical systems. The modelling of dynamic processes is also the scope of FEM. History of the development of the finite element method begins in the 20th century. The FEM algorithms are universal in solving the problems of various physical systems, so there is no need to go deep into many solution methods of traditional analytic equations. The main drawback is the fact that they are specific for each task class.

Essential quadratic finite element method steps:

- the area of any complex geometric shape is represented by the finite number of elements of a simple form;
- in the domain of each element, the differential phenomenon describing the equation in flabby derivatives is roughly replaced by an algebraic equation system;
- elemental algebraic equations are connected to a uniquely solved algebraic level system.

The physical process examined in each finite element is fully described, with small areas with initially unknown boundary conditions. A mathematical problem is formulated as a differential equation or a change in the algebraic equations of the energy functional, which describes the issue under consideration. For each element, a system of PDE is solved by numerical linear algebra methods (Logan *et al.* 2007). The elements are joined via nodes, which are indexed by numbers. The elements have to be small enough to give useful results and large enough to save computation resources.

### 1.5.1. Finite Element Method in Electromagnetics

The numerical solution of the problem is carried out by the method of FEM. The application of FEM is straight-forward if potential functions are introduced. Two options are open: the field quantities can either be represented by a magnetic vector potential  $A$  and an electric scalar potential  $V$  (Bíró *et al.* 2014).

The magnetic vector potential is introduced as an artificial quantity without Electrical potential. Therefore, to present the vector potential solution, the definition of magnetic vector potential can be used:

$$\nabla \times \{A\} = \{B\}. \quad (1.6)$$

The electric scalar potential is to model fields inside conducting regions (Rodger and Leonard 1993):

$$\nabla \times \{E\} = -\frac{\partial B}{\partial t}. \quad (1.7)$$

Continuing the derivation of the matrix:

$$\{E\} = -\left\{ \frac{\partial A}{\partial t} \right\} - \nabla V. \quad (1.8)$$

It can be shown that vector potential  $A$  obeys the following equation (Beno 1991):

$$A(\mathbf{r}') = \frac{\mu}{4\pi} \int_{V'} \frac{\mathbf{j}(\mathbf{r}')}{|\mathbf{r}-\mathbf{r}'|} dV', \quad (1.9)$$

here  $V'$  is the volume of space filled with charges, the quantities of  $\mathbf{r}'$ ,  $\mathbf{r}$  are the distance from zero points till current carrying point and from zero points till calculating point. The integration performs in all region of space includes all current sources of conductor and nonconducting regions.

The vector potential formulation is applicable to both static and dynamic fields with partial orthotropic nonlinear permeability. The basic equation to be written (Zienkiewicz 1977; Bíró and Preis 1989):

$$[S]\{\dot{o}\} + [Z]\{o\} = \{J_i\}, \quad (1.10)$$

here:

$$\{o\} = \left\{ \begin{array}{c} \{A_e\} \\ \{V_e\} \end{array} \right\}. \quad (1.11)$$

Electric scalar potential:

$$\{V_e\} = \left( v_e = \int V dt \right). \quad (1.12)$$

The method is the basis of all FEM methods in EM behaviour investigation.

In these days the numerical calculations are used for each investigation regarding the distribution of magnetic and electric field or current distribution in current carrying conductor. The most of papers deliver the 2D models which present the investigation at particular slice which usually described certain boundary conditions (Jarnieux *et al.* 1994; Ren *et al.* 1995; Keshtkar 2005; Keshtkar *et al.* 2008). This type of FEM investigation lets to see the principal view of what happens in the local paces of construction. The 3D models become more and more popular. This type of modelling has been applied to three-dimensional problems regarding a magnetic vector potential and an electric scalar potential employing a current vector potential and a magnetic scalar (Liebfried *et al.* 2011; Koczka *et al.* 2009; Parker 1998; Schneider *et al.* 2009).

The FEM software such a MEGA, COMSOL, Ansys Maxwell are the most known for EM launcher problems investigations. Also, the other packages which let to operate with magnetic vector potential and electric scalar potential.

### 1.5.2. Finite Element Method in Mechanics

From physical point, the EM launcher looks like a sandwich beam. Most papers are modelling the EM launcher construction as a beam. The mechanical deformation behaviour of the EM launcher structure under static action and dynamic loading using different finite element models.

The sandwich beam theory is available to study their suitability for application in 1D sandwich plates using the Fourier-Galerkin method and FE model. For nowadays the 1D investigation is not popular. The 2D and 3D investigations are at the top of science. The studies of free and forced vibration of sandwich beams under the action of double moving harmonic loads. The load travelling with constant velocity by using Timoshenko beam theory and studies of the elastostatic behaviour of sandwich beams based on a quasi-3D theory. The symmetric smoothed particle hydrodynamics method exists in mechanical investigation (Kahya and Turan 2018).

The method of linear elasticity and equations of the stress field in the tensor form is expressed as follows (Bengui *et al.* 2011):

$$\begin{cases} \sigma_{ij,j} + f_i = 0, \\ \varepsilon_{ij} = \frac{1}{2}(u_{i,j} + u_{j,i}), \\ \varepsilon_{ij} = \frac{1+\nu}{E}\sigma_{ij} - \frac{\nu}{E}\sigma_{kk}\delta_{ij}. \end{cases} \quad (1.13)$$

From the controlling equations of the EM field, electromagnetic force equations, and controlling equations of stress field, it is known that the strength of the armature is a coupled problem considering the interaction between the magnetic field and structure. On the one hand, the electromagnetic forces acting on the armature cause structural deformation; on the other hand, the shape and position of the armature are changed by structural deformation, which leads to a variation of the eddy current and the electromagnetic forces.

Other way of investigation is based on the full construction behaviour during the launch operations (Wagg and Neild 2010).

$$[M]\ddot{u}(t) + [C]\dot{u}(t) + [K]u(t) = F_N(t). \quad (1.14)$$

To calculate the magnetic force into mechanical construction rail in literature mostly usable method to calculate the current carrying conductor produce the magnetic pressure which is proportional to the electric current flowing in the current carrying conductor (Schuppler *et al.* 2013a).

The idea of FEM method is to divide construction into small bodies and perform the linear equation system to solve the static and dynamic models. Figure 1.5 visualizes the finite element of cube shape. The finite element model performed on the models using Eq. (1.13) for the static investigations and equations (1.13) and (1.14) for the dynamic investigations. The scientist are divided into two groups. One of them works with local investigations which concentrate on rail armature contact area to investigate local behaviour (Feng *et al.* 2015; Yang *et al.* 2016; An *et al.* 2017). Other groups of scientists work on a conventional system of EM launcher to investigate the construction behaviour (Fahrenthold *et al.* 1989; Che *et al.* 2017). Both groups of scientist use the same modelling method with different simplifications and different boundary conditions.

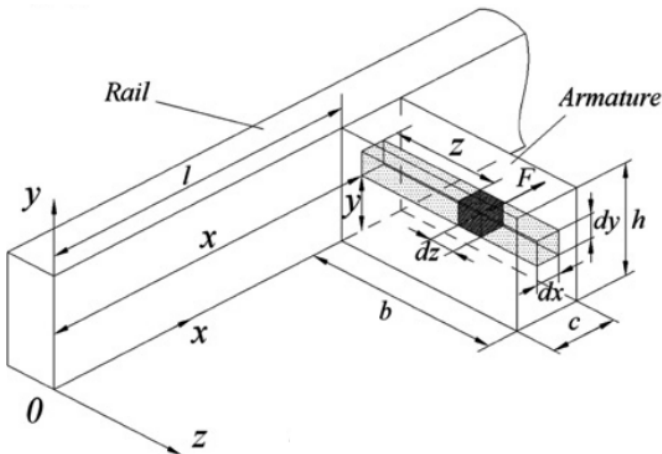


**Fig. 1.5.** The visualization of electromagnetic launcher construction finite element at one point on the armature (Xu and Geng 2012)

The FEM software such an ABAQUS, COMSOL, Ansys are most knows for EM launcher structural problems investigations.

## 1.6. Applications of Finite Element Method in Electromagnetics

The two techniques exist of EM launcher investigations. One of these techniques related to EM launcher operational behaviour. This type of technology is necessary to simulate the launching algorithm to calculate the power supply operation and compute the armature speed which is vital to launching target calculations.

To describe the function numerically one of the great codes is PSPICE where constitutive equations are converted into circuits consisting of essential circuit elements (Wey *et al.* 1997; Liebfried *et al.* 2013a). Another possibility is to use the MATLAB software with Simulink package which also allow to works with function blocks. Even there are already programmed libraries, which are let to introduce the solving equations for EM launcher operating behaviour. In days of IT technology, the free software such as Scilab is available (Siaenen *et al.* 2015). It is the software based on block diagram model of the differential equation system of the launcher and its power supply. The model is easily extendible to comprise side effects, solves reliably, and allows the inclusion of sophisticated control systems.

The second technique of EM launcher investigation is based on the time-varying electric field which generates a time-varying magnetic field and vice versa. It is the oldest study which investigates the magnetic and electric effects. This variation can be described by Maxwell's equations which have been developed in 19th century by James Clark Maxwell (Knoepfel 2000).

This technique is usable for local construction investigations and satisfying at all points of space. Using Maxwell equations, the magnetic and electric field is investigated. The interaction between the total current at the input into a rail and at armature/rail interface in the result of solving Maxwell's system of equations (Galanin *et al.* 2003).

The investigation based 2D current distribution and magnetic field in the current carrying conductor and around it. The current density distribution and magnetic flux density for different cases and their corresponding different dimensions sizes have been calculated by FEM. This investigation is done by Bayati and Keshtkar (2015).

The magnetic field distribution inside and around the construction also was done by ISL scientist. 2D investigation on moving armature analysis was done by Stankevic *et al.* (2013). In the study, the measurements were made experimentally of the magnetic field and the numerical model using Comsol software was created and verified. The next 2D investigation was performed by Keshtkar *et al.* (2008) study, where 2D magnetic field distribution inside and around the EM launcher rails cross-section was investigated. The numerical investigation was done using Ansys software. The scientist's group of Tan (Tan *et al.* 2017) did a numerical investigation and presented the differences by numerical calculation on 2D and 3D investigation modes. The results of current distribution inside the rail and armature are presented.

The numerical model using Comsol software was performed by Liebfried *et al.* (2013b). These researchers investigated the electric current distribution inside the armature. The 3D model was performed, and validation of the model was done by measuring magnetic field inside the armature.

The contact pressure between the rail and armature investigation was done by Feng *et al.* (2015). The group of scientist investigated the 3D modelling of contact pressure distribution which was carried out with the FEM. The 3D contact calculations, current entered the armature from the trailing edge.

## 1.7. Applications of Finite Element Method in Mechanics

In literature, the mechanical investigation of EM launcher is based on two different ways. One way when the structure of construction is investigated locally. All local structural mechanical problems can be solved according to static analysis of mechanical theory at a given time, and calculation of stress and deformation.

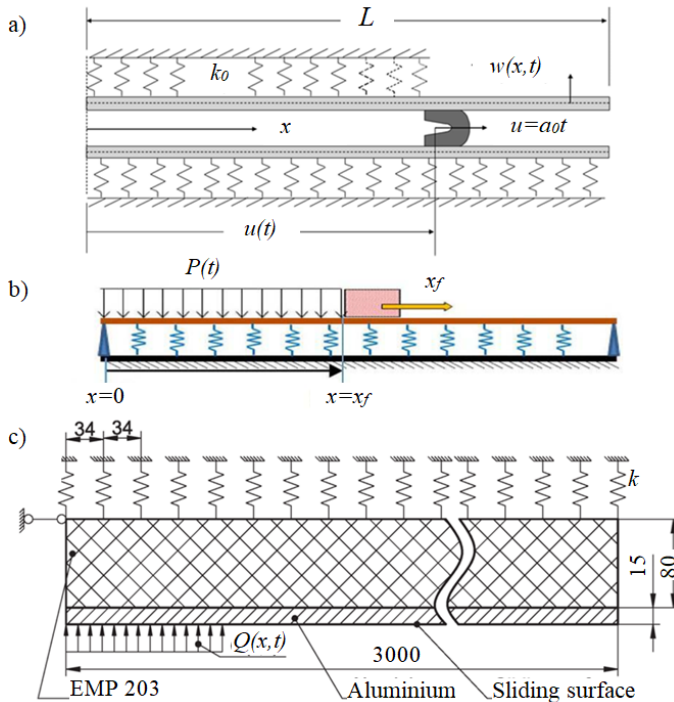


**Fig. 1.6.** Simplified electromagnetic launcher geometry: a) (Johnson and Moon, 2007); b) (Lee *et al.*, 2017); c) (Tumonis *et al.*, 2011)

To capture the large-scale dynamics, the model of the electric current conducting guide rails as Timoshenko beams and the rest of the insulator-support structure as an excellent elastic foundation as shown in Fig. 1.6. In literature, most



of the authors investigate the different forms of mechanical EM launchers. However, often they make the model more straightforward to save calculation resources.

The mathematical model describes the dynamic behaviour of the FEM of the railgun structure under the influence of the expanding pressure load moving along the rails. The dynamical behaviour of the rail is modelled using

$$m_{rai} \frac{\partial^2 \omega_{lat}}{\partial t^2} + EI_{in} \frac{\partial^4 \omega_{lat}}{\partial x^4} + k\omega_{lat} = q[1 - H(x - Vt)]. \quad (1.15)$$

The elastic constant from the elastic foundation will be derived from either a closed form or numerical solution such as finite-element analysis. The loading function  $q[1 - H(x - Vt)]$  represents the magnetic pressure front travelling along the rail with a constant velocity represented by a Heaviside step function. The magnetic pressure is assumed to be constant also (Tzeng 2005; Johnson and Moon 2006, 2007).

## 1.8. Coupling Concept

In the literature vary types of coupling calculating models exist. The EM launcher related to three types of coupling: magnetics, mechanical and thermal. These three physical states appear during the EM launcher operation. Full coupling of all physical states investigation is poured an only few papers present the idea of investigation (Hsieh 1995; Yang *et al.* 2017). The full EM launcher construction investigation with three state coupling is not yet known. The magneto-thermal coupled and magneto-mechanical coupled investigations are favourite nowadays.

The magnetic-structural coupling relationship is very complicated. Solving this problem with the analytic method is difficult. Finite element method is adopted to analyze the complex problem. The numerical algorithm based on variational principle and subdivision interpolation is suitable to solve the magnetic-structural coupling issues (Bengui *et al.* 2011).

Two types of models are possible to solve a coupled magneto-mechanical problem. The first is the weak coupling, in which the magnetic equation and the mechanical equation is solved separately. In general, there was no link between those two calculations. In the Eq. (1.16) the calculation matrix of weak coupling is presented (Gros *et al.* 1998). The Eq. (1.16) shows that only calculated results from electromagnetic calculation transfers to mechanical calculation and after mechanical calculation the results do not return to electromagnetic calculation for next iteration calculation.

$$\begin{bmatrix} \begin{bmatrix} \text{Magnetic} \\ \text{term} \end{bmatrix} & \begin{bmatrix} \text{Coupling} \\ \text{terms} \end{bmatrix} \\ 0 & \begin{bmatrix} \text{Mechanical} \\ \text{term} \end{bmatrix} \end{bmatrix} \begin{bmatrix} \text{Magnetic} \\ \text{Mechanical} \end{bmatrix} = \begin{bmatrix} \text{Coercitive field} \\ \text{Coercitive stress} \end{bmatrix}. \quad (1.16)$$

The second type of modelling is a robust coupling model. A “prediction–correction” procedure realizes the coupling model. First calculates the magnetic field and then the magnetic force distribution. After that, the magnetic force is inserted into the mechanical equation to calculate the displacement field (Jarnieux *et al.* 1994).

$$\begin{bmatrix} \begin{bmatrix} \text{Magnetic} \\ \text{term} \end{bmatrix} & \begin{bmatrix} \text{Coupling} \\ \text{terms} \end{bmatrix} \\ \begin{bmatrix} \text{Coupling} \\ \text{terms} \end{bmatrix}^T & \begin{bmatrix} \text{Mechanical} \\ \text{term} \end{bmatrix} \end{bmatrix} \begin{bmatrix} \text{Magnetic} \\ \text{Mechanical} \end{bmatrix} = \begin{bmatrix} \text{Coercitive field} \\ \text{Coercitive stress} \end{bmatrix}. \quad (1.17)$$

The coupled system is non-linear because of the magnetic saturation and the dependence of the magnetic field and force on the magnetic vector potential and the displacement. In consequence, an iterative procedure should be used. System solves for each iteration independly the following algebraic Eq. (1.17) for unknown magnetic and mechanical increments (Ren *et al.* 1995; Besbes *et al.* 1996).

## 1.9. Conclusions of Chapter 1 and Formulation of the Objectives of the Thesis

There are different analyzation methods for EM launcher electromagnetic and mechanical investigations existing in the literature.

1. In this chapter, the construction types of EM launchers and their analyses methods were reviewed. The EM launchers analyses methods show that there are various calculating methods which are related to EM launcher construction investigations seperatly. On the other hand, there is a lack of coupled numerical methods that are suitable for investigating EM launchers construction behavior.
2. In the literature is possible to find the EM investigation based on Maxwell equations and vector potential, but most of the investigations are performed on the local problems, regarding EM launcher projectile speed.

3. The EM launcher is under investigation in the literature. Scientist groups divided into different investigations areas. EM investigation, mechanical and some of them working with coupling between different activities such a mechanical, thermal or electromagnetic. The electromagnetic investigation is most difficult and requires many hardware resources to find the solution numerically.

To achieve the aim, the following tasks have to be solved:

1. To develop the 3D electromagnetic and structural FE models for the two-rail open-bore RAFIRA EM launcher.
2. To evaluate 3D variation of the magnetic field and magnetic load in the vicinity of the moving armature using developed EM model se-quence.
3. To evaluate the difference between the EM load into the EM launcher construction volume and the mechanical load on the EM launcher rail surface.
4. To investigate the influence of electromagnetic load on the mechanical behaviour of the EM construction.



# 2

---

## Data of the RAFIRA Electromagnetic Launcher

In this Chapter, the physically electromagnetic launcher model based on RAFIRA EM launcher is presented. The physical parameters, experimentally measured data and geometry of application are showed in detail. The main parameters are presented to set the boundary conditions for electromagnetic and mechanical calculations.

Parts of this chapter are published in Schneider *et al.* (2013), Stonkus *et al.* (2015) and Račkauskas *et al.* (2018).

### 2.1. The View of RAFIRA Electromagnetic Launcher

RAFIRA is one of the EM launchers ISL. It has proven its multishot capability by launching two projectiles at a repetition rate of 30 Hz. The next step was to extend its ability to accelerate more than two projectiles in a row. This task seemed to be straightforward because existing electrical and mechanical components were copied and added (Schneider *et al.* 2009). This kind of railgun was produced to investigate the multishot capacity of the multiple fibre brush and C-shape armatures technology. The calibre of the projectile is  $25 \times 25 \text{ mm}^2$  where the length can be changed.

The main components of EM accelerator are two rails, current injection units (perpendicular to rails), housing bar and supporting bolts. The RAFIRA railgun, which has an open bore construction is presented in Fig. 2.1. The biggest part of a railgun is the main accelerator. RAFIRA also has two pre-accelerators which are used to push projectiles into the main accelerator for multi-shot purposes (Schneider *et al.* 2009).

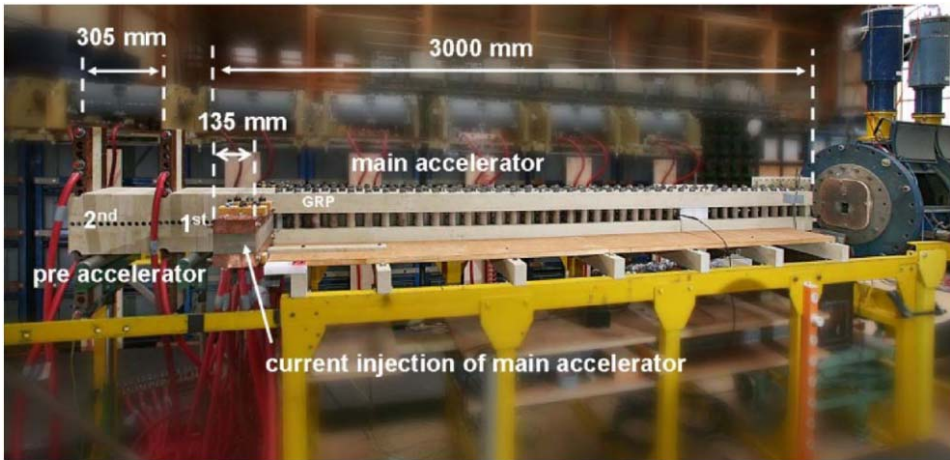


**Fig. 2.1.** Electromagnetic launcher RAFIRA (Schuppler, Alouahabi and Schneider, 2013)

The calibre of RAFIRA railgun is of  $25 \times 25 \text{ mm}^2$ . It means that the projectile of this railgun is with  $25 \times 25 \text{ mm}^2$  cross-section. The main conducting parts are rails with a cross-section of  $20 \times 25 \text{ mm}^2$  and injection units with a  $45 \times 45 \text{ mm}^2$  cross-section (Schuppler *et al.* 2013b). The cross-section of the injection bar is more than three times bigger than the rail cross-section. This is because the cables are plugged into it. The injection unit connects the main accelerator's rails with energy supply via coaxial cables.

## 2.2. Parameters of an Electromagnetic Launcher

In this dissertation, the major attention is dedicated for main accelerator investigation. This part of EM launcher construction is most significant. The structure consists of a combination of two bars made from glass fibre reinforced plastic connected by 160 steel bolts, which are positioned in four rows. The length of this part is 3 meters.

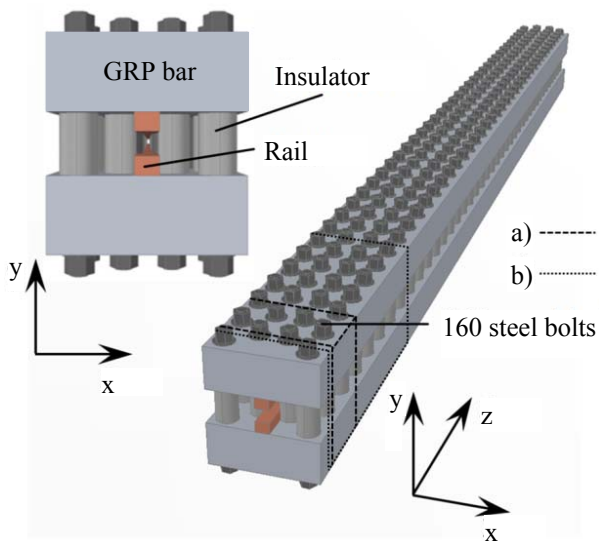


**Fig. 2.2.** Electromagnetic launcher main accelerator structure of RAFIRA: a) part for electromagnetic calculations; b) part for mechanical calculations

**Table 2.1.** Material parameters used for numerical simulations

Structural member	Material	Physical properties
Rail, armature	CuCr1Zr (CRM 16N)	Density: $\rho_r = 8900 \text{ kg/m}^3$ Young's modulus: $E_r = 120 \text{ GPa}$ Poisson's ratio: $\nu_r = 0.3$ Electrical conductivity: $\sigma = 5.8 \cdot 10^7 \text{ S/m}$ Relative permittivity: $\epsilon_r = 1$ Relative permeability: $\mu_r = 1$
Housing	GRP	Density: $\rho_h = 1850 \text{ kg/m}^3$ Young's modulus: $E_h = 18.0 \text{ GPa}$ Poisson's ratio: $\nu_h = 0.3$ Electrical conductivity: $\sigma \ll 1 \text{ S/m}$ Relative permittivity: $\epsilon_r = 1$ Relative permeability: $\mu_r = 1$
Bolts	Steel	Density: $\rho_h = 7850 \text{ kg/m}^3$ Young's modulus: $E_h = 210.0 \text{ GPa}$ Poisson's ratio: $\nu_h = 0.3$ Electrical conductivity: $\sigma = 6.9 \cdot 10^6 \text{ S/m}$ Relative permittivity: $\epsilon_r = 1$ Relative permeability: $\mu_r = 1$
Ambient	Air	Electrical conductivity: $\sigma \ll 1 \text{ S/m}$ Relative permittivity: $\epsilon_r = 1$ Relative permeability: $\mu_r = 1$

In the Fig. 2.2 the main accelerator presented without current injection unit which is necessary for cable connection. The influence of current injection unit is not taken into account. Only main accelerator is under investigation.

The construction of main accelerator is made from various materials such as copper, GRP, steel and the modelling ambient (in EM investigation the ambient is necessary for magnetic field calculations). All these materials and their parameters needed for electromagnetic and mechanical models' investigations are presented in Table 2.1.

## 2.4. Power Supply

At present RAFIRA can fire not more than three shots in a multi-shot experiment. The first projectile placed in the main accelerator, the next two in two pre-accelerators (see Fig. 2.1). RAFIRA has eighteen power supplies, while fifteen of them are separated into three parts (Wild *et al.* 2015). A five power supplies are for each shot at the main accelerator and two power supplies for each pre-accelerator. In two-shot case, the different variations of power supplies can be used. For example, eight power supplies can be used for each shot and one power supply for pre-accelerator.

The power supply is an essential element of the electromagnetic launcher. This device enables to store energy from a low power source (from standard electricity point) during a long time (some minutes) and release the very high energy in very short time (nanoseconds or milliseconds). In Fig. 2.1 the power supply has eight capacitors with 385  $\mu\text{F}$ . The capacitors can be charged to 10.5 kV. The power supply also has a PFU (Liebfried *et al.* 2013a), which consists of spark gap switch, initial resistance, crowbar diodes and pulse forming inductances. This type of one PFU can form pulse with the shape as shown in Fig. 2.3 (Current I1–I5 lines). The full charged power supply generates a pulse with a duration of 5 milliseconds, and the amplitude of pulse current reaches 205 kA. The current pulse is unsymmetrical: it increases and achieves the maximum value very fast while a decreasing process is slower. The maximum amplitude during discharge of capacitor is reached in 0.2 ms, and other time of all pulse duration (5 ms) the value of pulse current is decreasing.

There are also possibilities to use more than one power supply and to trigger each of them separately. This connection of different power supplies allows increasing the electric energy which is necessary for railgun operations. The variation of triggering is producing different pulses. The total current pulse produced with five PFU is shown in Fig. 2.3 (red curve). This shape of the pulse was used in railgun experiment. The current maximum value was reached at



640 kA, which was used for calculations in the time-harmonic case and later in the transient case.

The triggering process is one of most important task for preparation of the EM launcher launch experiment. Each current pulse depends on energy stored in the capacitor, which can be calculated according to following equation (Knoepfel 2000):

$$E_{cap} = \frac{1}{2}CU^2, \quad (2.1)$$

here  $C$  is capacity of the capacitor and  $U$  is the voltage of the capacitor.

The different triggering algorithm of PFU receives different current pulse which directly affects the launching process that plays a vital role in construction behaviour. In case of triggering a large number of capacitors, the construction can be damaged or destroyed.

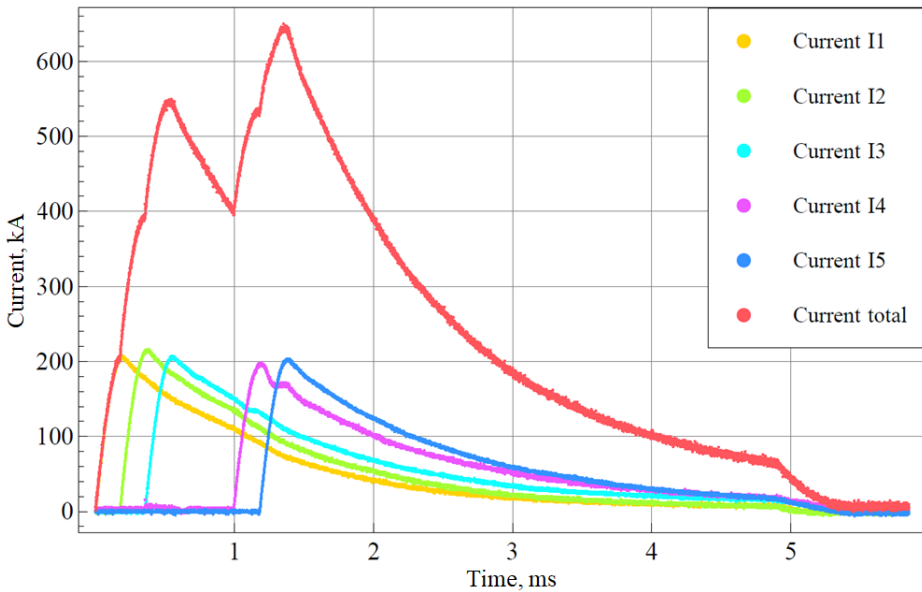


**Fig. 2.3.** Experimental current pulse gained during the experiment with five capacitors.

The graph presented in Fig. 2.3 shows experimental measurements. The measurement was done by using Rogowski coil. The Voltage measurement between the rails of a railgun is regularly performed at the breech and the muzzle of railguns. At ISL, the measurements are performed using voltage dividers,

optoelectronic transmitters, and oscilloscopes. Such a measure gives valuable information on the contact behaviour between the armature and the rails (Liebfried 2011).

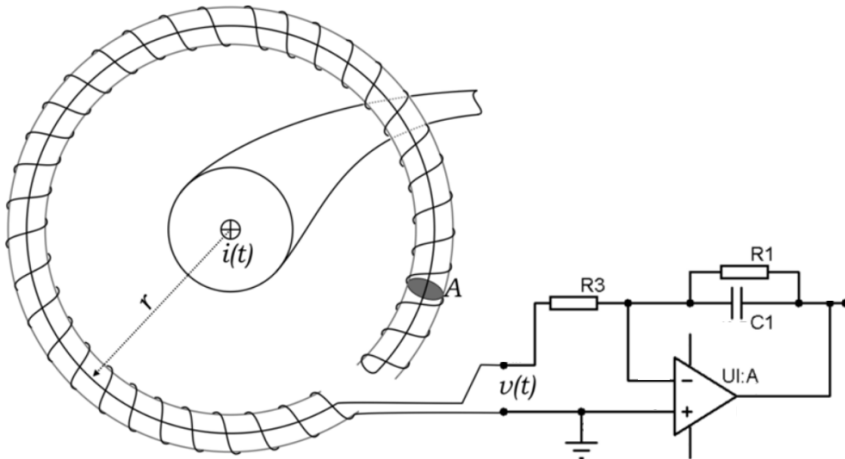


Fig. 2.4. Rogowski coil visualisation (Wikipedia 2017)

A Rogowski coil is an electrical device for measuring alternating current or high-speed current pulses. It works by sensing the magnetic field in the space around the current carrying conductor (see Fig. 2.4). Ampere's law provides the relationship between the current in the conductor and the magnetic field around it (Metwally 2013). These coils are placed around the current feeding cables. It measures each cable separately. Using superposition principle, the current can be summed and the full current pulse loaded with EM launcher can be measured (see Fig. 2.4).

## 2.5. Types of Armature

The armature is central moving part of EM launcher which is necessary to propel the payload. This part of EM launcher makes a short circuit between rails to get current flow. The RAFIRA EM launcher can operate with two types of armatures: C-shape armature and brush armature (see Fig. 2.5).

The brush armatures (see Fig. 2.5b) has advanced things in case of material loss is permitted. The brush, being initially greater in length than the distance between the rails, is shortened by erosion and wear during the shot and finally loses direct contact due to insufficient length (Schneider *et al.* 2003). For several years, the EM launcher research at ISL has concentrated on the application of the so-

called brush armature technology to low and high-energy railgun experiments. To reduce the parasitic mass of the projectile body, the standard material being used for the sabot is GRP (Hundertmark *et al.* 2013; Lee *et al.* 2017).

The C-shape of armature is different than brush armature. It is the excellent construction of armature that is under investigation nowadays. The main advantage of this armature type is that the shape is “C” makes good contact between rail surface and armature body (see Fig. 2.5a). The force which deflects the rails near the armature also deflects the armatures C shape stem (Bourell and Persad 1999; Zielinski *et al.* 2003). This ability to change the shape of armature during the launch process ensure the current flowing through the rail to the armature. The C-shape armature is very difficult to vary parameters during the experiments (Stefani and Parker 1999).

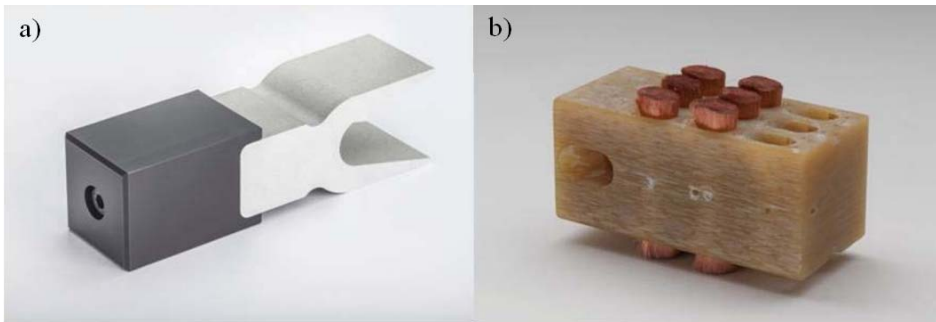


**Fig. 2.5.** Armatures which used during the experiments: a) is the C-shape armature; b) is the brush armatures (Wild *et al.* 2017)

In literature, it is possible to find the investigations of solid cube armature. The solid cube armature is convenient to investigate the EM effects distribution in EM launcher construction. The simple cuboid armature is useful as a simple model in calculating modes to present the magnetic and electric field distributions in EM launcher construction (Rodger and Lai 2001). In real structure, this type of armature is not useful, because the launching process the gap between the rails increase and the contact between rail surface and armature became poor. The erosion due to plasma appears. More armatures shapes and structures can be found in the studies of McNab *et al.* (2011).

Approximately half of the literature regarding EM launcher investigation is focused on armature investigation locally. In this type of study, the shape and dimension are essential. In our investigation armature used to investigate the influence of rails, the effects of armature and armature construction behaviour were not studied locally. All models in this thesis presented with solid cube armature.

## 2.6. Load of the Electromagnetic Launcher

Electromagnetic and mechanical aspects occurring during launch are considered in this work. The mechanical load is given by the magnetic pressure repelling the rails. To calculate the spatial and transient properties of the magnetic pressure between the rails experimental results were used. The transient pressure profile was derived from current measurements. Experimentally measured current pulses produced with five PFU are shown in Fig. 2.3 (red curve). The shape of the total current pulse resulting from the superposition of the single pulses could be realised as want. The maximum current amplitude cannot exceed 1 MA.

$$p(t) = \frac{L'}{2wh} I(t)^2, \quad (2.2)$$

where  $L' = 0,44 \mu\text{H/m}$ ,  $w = 25 \text{ mm}$  is the width of the rails, and  $h = 25 \text{ mm}$  is the rail separation (Schuppler *et al.* 2013b). According to this formula, the electric current can be recalculated into the mechanical pressure and used in the mechanical model.

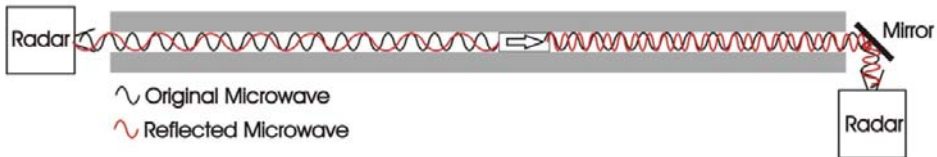


Fig. 2.6. The principle of the Doppler radar installation (Liebfried 2011)

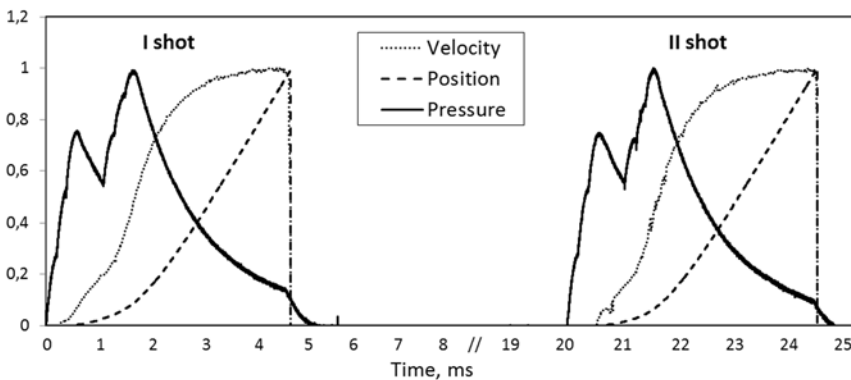


Fig. 2.7. Profiles of three relative parameters – electric current, projectile velocity and projectile position along the rail in time (Stonkus *et al.* 2015)

The position of the front of the pressure region (corresponding to the location

of the armature) was calculated using Doppler radar measurements of projectile velocity (see Fig. 2.6). Using velocity and time data the position was estimated. The results of armature position are presented in Fig. 2.7.

The Doppler radar is used for projectile velocity measurement. Due to this measurement, the projectile location in the EM launcher bore at each time can be set. This information is useful for creating the numerical model of EM launcher. During every experiment in ISL, the two radar systems for projectile velocity determination are installed: one installed at the breech and one at the muzzle of the EM launcher.

The independent measurement of the velocity helps for the evaluation of the projectile position. The profiles of the pressure, the velocity and the projectile position in the railgun are presented in Fig. 2.7. The curves are presented in relative scale to show the relation of the corresponding quantities. The maximum values are 185 MPa for the pressure, 1136 m/s for velocity and 3.017 m for rail position. This profile was gained with 726 kA in amplitude current pulse. The different magnitude of the current pulse and different algorithm of superposition single current pulses receive the different result of measured projectile speed at specific main accelerator position. The current pulse and projectile speed are experimentally measured parameters. The pressure of the rail surface is calculated using transformation Eq. (2.2). The projectile position in EM launcher construction is calculating according to time and measured the projectile speed at this time.

## 2.7. Analysis Idea and Algorithm

The numerical modelling gives the opportunity to solve the various types of problems. This thesis focuses on EM and mechanical investigation. The two models will be performed in series to see the mechanical behaviour of EM launcher. For EM analyses the numerical model will take only 5% of all EM launcher in length. This length was chosen to fulfil all requirements for EM calculations numerically.

The idea to investigate this way was necessary to solve the full EM construction by taking into account EM effects. The main issue of numerical EM model is a more significant number of finite elements. In case of a projectile moving the electric field can change up to 30 kHz. This requires that finite elements size could not exceed skin depth (Pitman *et al.* 2004) in the current carrying conductor. In our numerical EM model, the element size at the inside rail surface is 0.01 mm.

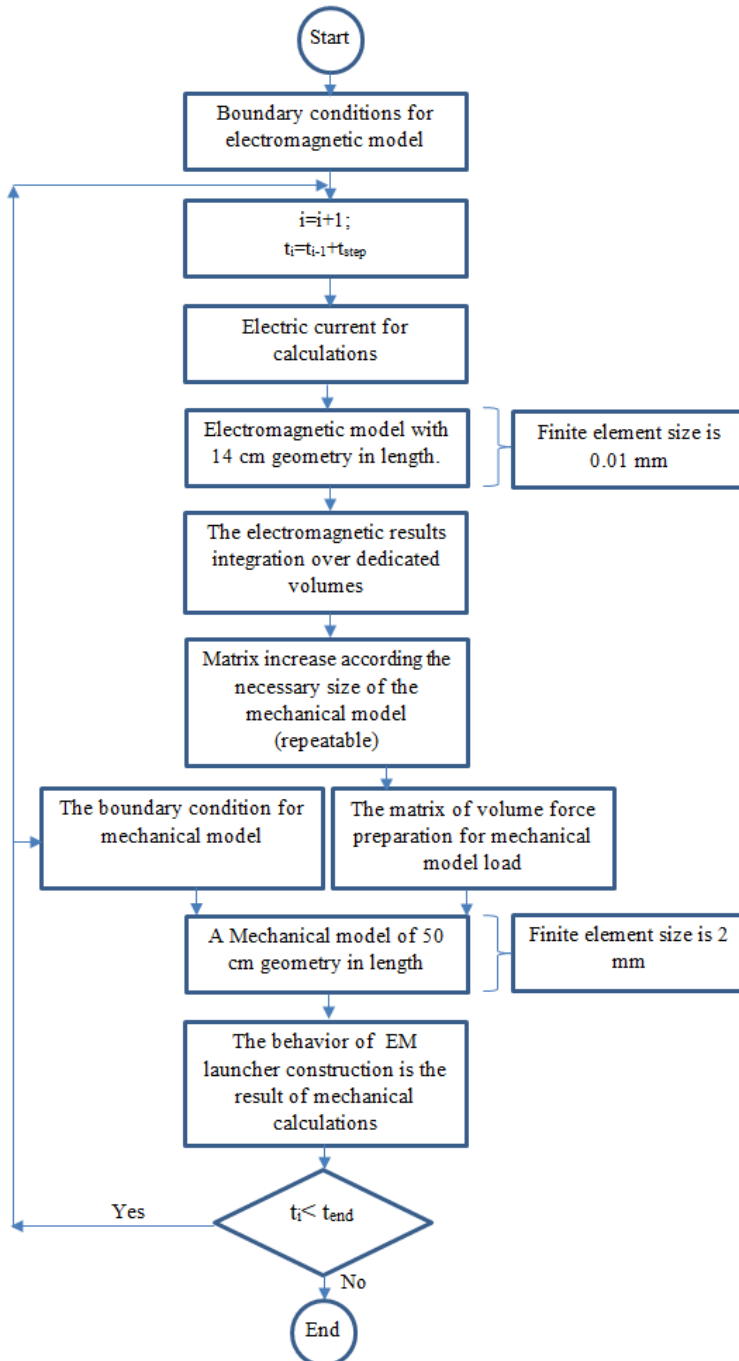


Fig. 2.8. The algorithm weak coupled consecutive model

For the numerical mechanical model to solve the mechanical effects, the size of the model should be big enough to see the behaviour of construction. In case of vibration investigation, it is necessary to analyse full EM launcher construction. To investigate the mechanical effects locally, we prepare the numerical model which is 17% of all EM launcher in length. This size of a numerical model for mechanical calculations can be solved more comfortable because the finite element size could be hundred times bigger than finite element size of EM numerical model. The finite element size influence for EM launcher construction behaviour was investigated in the paper (Gildutis *et al.* 2012).

The experimentally measured parameters such as current pulse will be used for EM numerical model as an input boundary condition. The measured magnetic field and projectile velocity are used for numerical model verification.

In this dissertation, the investigation of EM launcher rail will be done in two stages. Firstly, the electromagnetic model will be solved using Maxwell equations. After electromagnetic calculations, the load, which is gained from EM model will be used for mechanical model calculations. This concept is used due to a deeper investigation of EM and mechanical models. For EM model the FM mesh should be tiny, and due to computation power, to build the full-size model requires supercomputing machines. This type of full model investigation cost numerical calculation time and calculation resources. Step by step investigation does not require the calculating homogeneous data collection in EM modelling. For the mechanical model the mesh FE size coarser in comparison with EM model so for this calculation, the 3D model is a larger and can see the mechanical behaviour of the construction (Yang *et al.* 2017).

In EM model, only rail, bolt and armature were modelled. In mechanical calculation model, the real construction was built, and volume forces were applied for calculation.

Fig. 2.8 shows the structure of weak coupled model calculation. The cycle of the algorithm can continue with time steps according to the current pulse time. This type of analyses requires less computer hardware resources comparing with full model EM calculations. The algorithm calculation is performed in series.

## 2.8. Conclusions of Chapter 2

1. The experimental measurement of armature velocity during EM launcher operation prests that the movement of armature starts after 0.3 ms. The velocity was measured using two Doppler radars.
2. The pressure calculated using the time measured current pulse presents the same shape as a current pulse. The superposition principle using 18 capacitors allow to create the current pulse, which can be built the various

shapes. In this research thesis, only one shape of current/pressure pulse was used.

3. The RAFIRA EM launcher is open bore EM launcher. The open bore construction is convenient for investigation purposes. The flexibility of operating systems and ability to measure each point at the mechanical construction give the possibility to do experimental measurements and according to the measured data make model of EM launcher construction and improve models' validation numerically.
4. The coupling concept is available in the conventional numerical calculation software. The idea is to solve small model in the EM modelling system and apply small model results for full mechanical model investigations. This type of modelling does not require to solve full EM model in which the gradients far away from armature is homogenous and can be repeatable.



# 3

---

## Electromagnetic Analysis of the Electromagnetic Launcher

In this Chapter contribution, we analyze the foundations of our electromagnetics modelling using electromagnetic calculations. We calculate a 3-D distribution of the  $J \times B$  volume force density in the rails and use them as input for our structural mechanic's model.

Parts of this chapter are published in Schneider *et al.* (2013), Račkauskas *et al.* (2015), Račkauskas *et al.* (2016), Račkauskas *et al.* (2018), Račkauskas *et al.* (2018).

### 3.1. Electromagnetic Field Model

A 3-D FE electromagnetic model was generated for electromagnetic force calculations. The computational domain encompasses the volume required to determine the distribution of the magnetic field. It involves the structural part of the full model shown in Fig. 2.2a and the ambient air which is necessary for electromagnetic calculations.

The development of the model relies on several assumptions such as model symmetry, constructional reduction and simplification of bolts (in a model with bolts). Due to the symmetry of the cross-section lying in the Oxy plane, only one-

quarter of the structure outlined in the breech view (see Fig. 3.1) was considered as the model domain. Thus, the model includes the half of a rail and housing bar and one-quarter of the armature which are used for calculations. The air part of the model is not shown in Fig. 3.1. To save calculation resources, a section of the electromagnetic launcher of only  $L_{el} = 14$  cm in length (see Fig. 2.2a) was modelled. This length of the model chosen using the “four calibres” rule is sufficient to avoid numerical errors introduced by boundary conditions. The distance between the start point of rail and armature should be four times bigger than the gap between rails. The four calibre rule plays an essential role in force value. The rule indicates how far the armature should be inserted into the breech of an EM launcher to warrant that full propulsive force to be obtained when current is flowing (Marshall and Ying 2004).

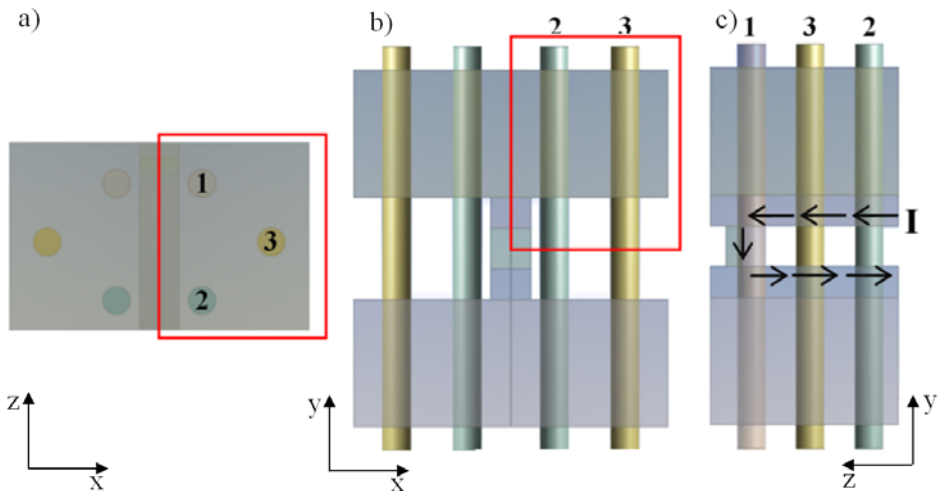


**Fig. 3.1.** The structural part of the 3-D model used for calculation: a) top view projection; b) breech view projection; c) side view projection, I – current flow

Two types of models were developed: a model without construction bolts and a model with construction bolts. Detailed geometry of the structure part of the models is presented in Fig. 3.1. The model without bolts is the same in size and structure just bolts are excluded.

In the model with bolts, the side view shows that only three steel bolts denoted by 1, 2 and 3, were included. The path of the current flow is also showed in black coloured arrows (see Fig. 3.1c). The top view shows the bolt positions in the construction bar. It was assumed that these conditions allowed to investigate the local effects of current flow and magnetic field distribution locally.

## 3.2. The Calculation Method for the Electromagnetic Case

These four equations are based on Ampere's, Faraday's and Gauss's laws and can be written in the differential form (Keshtkar *et al.* 2008; Özakın and Aksoy 2016; Yang *et al.* 2016):

$$\nabla \times \mathbf{H} = \mathbf{j} + \frac{\partial \mathbf{D}}{\partial t}, \quad (3.1)$$

$$\nabla \times \mathbf{E} = -\frac{\partial \mathbf{B}}{\partial t}, \quad (3.2)$$

$$\nabla \cdot \mathbf{B} = 0, \quad (3.3)$$

$$\nabla \cdot \mathbf{D} = \rho_e. \quad (3.4)$$

Most of the investigations are based on the quasistationary magnetic fields approximation because the effect of the magnetic field is predominant. Therefore, the displacement term  $\partial \mathbf{D} / \partial t$  can be neglected. The charge density variation is also ignored and Eq. (3.1) should be rewritten as:

$$\nabla \times \mathbf{H} = \mathbf{j}. \quad (3.5)$$

The investigation of magnetic and electric fields is based on these equations.

In this thesis, main calculation of electromagnetic fields is based on time harmonics calculations. These type of calculations is not requiring a computational cost for including the displacement current in Ampère's law (then called Maxwell-Ampère's law) as was presented in Eq. (1.1) the calculation model continues with equations:

$$\mathbf{J} = \sigma(\mathbf{E} + \mathbf{v} \times \mathbf{B}) + j\omega \mathbf{D} + \mathbf{J}_e, \quad (3.6)$$

$$\mathbf{E} = -\nabla V - j\omega \mathbf{A}. \quad (3.7)$$

In the transient case, the inclusion of this term leads to a second-order equation in time, but in the harmonic case, there are no such complications. Using the definition of the electric and magnetic potentials, the system of equations (3.1) and (3.2) becomes:

$$-\nabla \cdot ((j\omega\sigma - \omega^2\varepsilon_0)\mathbf{A} - \sigma \mathbf{v} \times (\nabla \times \mathbf{A})) + (\sigma + j\omega\varepsilon_0)\nabla V - (\mathbf{J}^e + j\omega \mathbf{P}) = 0, \quad (3.8)$$

$$(j\omega\sigma - \omega^2\varepsilon_0)\mathbf{A} + \nabla \times (\mu_0^{-1}\nabla \times \mathbf{A} - \mathbf{M}) - \sigma\mathbf{v} \times (\nabla \times \mathbf{A}) + (\sigma + j\omega\varepsilon_0)\nabla V = (J^c + j\omega\mathbf{P}). \quad (3.9)$$

The time-harmonic assumption uses for armatures speed initialisation. The electric frequency uses as a current pulse flow and the armatures changing between the construction bolts. That means the higher frequency of the current flow indicates higher armature velocity through the construction bolts. This way of calculations presents the current distribution at different armature velocities.

This method for calculations calculates the model with armature at a fixed position. No moving effect. The velocity which is mentioned in the equations 3.6, 3.8 and 3.3 is  $v=0$ . Most of the papers are based on this type of calculations. To calculate the moving armature effect, the velocity of Lorentz Transformation (Gavrilov 2003) can be used. The moving frame is created by adding the velocity of continuous bodies. In this model, the armature keeps at the fixed position, but the bolts and rail body move with a certain velocity. To indicate the moving effect the frequency set to 1 Hz, in case of fully frequency elimination the time transient case equation should be solved. The time transient case requires second-order equations in time which is asking for more powerful calculation hardware. So with adding the velocity and reducing the frequency the simplified time transient model could be used with certain armature velocities. The Eq. (3.9) can be rewritten as:

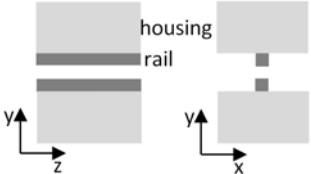
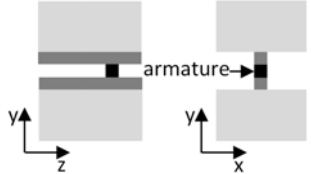
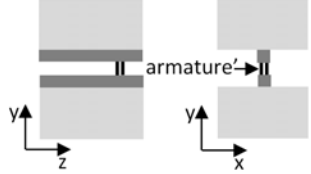
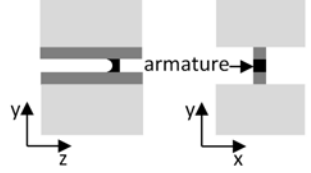
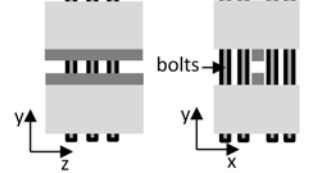
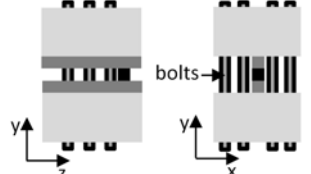
$$(j\sigma - \varepsilon_0)\mathbf{A} + \nabla \times (\mu_0^{-1}\nabla \times \mathbf{A} - \mathbf{M}) - \sigma\mathbf{v} \times (\nabla \times \mathbf{A}) + (\sigma + j\varepsilon_0)\nabla V = (J^c + j\mathbf{P}). \quad (3.10)$$

An operational definition of when it can be used is that the moving domain contains an induced magnetic source (magnetization plus eddy currents) that has to be stationary concerning the motion. Thus, used to model conductive with homogeneous bodies such as long electromagnetic launchers or magnets over a moving infinite homogenous plane (magnetic levitation trains) or flow of homogeneous conducting fluid past a magnet.

### 3.3. Models of an Electromagnetic Launcher

To investigate the magnetic force distribution and understand the current flow behaviour, the few EM model were built for EM analyses. Firstly, the calculation accuracy was checked by using  $J \times B$  approach and magnetic energy methods. The calculations starts with simple only rail model and in continuous work the different types of armatures were added, and constructed bolts were introduced into analyses. The schematic models of EM analyses are presented in Table 3.1.

**Table 3.1.** Schematic models for electromagnetic analyses

Model structure	Name of model
 <p>housing rail</p>	Rail model
 <p>armature</p>	Rail-armature model
 <p>armature'</p>	Rail-distributed armature model
 <p>armature</p>	Rail C-shape armature model
 <p>bolts</p>	Rail model with construction bolts
 <p>bolts</p>	Rail-armature model with construction bolts

### 3.4. Boundary Conditions for Electromagnetic Analyses

Since the structure is symmetric to  $x$ - $z$  and  $y$ - $z$  plans, only the one quadrant is modelled (Musolino 2001). Five surfaces must be set by individual boundary conditions which are described below. For electromagnetic simulations, special boundary conditions were set. At  $x$ - $y$  and  $x$ - $z$  and also at cylinder shaped surfaces (the air ambient usually set as a cylinder shape) the boundary condition  $n \times A = 0$  and  $n \times J = 0$  were set as “electrical wall”. This means that the current density and magnetic density vectors are normal to the surface. At  $y$ - $z$  plane the boundary condition  $n \times H = 0$ , which means that on this surface current density vectors are normal and the magnetic field vectors are always tangential to this surface – called “magnetic wall” (Hsieh 1995; Keshtkar 2008).

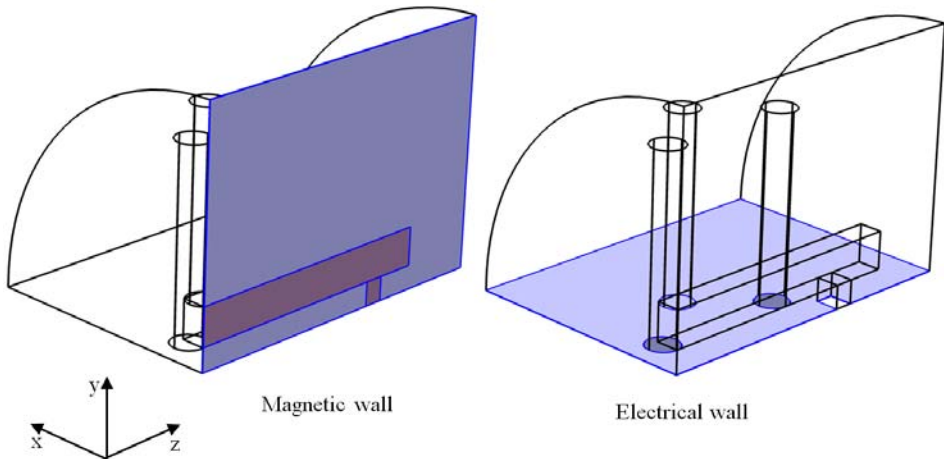


**Fig. 3.2.** The visualisation of boundary conditions for the electromagnetic model including the armature, rail, constructing bolts and air

In the Fig. 3.2 the “electrical wall” is not marked at the cylinder-shaped surface and at the cylinder shape ends which is covered the volume of air ambient are on  $x$ - $y$  planes.

### 3.5. Finite Element Mesh and Their Evaluation

The model calculation started with accuracy investigation. The time harmonic solver was used to investigate mesh of the FE. A rail-armature model was solved.

As was mentioned in Chapter 2 the FE method accuracy depends on finite element size.

The current density near the surface depends on alternating current frequency or pulse duration in pulsed power application. The current density at the surface increases when the frequency increases and vice versa. The main current carrying volume is at the surface and it can be described as the skin depth. This parameter explains how deep from the surface is distributed the main current (Knoepfel 2000).

$$\delta = \sqrt{\frac{2\rho}{\mu\omega}}. \quad (3.11)$$

The skin depth estimate the minimum mesh element size near the surfaces, where the skin and proximity effects appears.

A quarter of the rail-armature model is presented in Fig. 3.6, where half of one rail and a quarter of the armature are given. An important task for FE calculations is to find a good mesh type, which gives useful solutions and reduces computation resources. The volume of model must be meshed in 3D case. The meshing to uniformly finite elements in all volume produce a big number of finite elements and when the FE size decrease it leads to huge number of elements.

**Table 3.2.** Mesh element size (surface numbers fits with numbering in Fig. 3.6)

Surface number	Element size of meshes			
	mesh #1	mesh #2	mesh #3	mesh #4
1	6 mm	1 mm	0.8 mm	0.8 mm
2	6 mm	1 mm	0.5 mm	0.3 mm
3	6 mm	1 mm	0.5 mm	0.3 mm
4	6 mm	2 mm	1 mm	0.8 mm

The mesh element sizes can increase if they move farer away from these surfaces. For the investigation of accuracy it was decided to calculate inductance gradient according to Eq. (1.4). The force was calculated over all armatures volume according to Eq. (1.3). Four meshing cases were used to show the dependence between mesh size and calculate accuracy. Mesh #1 is the meshing type called “fine mesh” which is one of default in COMSOL software. This fine mesh divided model into tetrahedral elements, which have a similar size over all volume (to use finer mesh was impossible due to hardware power limitation). The other mesh types are presented in Table 3.2. These types of meshing have small elements at the marked surfaces and enough big elements far away from these surfaces.

It is interesting to determine the changes which appear in calculation results (inductance gradient magnitude), when the frequency is changing in time harmonic case calculations. The inductance dependence on frequency is shown in Fig. 3.3 four curves are presented. Each curve presents different meshing types and shows dependence on frequency.

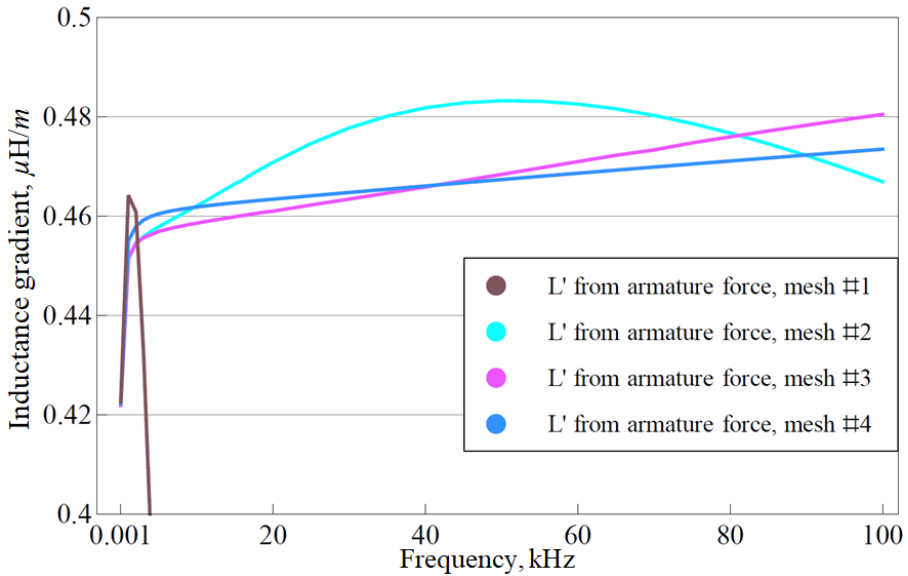


**Fig. 3.3.** Visualization of L-prime calculation using different meshes

According to accuracy calculations both good and bad solutions exist. The bad case is with mesh #1, which is default in COMSOL. The main drawback of this meshing is that there are a lot of small elements in air ambient. The regions which are far from armature have no influence on the force on the armature. The better case is with mesh #4. This case has the smallest elements at the marked surfaces (see Fig. 3.6) and big elements far from the railgun model (in air). Using the best meshing convergence is obtained. The differences between meshing are small when frequencies are low, but when frequencies are higher (bigger armature velocities) the effect of meshing on calculations accuracy is very big.

According to FE mesh evaluation and FE mesh recommendation in literature where the skin depth is taken into account (Pitman *et al.* 2004; Hsieh 2007). The final 3-D FE rail-armature model was generated by applying tetrahedral elements. The main parameters are the minimum element size and growth rate.



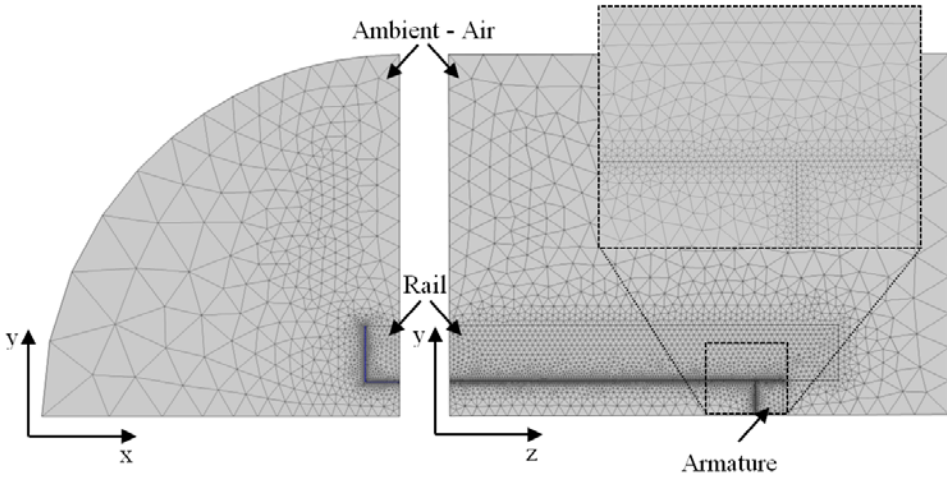


**Fig. 3.4.** The rail-armature model presented divided into finite elements. Electromagnetic numerically model requires the ambient volume for magnetic field calculations

The refined mesh has to be used in regions where the field gradients are the highest, and the size of the elements is increased with growing distance from these regions. An accuracy check was performed with a minimum size of an element of approximately 0.04 cm at the inner surface of the rail and armature and 0.005 cm at the inner conducting parts surface edges to evaluate the proximity effect. The element size corresponds to the minimal mesh density required to capture a 3-D behaviour of the entire railgun structure at acceptable computational expenses. The finite element mesh that was used for calculations consisted of 2012122 3-D tetrahedral elements and 15493339 nodes.

The accuracy of calculations allowed to model with an appropriate meshing for simple EM launcher simulation. According to this simulation, the doublecheck of RAFIRA's inductance gradient were calculated. The same model with the best meshing was used. The gradient was calculated according to two methods:  $J \times B$  approach (as was used for accuracy investigation) and magnetic energy. The results of inductance gradient are presented in Fig. 3.5.

Two different calculating methods are demonstrated in Fig. 3.5 to validate the mesh size. The inductance gradient was calculated in two different ways and compared with real inductance gradient, which can be experimentally measured. Inductance plays an essential role in defining how to transfer electromagnetic energy into the kinetic energy. The force pushing projectile is related to the inductance gradient according to Eq. (1.3). Inductance gradient is using energy conservation method. The decreasing curve indicates that calculations were done by

magnetic energy method, which calculated the magnetic energy in volume between two rails far away from the armature. The inductance gradient was found according to Eq. (3.11) when magnetic energy was known (Leferink 1995):

$$W_m = \frac{1}{2} \sum_{i=1}^n L_i I_i^2. \quad (3.11)$$

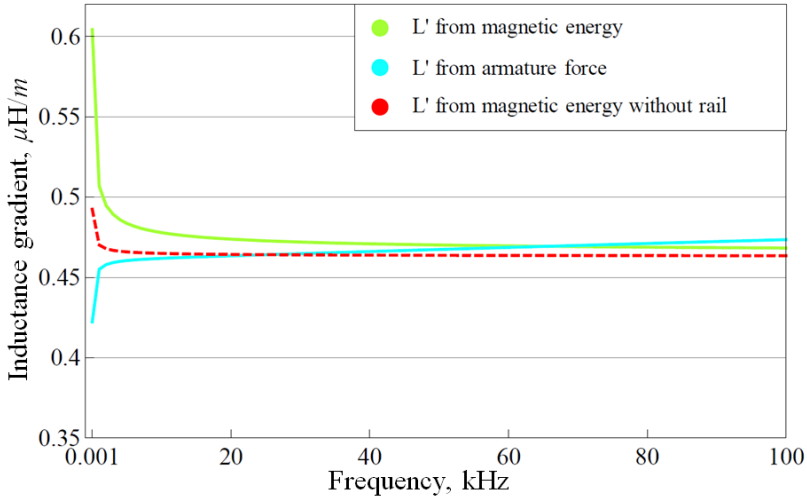


**Fig. 3.5.** Visualization of L-prime calculation using different methods

The green curve presents the inductance gradient difference at low and high frequencies is 20%. At high frequencies, the magnetic field is pushed out of the conductor due to current distribution changes. The red dashed line in Fig. 3.5 presents the inductance gradient value according to magnetic energy method. The picture (see Fig. 3.5) shows that the inner inductance gradient at low frequencies consists of 17% of full inductance gradient magnitude. However, it does not influence the propulsive force on the armature. As a contrast, the second case is according to  $J \times B$  method. This method showed that the inductance gradient was the lowest when the frequencies are low and converged to the same value as the magnetic energy method. At low frequencies, the magnetic field penetrates inside the rail, and the efficiency of the inductance gradient is increasing when the current frequency is increasing too. This simulation shows that when the magnetic energy is the highest the efficiency of propulsive force is the lowest. The effective inductance gradient depends on the current frequency and converges to a steady value. In the case of RAFIRA with copper rails,  $L' = 0.467 \mu\text{H/m}$  was obtained for the high-frequency case. The L-prime values which are obtained within the margins of accuracy should merge in both methods, at high frequencies.

### 3.6. Results and Discussion of Electromagnetic Models

The results of each model numerical calculation are presented below.

#### 3.6.1. Rail-armature Electromagnetic Model

A quarter of the simple railgun model is presented in Fig. 3.6, where half of one rail and a quarter of the armature are given. In the picture zones with different colours show normalized current distribution on the model at 0.88 kHz frequency. There are two well-known effects are visible: the skin effect, which appears that the main current distributes at the surfaces and the proximity effect which define, that the current mainly distributes on the inner surfaces.

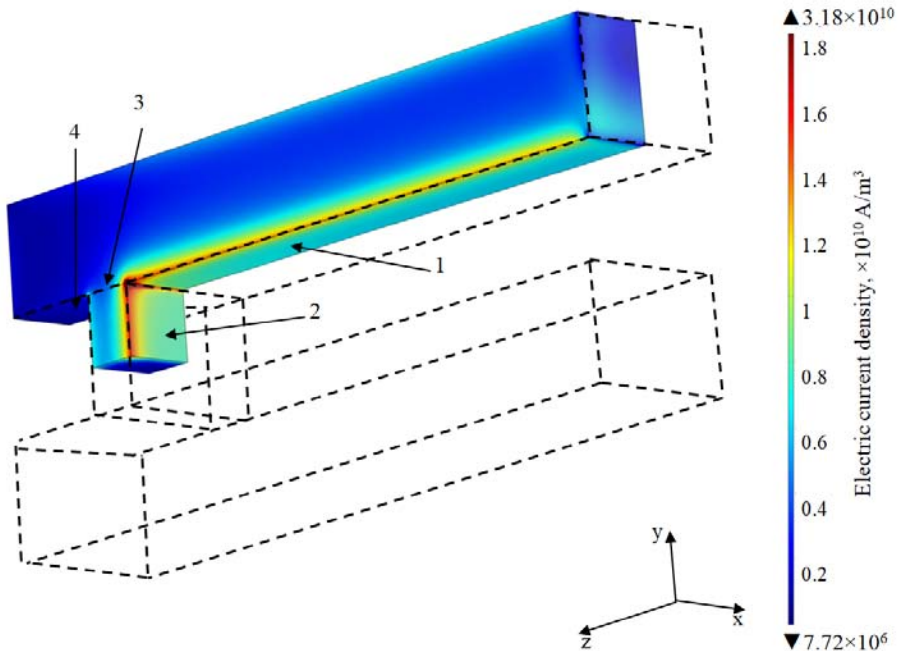


**Fig. 3.6.** Colour plot of electric current density distribution in the rail-armature model

An important task for numerical calculations is to find a good mesh type, which gives useful solutions and reduces computation resources. The volume of the model must be meshed in 3D case. The meshing of uniformly finite elements in all volume produce a significant number of finite elements and when the finite

element size decreases it leads to considerable number of elements. This type of meshing is expensive regarding computation resources and calculation time.

The current distribution shows (see Fig.3.6) that the skin and proximity effect appears. Due to these effects, the biggest gradients are at the inner surfaces. Thus, the fine meshing only at these surfaces can be used to reduce the number of mesh elements in the EM numerical model. The mesh element sizes can increase if they move far away from these surfaces.

### 3.6.2. Moving Armature vs Static Armature

The first example deals with the repelling magnetic forces acting on the rails. In purely mechanical calculations, the magnetic pressure is assumed to act on the rail surface only (high-frequency approximation). Here, we calculate the  $J \times B$  distribution in the rail volume. The rail-armature electromagnetic model was solved and case of Fig. 3.7a. illustrates a high-frequency approximation when the armature is fixed at the absolute position (880 Hz).

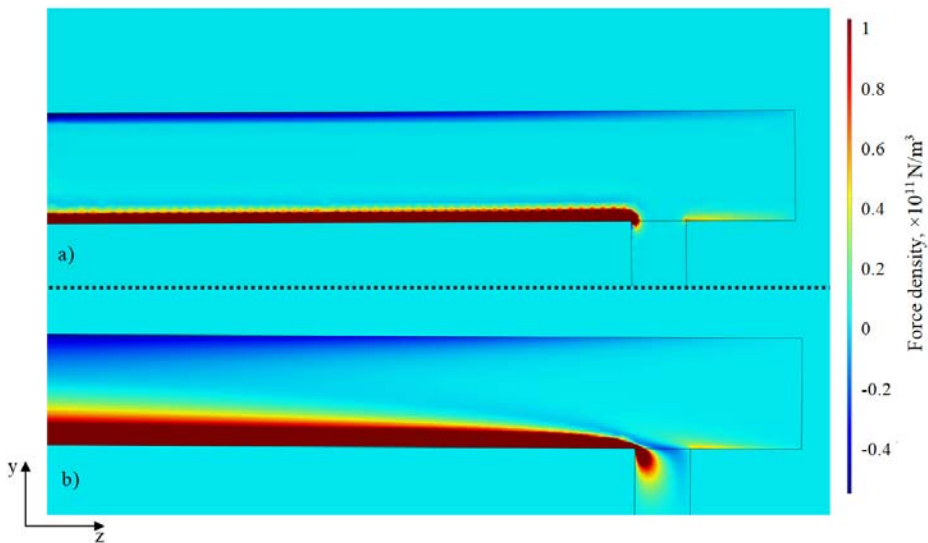


**Fig. 3.7.** Colour plot of  $J \times B$  y-components:  
a) high-frequency case; b) moving armature case

Figure 3.7b illustrates the case of an armature moving with a velocity of 65 m/s. The colour plots of the y-component of the force are presented in Fig. 3.7. Here, two results obtained for two cases are presented in subfigures A and B, respectively. The colour scale indicates force density defined in  $N/m^3$ . Note that the velocity was chosen to fit the frequency of 880 Hz at the position of the armature.

Differences in local force distributions are presented. The high-frequency approximation model leads to a distribution dominated by the skin effect. The force is concentrated in a thin layer with a thickness of 2 mm. In the case of the moving armature, magnetic diffusion plays a vital role in the local force distribution. The force distributions show significant differences, in the region close to the armature. In the context of our current investigation, the question had to be answered: do these differences lead to significant changes in the mechanical construction. The different moving armature magnetic force distribution depends not only on skin effect based on current pulse frequency but also depends on velocity skin effect which is due to moving (Engel *et al.* 2008).

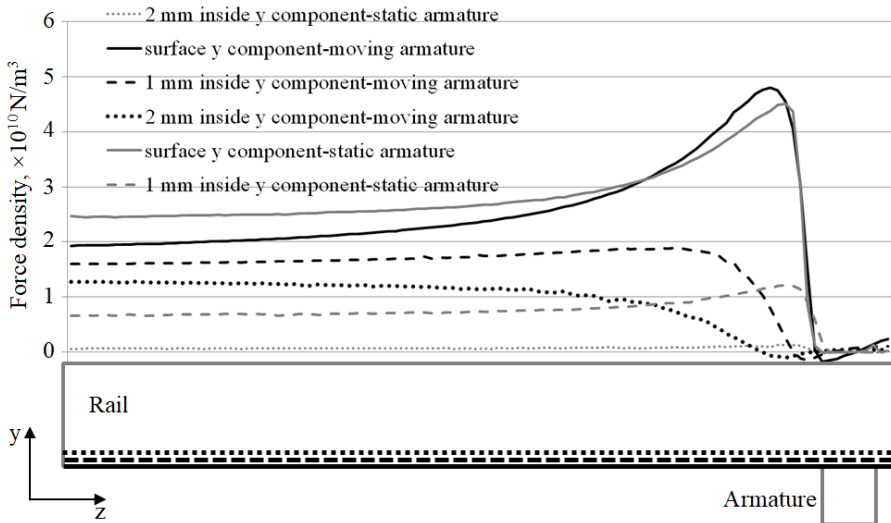


**Fig. 3.8.** The Lorentz force density distribution along the rail on static and armature moving the numerical case

In the Fig. 3.8 the force density concentration is presented along with the rail on three different slices inside the rail. These slices present the force density of static armature model with velocity frequency approximation and the force density results of the moving armature model. The results present that the force density concentration on the rail surface is higher in the static armature model. At 1 mm slice inside the rail, the force distribution in static armature model with frequency approximation drastically decreases. The extremely force concentration changing in the volume confirm the skin effect theory. The skin depth at this frequency is 1.38 mm. In the model with moving armature, the force concentration distributed more inside the rail volume, and the force distribution changes more smoothly over the different slices inside the rail volume.

### 3.6.3. Local Effect Induced by the Armature

The next example uses the “rail-armature” model (see Table 3.1) to illustrate effects caused by the presence of an armature. The results are presented in Fig. 3.9. The black curves represent the norm of  $J \times B$ , and the grey ones represent the y-component.

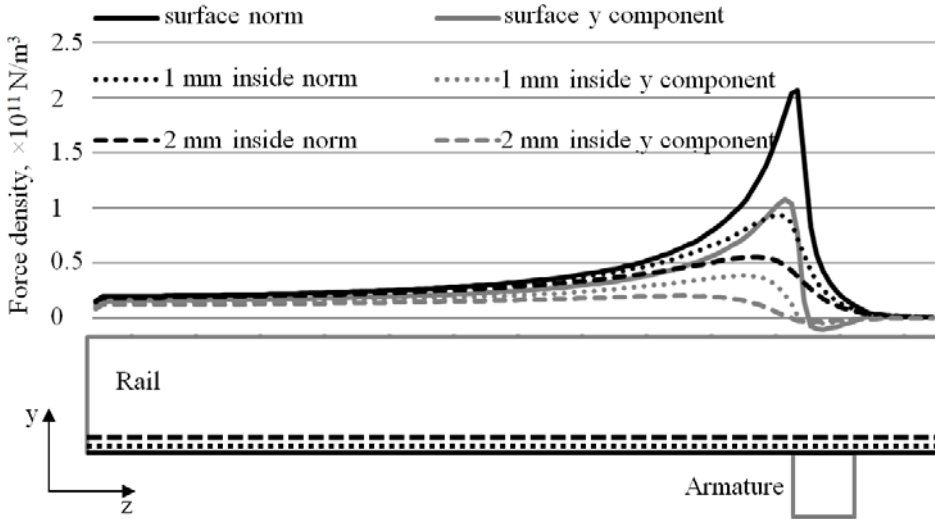
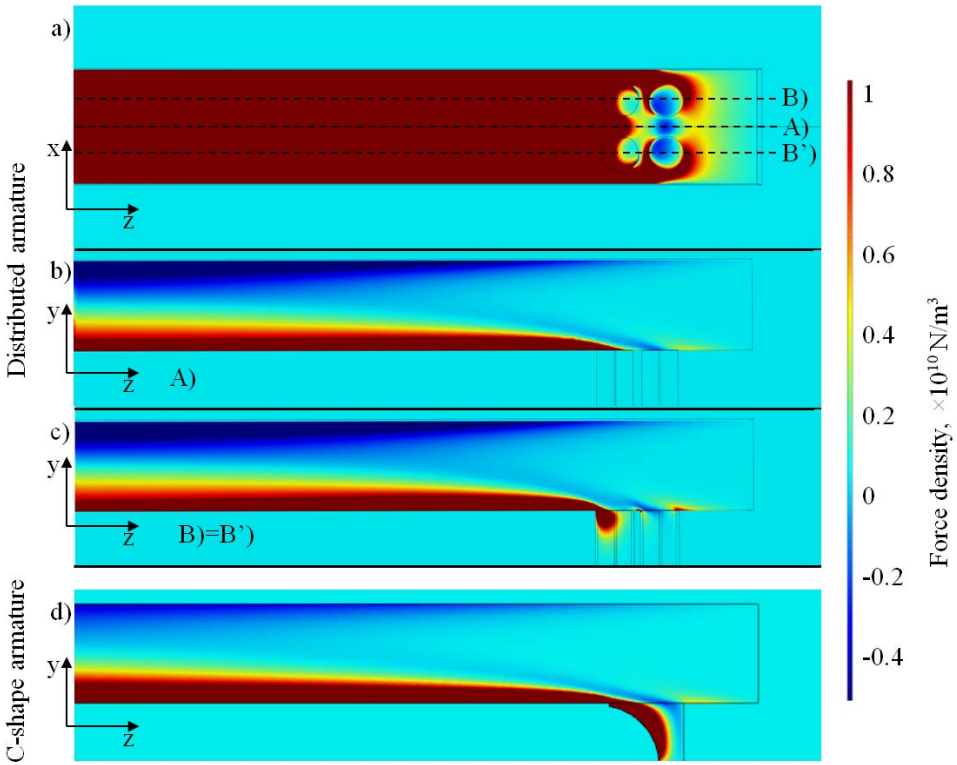


Fig. 3.9. The Lorentz force density distributions which are presented along the rail

The calculation results show that the armature influences the Lorentz force distribution in the rail volume. The  $J \times B$  force increases in the region near the armature. The difference between the norm calculation and the calculations of the y-component means that the presence of the armature effects all vector components. However, the most significant influence exists for the y-component being responsible for the repulsion between the rails. The measured parameters with CMR-B-scalar sensors also preset the magnetic field distribution inside the rail volume. The created numerical model fit the measurements of the magnetic field distribution done by ISL (Liebfried *et al.* 2013b; Stankevici *et al.* 2013).

### 3.6.4. Types of Armature

The EM launcher has three different types of the armature for analyses. The most common case for rail EM investigation uses pure current conducting cuboid to imitate the armature between rails (see Fig. 3.7). For this investigation, the two additional models were created which are described in Table 3.1.



**Fig. 3.10.** Colour plot of  $J \times B$  y-components: a) top view projection of rail-distributed armature model, b) side view projection at the slice A; c) side view projection at the slice B; d) side view projection of rail C-shape armature model

Essential results of EM simulation are illustrated in Fig. 3.10, where 2D distributions of the y-component of EM force density in the form of coloured contour plots are presented: the distributed armature, which consists of four cylinders and C-shape armature. The results of force density distribution of y-component are presented in collared pictures to see the locally biggest concentration of force in the rail and armature. The results obtained for distributed armature show the local armature shape dependent distributions of the force density. Uniform force distribution on the sliding surface (see Fig. 3.10a) illustrates the dominance of the skin effect occurring outside the contact. Two different variations in vertical longitudinal sections, central section A (see Fig. 3.10b) and section B (see Fig. 3.10c) illustrate inhomogeneity of cross-sectional loading. This undesirable effect indicates available imperfection of the sliding surface, which may lead to instability of projectile motion.

All model was modelled one-quarter of full model except distributed armature model because the distributed armature the symmetry not continues over all

rail cross-section. The results indicate the different force distribution in the region near armature of all three armatures.

### 3.6.5. Constructing Bolts Influence for Electromagnetic Calculations

The construction bolts which are in the mechanical construction have influence not only direct for mechanical model: the up and top housing bars are connected using the bolts which are made from steel alloy (see Table 2.1). The investigation which is present below presents the fact which construction bolts made from steel alloy located near the current carrying rails have a negative impact on launching process. The rail model with construction bolts and rail-armature model with construction bolts (see Table 3.1) were solved.

The construction bolts investigation starts on rail model with construction bolts (see Table 3.1) numerical investigation. The housing under investigation is characterised using discrete steel bolts to counter the repelling forces (see Fig. 2.2). Considering the question if the presence of these conductors has to be considered for appropriate electromechanical modelling. Figure 3.11 illustrate the results of similar calculations. The two-coloured images show the  $J \times B$  distributions in two rail cross-sections, while the upper image shows the cross sections (parts a and b). At the z-coordinate of section a) was chosen to coincide to that of a bolt, whereas the z-coordinate of section b) lies in the middle between two bolts. Minor deviations can be stated which motivated us to further elaborate on this topic. Only two construction bolts no. 1 and 2 (see Fig. 3.1) are taken into account because they are nearer to the rails. Construction bolt no. 3 (see Fig. 3.1) do not influence conducting part of EM launcher. This bolt far away from the current caring part and do not have any influence on magnetic field distributions. The Eq. (3.12) estimate the magnetic field influence for bodies any point in 3D-space:

$$B(\mathbf{r}) = \frac{\mu_0}{4\pi} \int_C \frac{I d\mathbf{l} \times (\mathbf{r} - \mathbf{l})}{|\mathbf{r} - \mathbf{l}|^3}. \quad (3.11)$$

Biot-Savart law is an equation describing the magnetic field generated by a stationary electric current. This law explains the magnetic field concentration influence for near constructions and why only two constructing bolts influencing the conducting part of EM launcher (Knoepfel 2000).



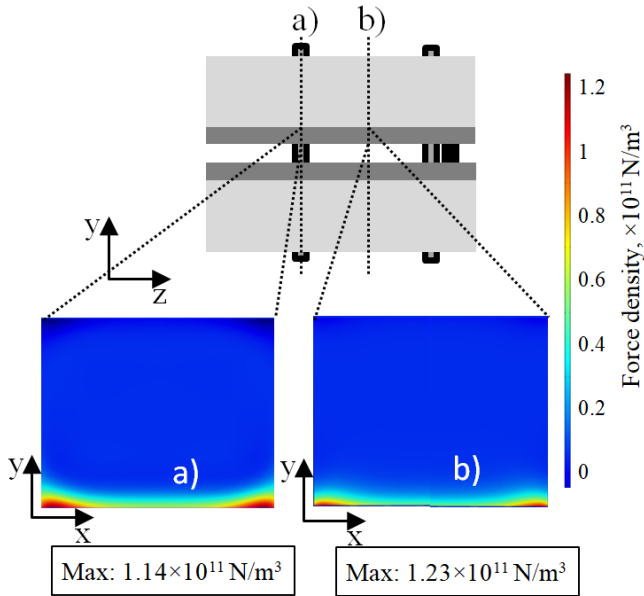


**Fig. 3.11.** The colored view of the rail cross section: a) at the region of construction bolts; b) in the pure rail region

The coloured graph above presented the distribution over the rail cross-section. The different magnetic force concentration near the bolts away from bolts are visible. The Fig. 3.12 presents the force densities distribution in the longitudinal sections way. The model was solved using the time-harmonic approximation algorithm to see the armature and bolt influence for EM launcher rail magnetic force distribution. The armature effect still exists but also the construction bolts make an influence on EM force concentration distribution in rail volume. The EM force distribution is different at a different frequency. With the highest frequency, the effect of construction bolts is bigger. The effect mainly appears at the inner surface, in the next layer inside the rail volume the effect of construction bolts decrease (dashed line is 1 mm inside the rail measuring from the inner rail surface).

To elucidate the influence of the bolts overall rail volume the integral at any point in the  $x$ - $z$ -plane:  $\int dy (jxB)_y$  was calculated. This integral was taken across the whole rail. In Fig. 3.13 a map of the results obtained for two cases is drawn: presents the rail model with constructing bolts (b) and the rail model without bolts (a). The integral is calculated using the harmonic approximation solution at 5000 Hz corresponding to an armature velocity of around 370 m/s. One can clearly see the local influence of the bolts. In agreement with Lenz’s rule the eddy currents induced in the bolts reduce the repulsive force. The relative reduction is

at maximum 17.5%. Also, the soundness of results were checked by calculating  $F_y$  acting on the rail section which corresponds to  $\int dV (jxB)_y$ . In agreement with Lentz' rule the 7% reduction of the total repulsive force was found.

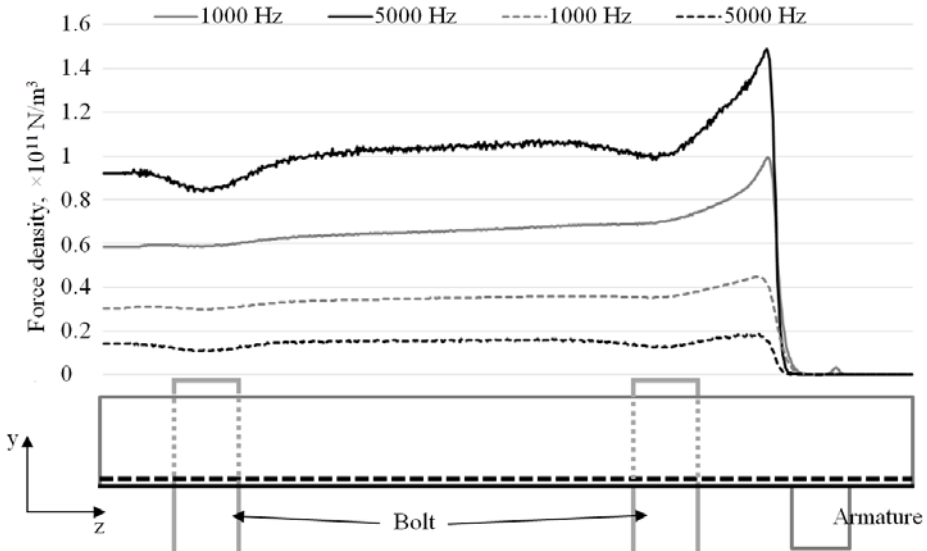


**Fig. 3.12.** The rail-armature model with constructing bolts is presented. Black colour presents the force density distribution at 5000 Hz. Grey colour presents the force density distribution at 1000 Hz. The results presented at the surface (solid curve) and 1 mm inside the rail (dashed curve).

**Table 3.3.** The repulsive force calculated over all rail volume (model with 14 cm rail length)

Name of the model	Frequencies					
	20 Hz	1000 Hz	5000 Hz	10000 Hz	15000 Hz	20000 Hz
Rail-armature model	111170 N	118595 N	119636 N	119938 N	120153 N	120360 N
Rail-armature model with construction bolts	111165 N	113846 N	109395 N	108438 N	108089N	107956 N
Rail model with construction bolts	87928 N	95910 N	94269 N	93980 N	93940 N	93973 N

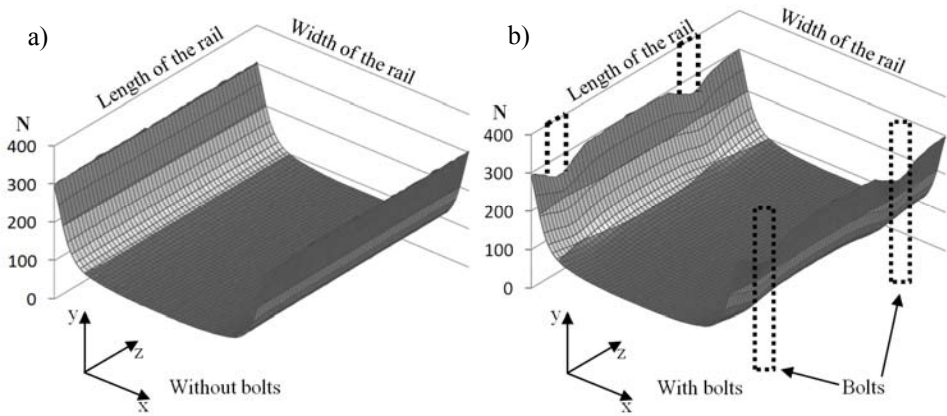


**Fig. 3.13.** Influence of steel bolts on repulsive  $J \times B$  force: a) a map of force without bolts; b) a map of force with bolts

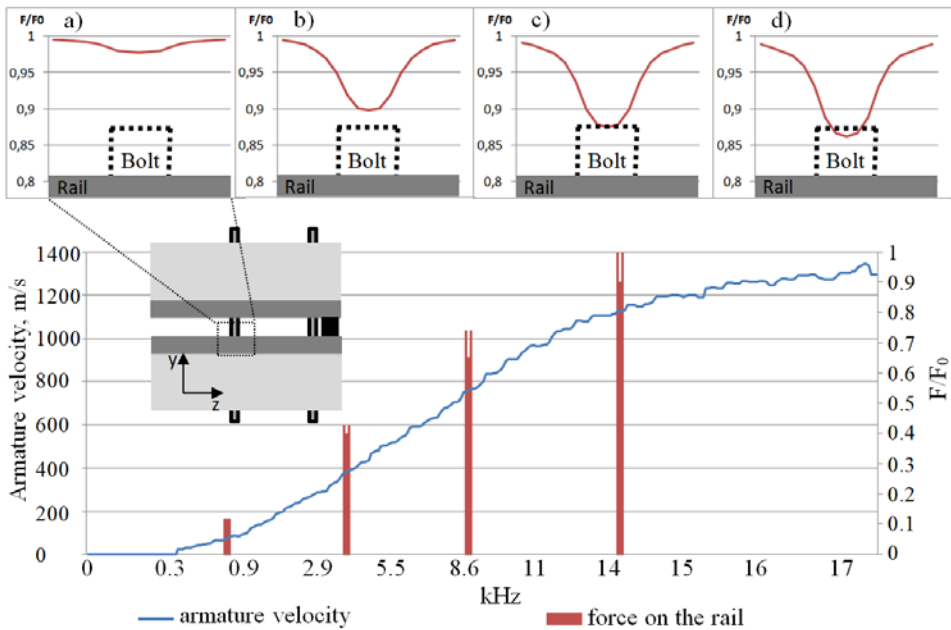


**Fig. 3.14.** The influence of constructions bolts on the rail force at different frequencies (velocities). The subgraphs a–d present relative force distribution along the rail in bolt region: a) at 65 m/s, b) at 400 m/s, c) at 800 m/s, d) at 1100 m/s

The repulsive force using the volume integral  $\int dV (j \times B)_y$  according to different frequencies using the frequency approximation model were calculated. Three different models of repulsive force are presented in Table 3.3. It is seen that

the force generated in 14 cm length rail is different according to different velocities (frequencies in frequency approximation model) while in mechanical model pressure is calculated according to Eq. (2.2). The projectile velocity is do not taken into account for mechanical behavior.

The next view of constructing bolts continuing the constructing bolts influence for EM launcher force distribution in the rail. In Fig. 3.14 the bolt effect for  $J \times B$  concentration at inner rail edge is presented. The different frequencies present different projectile speed. The solid curve at main graph indicates the armature velocity at particular frequencies. The armature velocity is measured using Doppler radar which was described in saubchapter 2.6. According to the different armature velocity, the different frequencies were calculated to estimate the armature velocity in frequency approximation model. The columns present the results that the force concentration is lower in the constructing bolts region. In the region far away from constructing bolts, the force concentration is higher.

The subgraph of Fig. 3.14 presents how force concentrations distribute at different frequencies (armature velocities on frequency approximation case). At low frequencies (low armature velocity) the difference between highest and lowest force concentration is 0.02 (see Fig. 3.14a) in relative quantities while at high frequencies (high armature velocity) difference between highest and lowest force concentration is 0.14 (see Fig. 3.14d).

### 3.7. Conclusions of Chapter 3

1. The model finite element meshing has to be set with additional meshing parameters in the places where the calculating gradients are highest. This manual adjusting of meshing algorithm increase the calculating accuracy and save calculating resources. The minimum element size calculating according to skin death formula set at EM launcher inner surface receive sufficient calculating result.
2. The moving armature model receives different pulse current distribution over the rail result comparing with pulse current distribution over the rail of the time-harmonic calculating model. This depends not only on skin effect based on current pulse frequency, but also depends on velocity skin effect.
3. The shape of armature playing an essential role of Lorentz force distribution inside the rail volume. The main differences are apeared in the region near the armature. This effect directly reflects the armature's shape. The concentration of the Lorentz force and the scalar amplitude depends on armatures geometrical parameters such as contact area, armature size and armature shape.
4. The used force for mechanical models is commonly used as homogeneous forces distribution over the surface. The results of EM calculations the force

distributes not homogeneous over the surfaces and also over the rail volume. The most significant concentrations of electromagnetic forces are distributed at the rail edges and in the region near the armature. The different calculating methods regarding armature moving and frequency approximation method became the same maximum force concentration in the armature region, but far away from the armature, the Lorentz force density is 21% lower in according armature moving model than frequency approximation model.

5. The bolts of construction receive the adverse effect. In the regions near the bolts the EM force concentration decreases. These changes of force decrease could affect all EM launcher mechanical construction. According to different velocities (frequencies on the frequency approximation model), the negative effect of construction bolts reduces the rail repelling force from 3.7% on 65 m/s till 9.5% on 1332 m/s armature velocity. This fact presents that the negligible effect of constructing bolts depends on armature velocity.



# 4

---

## Mechanical Analysis of the Electromagnetic Launcher

In this chapter two mechanical models and their investigations are presented. The mechanical effects occurring in the simplified electromagnetic launcher construction are demonstrated. The first model investigates the local EM forces impacts of construction. The second model presents the full EM launcher behaviour during its operation.

Parts of this chapter are published in Stonkus *et al.* (2015) and Račkauskas *et al.* (2018), Račkauskas *et al.* (2018).

### 4.1. The Elastic Foundation of a Mechanical Model

A 3-D structural model of the RAFIRA railgun was worked out (see Fig. 2.2). This model uses several assumptions for the sake of simplifications. Considering the symmetry of the barrel is sufficient to simulate only one half of mechanical construction. The steel bolts representing discrete supports were replaced by an elastic foundation layer continuously supporting the bar (see Fig. 4.1 and Fig. 4.9). In these figures, the springs initialize discrete supporting bolts. The elastic support layer is characterized by an adequate foundation stiffness per unit length  $k_{\text{eff}}$ .

$$k_{eff} = \frac{E_b A_b 1}{L A_{top}} n, \quad (4.1)$$

where  $E_b$  is the elastic modulus of a steel bolt.  $A_b = 2.53 \cdot 10^{-4} \text{ m}^2$  is the cross-sectional area of one bolt,  $L = 0.1125 \text{ m}$  is the length of the bolt,  $n = 160$  is a total number of bolts in railgun, and  $A_{top} = 3.0175 \text{ m} \cdot 0.2 \text{ m} = 0.6035 \text{ m}^2$  is the area of the elastic support layer.

## 4.2. A Mechanical Model for Local Effects Investigation

The mechanical model was created for structural mechanic's calculations. The 3-D simplified mechanical model involves the structures such as rails and housing bars.

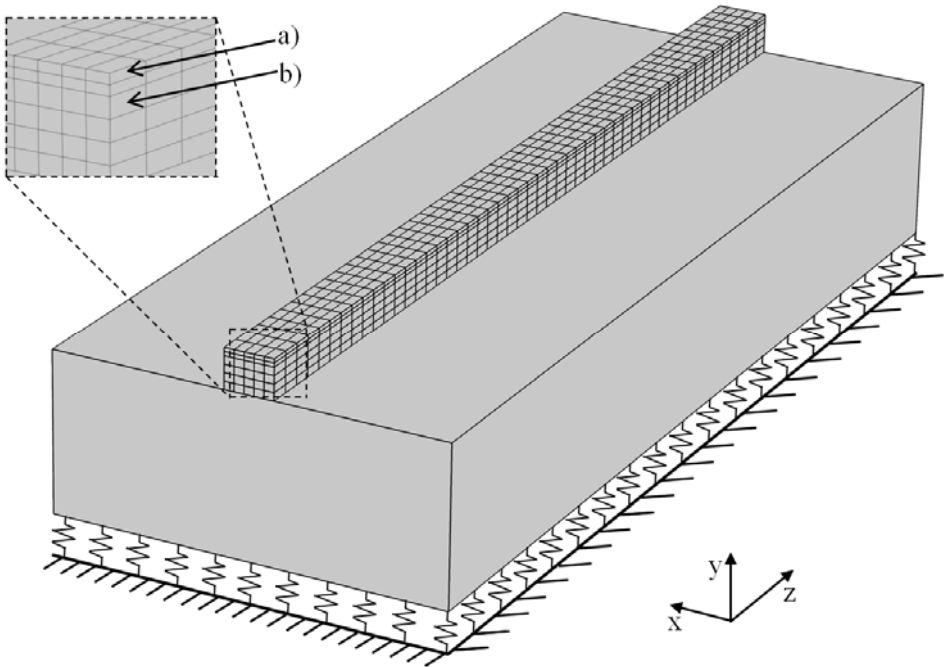


**Fig. 4.1.** The 3-D mechanical model used for calculation.  
One half of full construction structure is used



To investigate the influence of local EM effects on structural mechanics, a section of the EM launcher only  $L_{el} = 50$  cm in length (see Fig. 2.2b) was modelled. The simplified model geometry is presented in Fig. 4.1. Instead of constructing bolts the elastic foundation was used.

In this calculating model, the rails are divided into small cuboids ( $5 \times 2 \times 10$ ) mm (see Fig. 4.1a) and ( $5 \times 4 \times 10$ ) mm (see Fig. 4.1b). These cuboids are necessary to load the structure with volume forces received from EM calculations. The mechanical model load was obtained by integrating the Lorentz force  $J \times B$  over the volume size of the cuboid in EM model calculations. The two different volumes cuboids were set because the EM force concentration is different inside the EM launcher rail. All calculated forces in the previous chapter were used to investigate influence of the EM effects for the mechanical model. Each cuboid was used as a force load for the mechanical calculations. In such a manner, the local structural behaviour of the railgun could be investigated. Due to the symmetry of the problem, only one half of the full EM launcher structure was simulated.

### 4.3. Finite Element Model of the Mechanical Model

The corresponding 3-D FE model was generated using tetrahedral elements. In the case of mechanical modelling, the field gradients distribute uniformly, and no special refinement is necessary (Gildutis *et al.* 2012). In the EM model, the air ambient was necessary for magnetic field distribution calculations and in the mechanical model the air ambient is not necessary, and the bigger model can be built under lowest hardware resources.

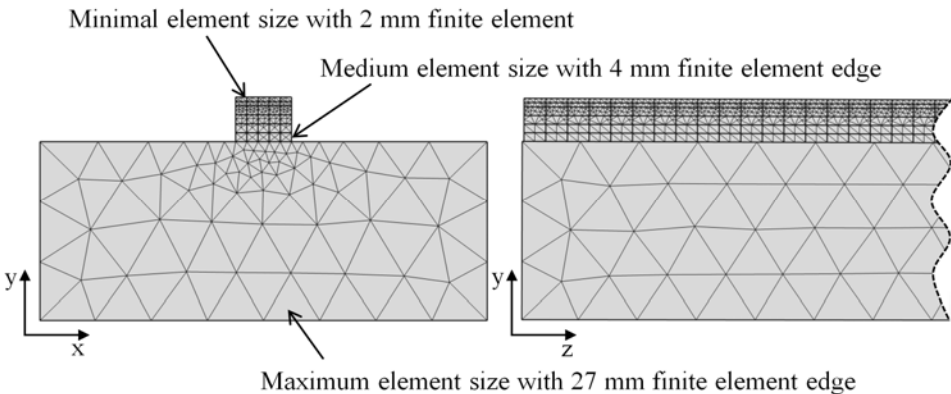


**Fig. 4.2.** The mechanical model presented divided into finite elements

The finite element size distributed in three groups. One group is smallest elements which are distributed in the inner rail surface were the size of the cuboid is  $(5 \times 2 \times 10)$  mm (see Fig. 4.1a). Here due to highest gradients in EM model, the most significant forces are transferred as a load force. The second group of elements are called medium elements group and are distributed in the inner rail surface were the size of the cuboid is  $(5 \times 4 \times 10)$  mm (see Fig. 4.1b). Moreover, the third finite element group which is distributed in the construction housing bar. There the finite element size reaches up to 27 mm in size.

In Fig. 4.2 the mesh of mechanical model is presented. All three groups of elements are described. Using these groups of element the FE number is extremely smaller than in the EM model. The FE mesh consists of 111206 3-D tetrahedral elements and 507354 nodes.

#### 4.4. The Mechanical Models With Different Loads

In Fig. 4.3 the technical drawing of force distribution in rail construction is shown. The two load principles are presented. First principle (see Fig. 4.3a) for the load force is set as the pressure on the surface. This type of force distribution is used for most mechanical calculations in literature. This principle can be used at high armatures velocities when the current is vanished from the rail body and mainly concentrated at the EM launcher inner surface. The second principle of the load force is to distribute rail volume into EM launcher. This principle is used in this thesis investigations. The idea is shown in Fig. 4.3b. The force distributed homogeneously over cuboid volume, in Fig. 4.3b the resultant force is marked as  $F_{1-6}$ . These cuboids are used to simplify the calculating model. The force  $F_1$  is presented as the highest force, and the  $F_6$  force is indicated as a smallest load force because the main EM force concentration is near the surface. As the EM investigation started from simple rail model, so the mechanical began using different load principles over the rail volume. The rail model (see Table 3.1) was solved using the EM model, and the results of EM calculations were integrated over cuboids size volumes (see Fig 4.1). The forces  $F_1 \dots F_6$  are the integral of Eq. (1.3) over the cuboid size volume. The integrated Lorentz force was used as the mechanical model load into each cuboid.

Of both force load principle, the repelling forces play an essential role in the EM launcher technology because due to high currents in the rails and the injection bars several hundred MPa of pressure appear. These forces try to increase the distance between rails. Because of this a gap between rail and armature appears and conducting properties in the contact zone between rail and armature decrease. This decrease lowers the efficiency of railgun system.

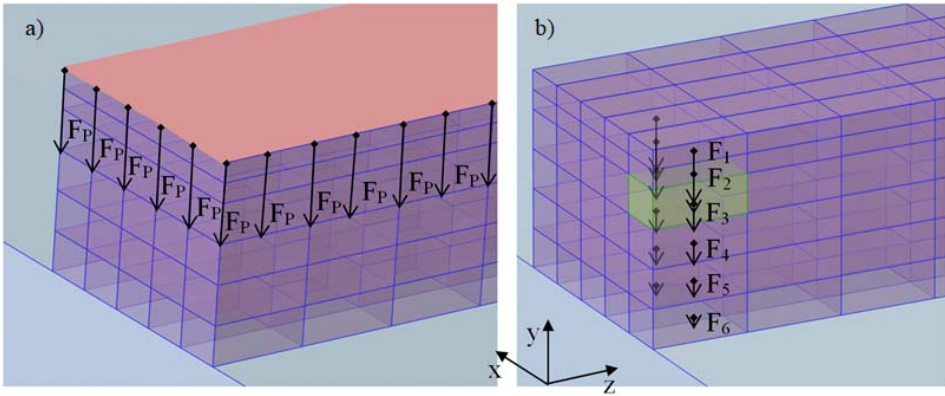


**Fig. 4.3.** Technical drawing of load force principle: a) the load force set as pressure homogeneously overall rail surface, b) the load force distributed over rail volume

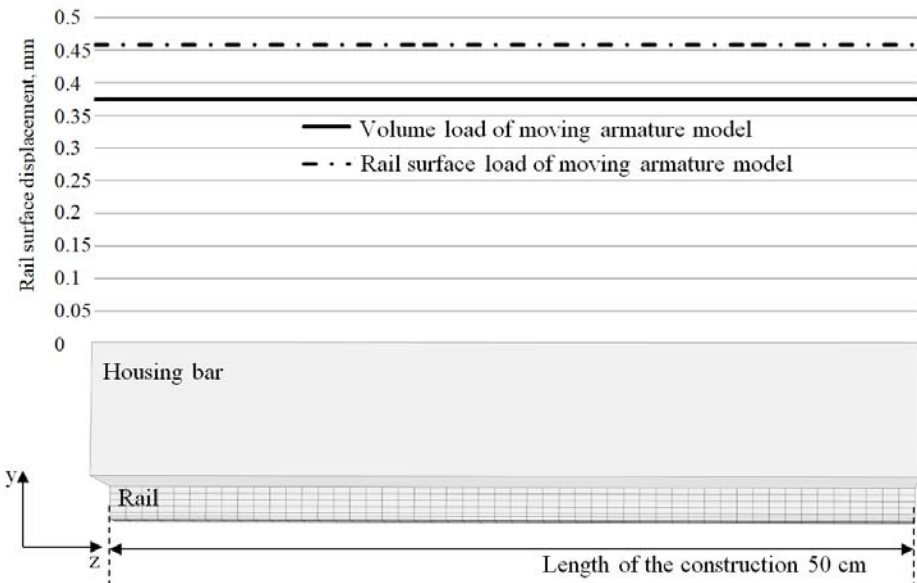


**Fig. 4.4.** The rail displacement of the mechanical model using two mechanical load types

The variation of the mechanical behaviour due to different loads is demonstrated by considering the rail deformation under compression. The force was distributed uniformly over the cuboid volume. The rail model was solved using two types of EM launcher calculations: the harmonic case and the case with moving armature. Both cases indicate the rail displacement far away from armature to eliminate the influence of armature. Longitudinal variation the rail surface

displacement is given in Fig. 4.4. Solid curve indicates displacement profile obtained under the action of numerically acquired Lorentz forces loaded in all rail volume; the dashed curve demonstrates the rail displacement profile obtained by the time-harmonic case drawn for the sake of comparison. The calculation results are show the significant difference in the mechanical model without an armature.

## 4.5. Armature Influence on a Mechanical Model

The next investigation continuous by adding the armature and including the armature effect into the mechanical calculation. The results of EM calculations were different when comparing the time-harmonic case and armature moving case.

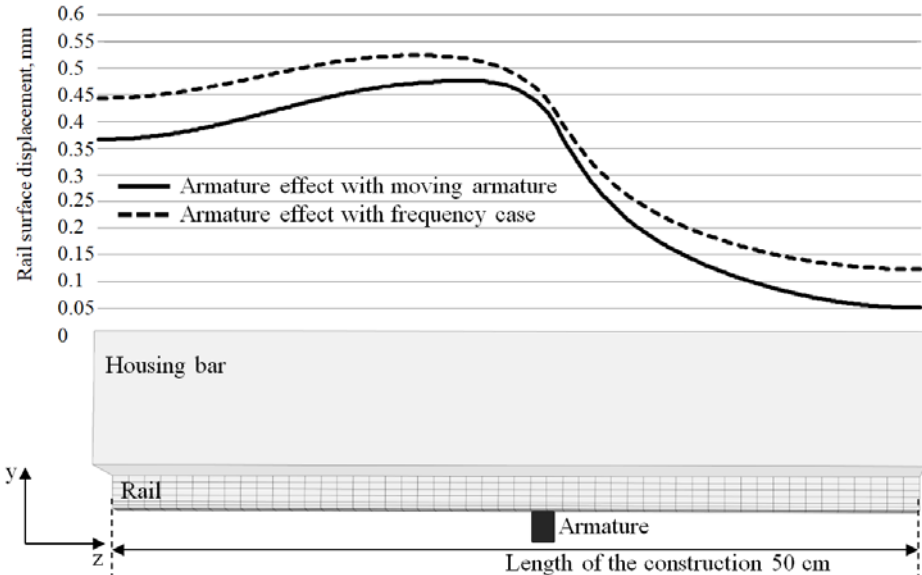


**Fig. 4.5.** Rail surface displacements for two different types of electromagnetic calculating modes: moving armature model and frequency approximation model

The results of the electromagnetic calculations were again used as a load for mechanical calculations. As in the previous figure, the displacement of the rail surfaces was calculated for the high-frequency case and the volume load case. As it was expected from result presented in Fig. 3.7, an influence of the armature can be stated for both numerical cases. Both cases converge at the position of the armature. The amplitude changes in comparison to the case without armature (see Fig. 4.4) are about 0.1 mm and therefore in the same range as in Fig. 4.5. Again,

referring to earlier investigations (Schneider and Schneider 2007) the point out that at the position of the armature one should try to be as precise as possible because it is precisely there where rail displacements may influence the sliding electrical contact.

The most of the publications did not take the armature effect into account for mechanical construction behaviour investigation. The calculations with added armature effect show that the EM forces near the armature make sense for the mechanical model. The distance between rails is influenced. In both cases, the difference between displacement near the armature and far away from armature exists. It could influence mechanical construction stability because additionally bending effect appears in the rail.

Continuing the armature effect the different force distributions in EM model also influence the mechanical construction. In Fig. 4.6 the rail surface displacements according different shape of armatures are presented.

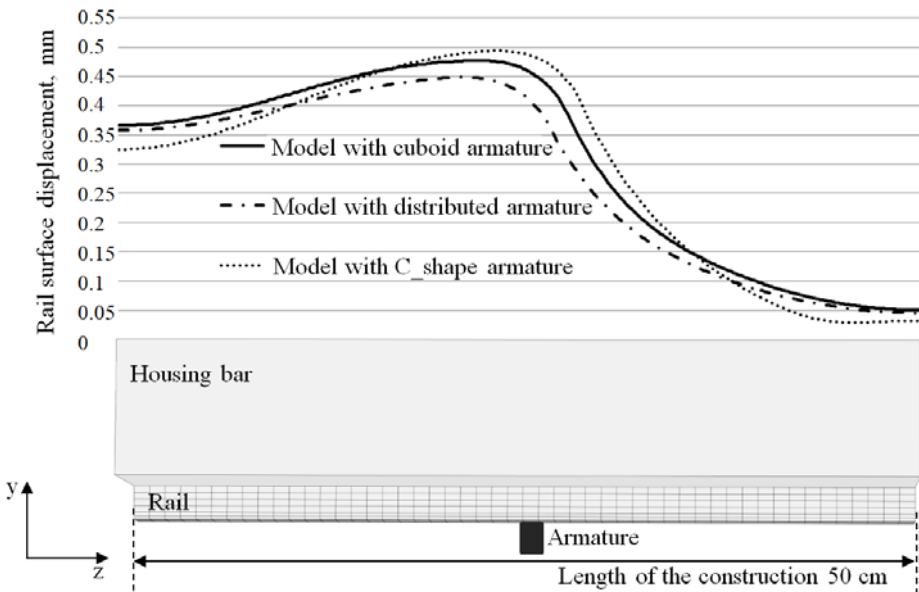


Fig. 4.6. The rail surface displacement of three different types of armatures

Figure 4.6 illustrate that, the Lorentz forces from rail armature model, rail distributed armature model and rail C-shape armature model (Table 3.1) are different not only for EM models but also for mechanical construction behaviour. The integration of force over the rail volume was done, and the results were used for a mechanical model with three different load force maps: force distribution

over the rail volume of 3 different armature shapes. The biggest influence for armature can be seen C-shape. It is because the rail influenced not only from EM force which is due to Lorentz force inside the rail but also from the C-shape armature (Zielinski *et al.* 2003; Li *et al.* 2013). This shape of armature has proper contact parameters because it repels the rails by itself. The lowest impact to the rail form armature was obtained with the distributed armature. This can be due to distributed Lorentz force distribution in the armature region. The current flow does not have a high concentration at each point. The effect of armature propulsion was not taken into account.

#### 4.6. Constructing Bolts Effect on a Mechanical Model

During the EM calculations, not only armature effect but also the influence of construction bolts were investigated. The Lorentz force distribution was used for mechanical model calculations.

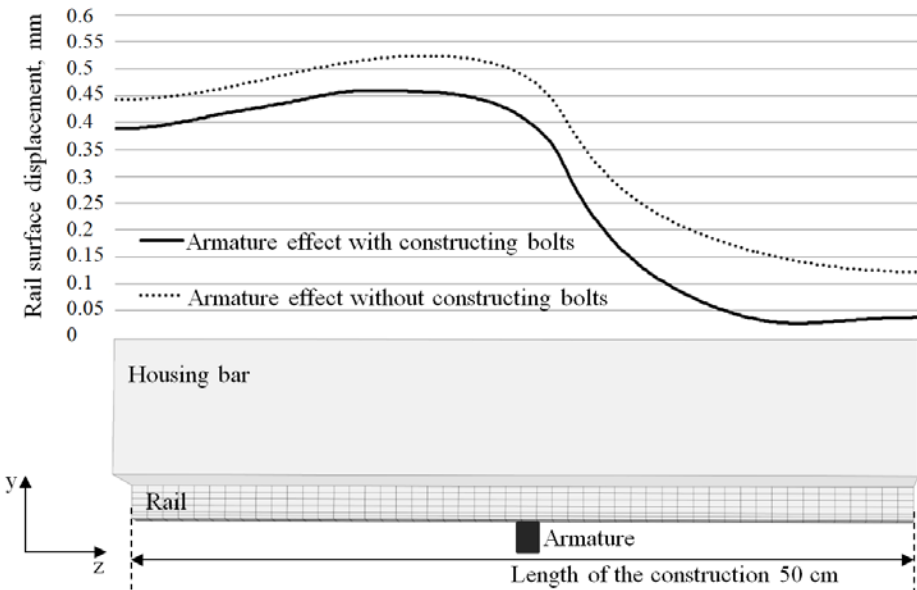
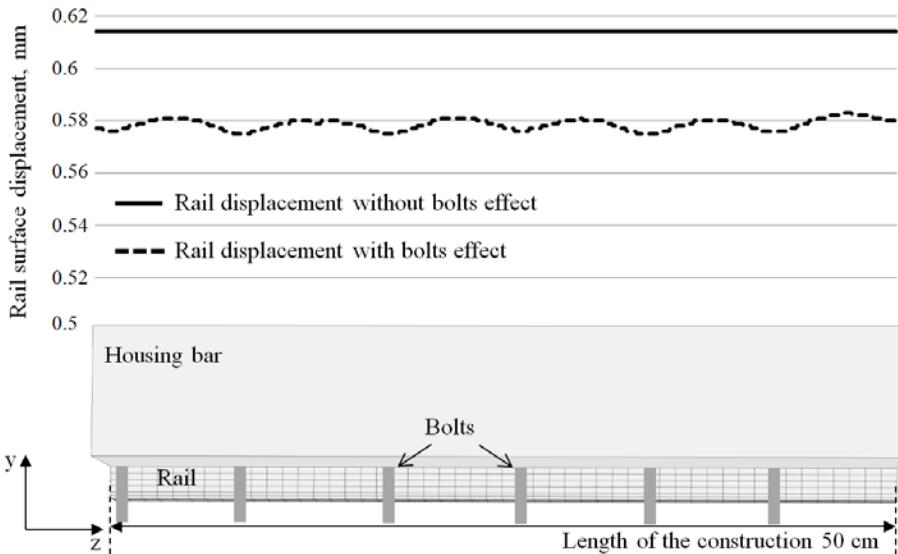


Fig. 4.7. The rail displacement with taken accounts the bolt and armature effects

The Fig. 4.7 shows two curves. Solid curve presents the rail surface displacement with the model when armature and construction bolts are taken into account. The dashed curve presents the rail surface behaviour during the operation when

the construction bolts are not taken into account. The difference between the calculation models is approximately 11%. The predictions of EM model were done on moving armature calculation model.

While this is, in general, a non-negligible effect, the context requires to examine the influence of the non-homogenous force distribution on the displacement of the rail surfaces. In Fig. 4.8 the results of static mechanical calculations are assuming the force distribution from Fig. 3.9 (5000 Hz) is shown. Results are presented at the rail edge in the x-direction. At first, we note that the 7% difference in  $F_y$  translates into a 7% difference in displacement as has to be expected if Hook's law applies.



**Fig. 4.8.** The displacement of rail surface using models with construction bolts and without construction bolts at 5000 Hz

The absolute difference in displacements at a current amplitude of 620 kA is only 0.4 mm which is acceptable for most armature types. The rippled structure is being presented in Fig. 4.8 could, however, lead to resonances which are not investigated in this work.

### 4.7. The Mechanical Models of Dynamic Behaviour

The next mathematical model describes the dynamic behaviour of FEM behaviour of the railgun structure under the influence of the expanding pressure load moving

along the rails. The dynamical behaviour of the rail is modelled using Eq. (1.7). In the approach taken here, damping phenomena is not considered.

It is evident that the vector of external time-dependent EM load in Eq (2.2) depends not only on the pressure value but also on the armature position on the rail. To fix the position of the load, the rail was divided into 20 segments (see Fig. 4.9). Therefore, the discrete model encompasses the discretization of the pressure load moving according to recalculated pressure profile, as shown in Fig. 2.7. This concept of a computational model can capture the temporal variation of the pressure along the rail.

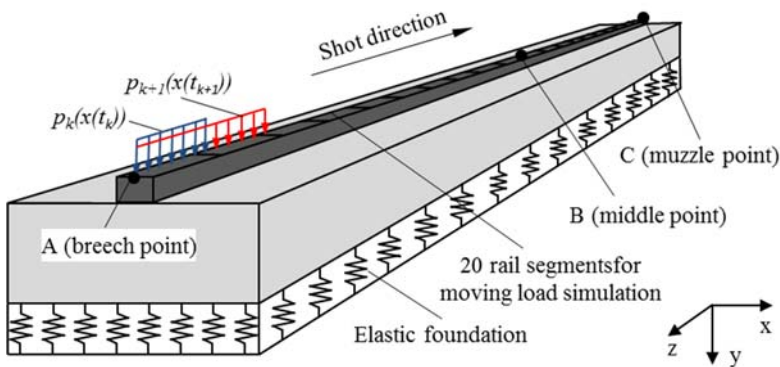


**Fig. 4.9.** RAFIRA 3-D model simplification for numerical calculations

Each segment was loaded by surface pressure according to the time calculated from armature position on the rail. Each segment behind the modelled armature position has the same surface pressure as the segment where the armature is. Only rail segments in front of the armature are without surface pressure. The mechanical model was used for experimental measured EM launcher operation with two shoots. For modelling two identical shoots was used.

## 4.8. Investigation of Two Shoots

The dynamic transient analysis was performed to illustrate the EM launcher behaviour during multishot loading. Two different multishot scenarios were considered, and two sets of different loading histories were generated for simulation purposes. Each of these scenarios comprises two shot periods where each of the periods consists of loading and loading-free, or post loading, intervals TL and TF.



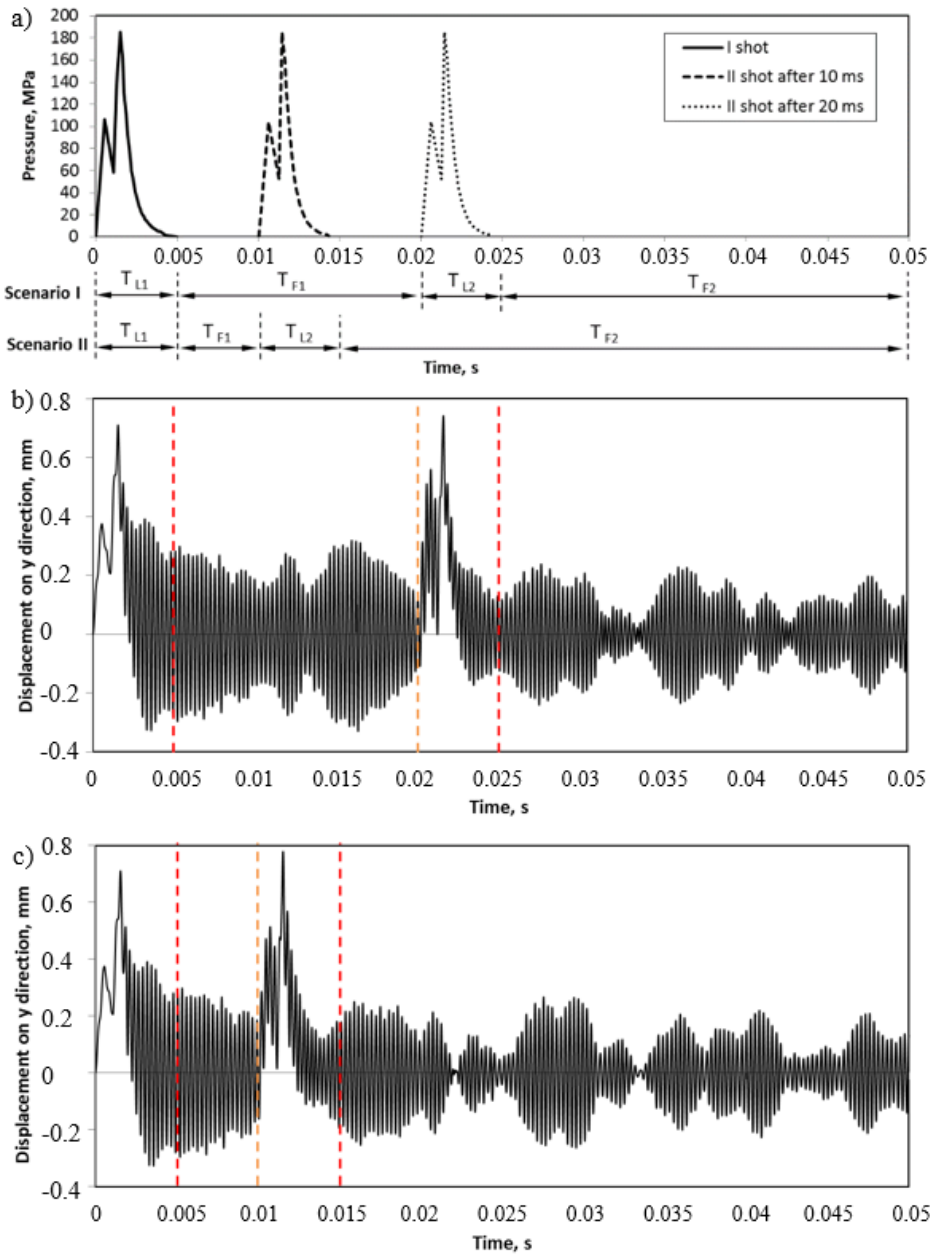


**Fig. 4.10.** Time history graph of the rail breech point: a) pressure load; b) the displacements responding to first scenario; c) the displacements responding to second scenario

The duration of a loading interval is predefined by the duration of the electromagnetic load,  $TL1 \approx 4.5$  ms, which is characterized by the pressure profile obtained experimentally and described in previous chapter (see Fig. 2.7). The loading duration also indicates the residence time of the projectile in the launcher.

The loading-free time interval between the first and the second shots is denoted by TF1, while TF2 indicates the post loading time interval after the second shot. In summary, the loading scenario I combine two shot intervals TL1 with freely chosen post loading intervals  $TF1 = 15$  ms and  $TF2 = 25$  ms, while the scenario II is characterized by post loading intervals  $TF1 = 5$  ms and  $TF2 = 35$  ms. Specified loading histories are shown in Fig. 4.10a.

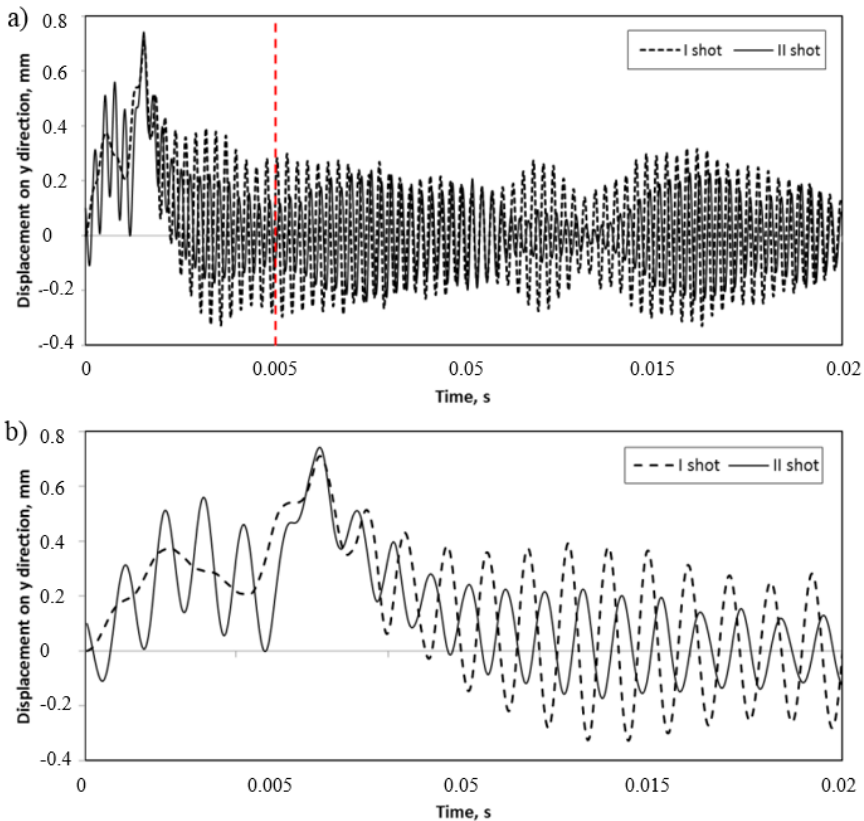


**Fig. 4.11.** The rail breech point displacement comparison of the I shot (curve 1) and the II shot (curve 2) for the scenario I – time histories on: a) full-time history; b) time history under load

Both scenarios simulation intervals were limited to 0.005 s. The deformation behaviour of the railgun under the action of the magnetic pressure is illustrated

regarding the displacement histories for the selected point in the central line of the loaded surface of the rail (see Fig. 4.10b, c). The vertical dashed lines represent the boundaries between the loading periods.

Note that both negative and positive displacements of the rail could have a negative influence on the sliding contact performance. The latter requires a sufficiently large contact surface, which can only be realized using enormous contact pressures. Depending on the armature technology, positive displacements can lead to contact transition due to reduced contact pressure (Schneider *et al.* 2009).

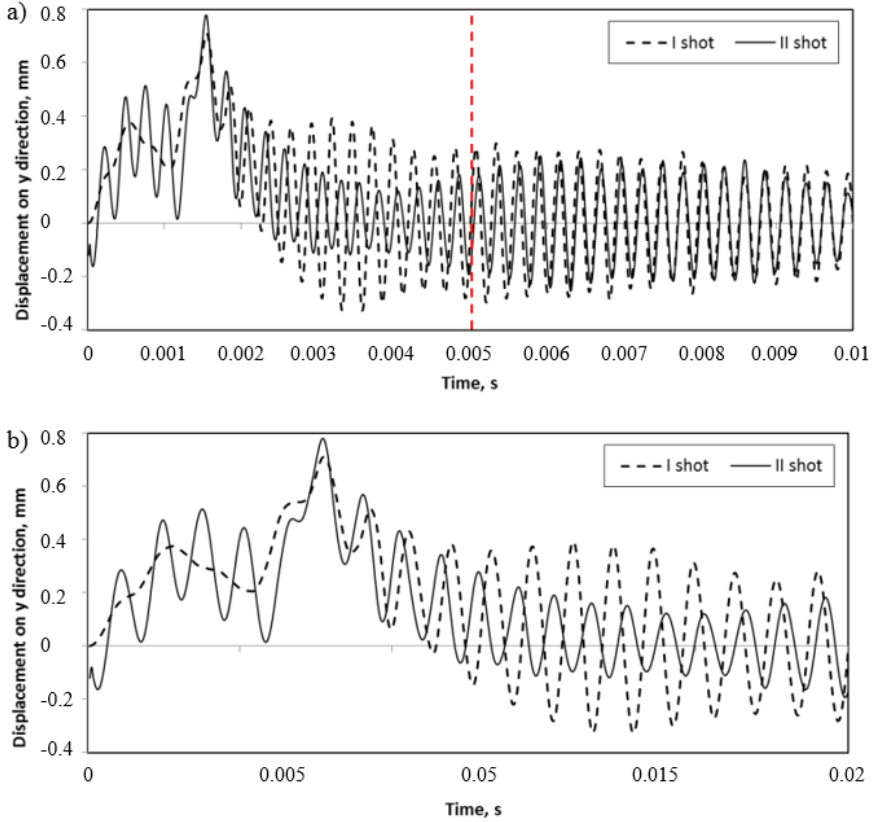


**Fig. 4.12.** The rail breech point displacement comparison of the first shot (curve 1) and the second shot (curve 2) for the scenario II – time histories on:  
 a) full-time history, b) time history under load

In the case of scenario II, the structure showed qualitatively the same response as it was observed in scenario I-the highest values of displacement take place at the breech point. Therefore, only these displacements are shown for illustration in Fig. 4.10c.

It is obvious that the highest values of displacement occur at the input zone which is limited by 0.3 m. Therefore, the limit of the displacement analysis was at the first point. The results obtained for the first scenario loading are presented in Fig. 4.11. To compare the behaviour of rail vibrations during the first and the second shot, both shots were set to the same reference time  $t_0$  indicating the start time instant. In our case, the start point of second shot  $t_{02}$  is shifted to zero. The full-time histories are presented in Fig. 4.11a while the fragment of time history in the vicinity of input point is presented in Fig. 4.11b. The results of the second scenario are presented in Fig 4.12 keeping the same style.

The second shot begins with the action of vibrations remaining from the first shot. Note that the initial vibration amplitude is larger for the triggering period. The general impression is that the vibration amplitudes during the second shot are smaller in comparison to the first shot. We assume that vibration during and after the first shot is damped by the vibration of the second shot. Therefore, the possibility to control the interval between consecutive shots could be used to influence vibrations after launch.

To understand the differences between first and second shots, the time history analysis was performed. Comparisons of the structures behaviour of first and second shots are presented in Fig. 4.11 for the scenario I and in Fig. 4.12 of scenario II.

## 4.9. The Local Effect on the Dynamic Model

As mentioned in the introduction, the most critical positions to be considered are that of the projectile or more precisely that of the armature. Note that both negative and positive displacements can have negative influence on the projectile performance. While this is clear for the negative displacements (e.g. momentum transfer) the case of positive displacements is characteristic for railguns using solid armatures.

Here, the sliding electric contact requires a sufficiently large contact surface which can only be realized using enormous contact pressures. Depending on the armature technology positive displacements can lead to contact transition due to reduced contact pressure.

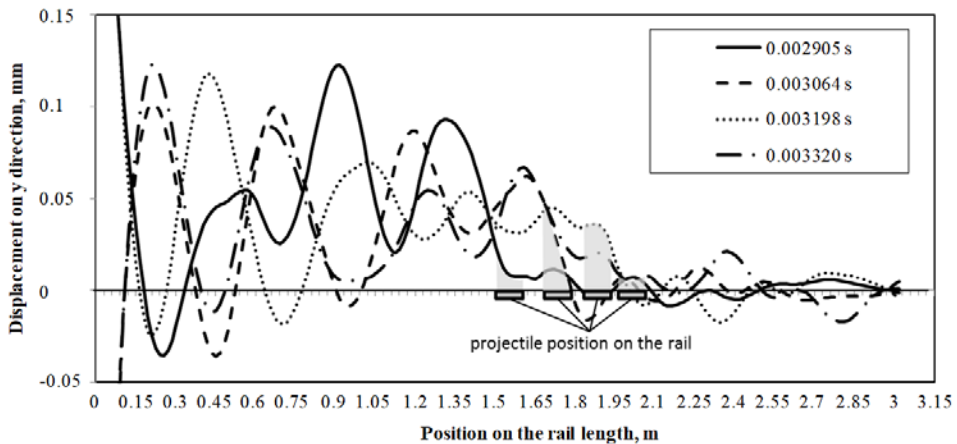


**Fig. 4.13.** The rail deformation according to the projectile position on the rail

In Fig. 4.13 the displacement profile at the position of the projectile is presented. It can be seen that the 3D results obtained for RAFIRA confirm former conclusions: dynamic displacements are observed at the position of the armatures. While they are acceptable for the current amplitudes investigated here it is safe to say that they have to be taken into account for high-speed experiments ( $>2$  km/s).

## 4.10. Conclusions of Chapter 4

1. The different load types were investigated. The mechanical load calculated from EM model and loaded overall EM launcher volume have a lower impact for EM launcher rail surface displacement than the mechanical load loaded over the rail surface. The difference is 0.1 mm. This amount of the gap has a negative impact on electrical contact.
2. The mechanical deformation rail surface has differences also the calculating type when using armature moving type and frequency approximation type. The armature moving model with armature effect on the case has lower impact for EM launcher rail surface displacement than frequency approximation model. The differences are 16% far away from the armature, and 7.7% is the maximum armature effect in the armature area.
3. The C-shape has biggest influence on armature because the rail is influenced not only from EM force which is due to Lorentz force inside the rail but also from the C-shape armature. The C-shape armature deflects the rail surface 4.2% more than cuboid armature and 11% more than distributed armature.

4. The bolts effect was taken into account in EM modelling case. However, also the bolts have influence onto the mechanical model. The rail displacement, not uniform, the sinusoidal waved the surface is obtained. The rail displacement in the calculating case with construction bolts is 4.9% lower than with calculating model, where the construction bolts are not taken into account.
5. The influence of residual oscillations of the first shot on the mechanical response obtained for the second shot was either amplifying or damping. Before the maximum pressure amplitude of the second shot, the displacement amplitudes are increased concerning the first shot. In contrast, after the pressure maximum the residual oscillations tend to damp the displacement amplitudes.

---

## General Conclusions

1. An overview of the results of the open-bore EM launcher researchers has shown that the experimental methods for determining the EM force induced by a magnetic field predominate when calculating the mechanical state of a structure. For determining the mechanical forces, the electro-magneto-mechanical models coupling has not been applied to the open-bore EM launchers. Absolute computational results for this kind of EM launchers were not investigated.
2. To assess the accuracy of the model electromagnetic launchers inductance parameter was used while calculating in different methods and, after performing experimental measurements. This showed a sufficient three-dimensional quality of electromagnetic and mechanical finite element models using two-rail open type RAFIRA EM launcher. The evaluation was carried out using a magnetic energy estimation method.
3. The local effects of armature and constructing bolts on the generation of electromagnetic force on the surface of the structure were investigated. The results indicate that the magnetic force density of the projectile increases 2.5 times in the armature area locally. The evaluation of structural bolts shows that the effect of magnetic forces on structural bolts is reduced by 17.5%. The findings suggest that coupled calculations are to be preferred locally.

4. High-power linear accelerators of the railgun-type require the careful electromechanical design of their components because of the high magnetic forces acting on current-carrying conductors during launch. The forces acting on the rails interfere the projectile and rail connection for proper operation. It has been calculated that the force in the volume of the electromagnetic launcher and the rail surface is distributed unevenly: in the transverse direction, the maximum force is at the edges of the rail, while in the longitudinal direction the maximum force lies between the construction screws.
5. The forces acting on a EM launcher structure can lead to oversimplifications. Calculations show the difference between considering magnetic pressure working on the rail surfaces only and accurate calculations of the volume forces. The EM effect in the rail volume causes an additional deformation of the rail surface, which varies according to the symmetry plane. The calculating simplification can lead to differences in rail surface separation of about 0.1 mm. For brush armatures, such differences may decrease the sliding contact performance.
6. A local electromagnetic launcher investigation reveals that the structural shape of the electromagnetic launcher armature does not only lead to a different localization of EM forces but also affects the behaviour of the electromagnetic launcher mechanical construction. The results show a slight variation in the displacement of the rail surface of the EM launcher using different mechanical shapes of the armature. The least mechanical deformation on the rail surface was obtained using a distributed armature. The deformation of the rail surface in the case of a distributed projectile is 10% less than the displacement of the rail surface when performing the launching process using a C-shaped armature.
7. Performed transient analysis of the 3D FE model describes the structural behaviour of the RAFIRA railgun operated in multishot mode. Two shot sequences, which are characterized by using residual oscillations after the first shot as preloading history for the second shot, were analysed.
8. The influence of residual oscillations of the first shot on the mechanical response obtained for the second shot was either amplifying or damping. Before the maximum pressure amplitude of the second shot, the displacement amplitudes are increased concerning the first shot. In contrast, after the pressure maximum, the residual oscillations tend to damp the displacement amplitudes.



---

## References

- Abdo, M. T., Elrefai, A. L., Adly, A. A. and Mahgoub, O. A. 2017. Performance analysis of coil-gun electromagnetic launcher using a finite element coupled model. *2016 18th International Middle-East Power Systems Conference, MEPCON 2016 – Proceedings*: 506–511.
- An, S., Lee, B., Bae, Y., Lee, Y. and Kim, S. 2017. Numerical Analysis of the Transient Inductance Gradient of Electromagnetic Launcher Using 2-D and 3-D Finite-Element Methods. *IEEE Transactions on Plasma Science*, 45(7): 1635–1638.
- Bayati, M. S. and Keshtkar, A. 2015. Novel Study of the Rail's Geometry in the Electromagnetic Launcher. *IEEE Transactions on Plasma Science*, 43(5): 1652–1656.
- Bengui, Z., Yanjie, C., Jie, W., Huijin, W. and Xuehui, C. 2011. Magnetic-structural coupling analysis of armature in induction coilgun. *IEEE Transactions on Plasma Science*, 39(1): 65–70.
- Beno, J. H. 1991. Three-Dimensional Rail-Current Distribution Near The Armature Of Simple, Square-Bore, Two-Rail Railguns. *IEEE Transactions on Magnetics*, 27(1): 106–111.
- Besbes, M., Ren, Z. and Razeq, A. 1996. Finite element analysis of magneto-mechanical coupled phenomena in magnetostrictive materials. *IEEE Transactions on Magnetics*, 32(3): 1058–1061.
- Biró, O., Koczka, G. and Preis, K. 2014. Finite element solution of nonlinear eddy current problems with periodic excitation and its industrial applications. *Applied numerical mathematics: transactions of IMACS*, 79: 3–17.

- Biró, O. and Preis, K. 1989. On the use of the magnetic vector potential in the finite-element analysis of three-dimensional eddy currents. *IEEE Transactions on Magnetics*, 25(4): 3145–3159.
- Bourell, D. L. and Persad, C. 1999. Simulation of railgun gouging. *IEEE Transactions on Magnetics*, 35(1): 214–216.
- Che, Y., Yuan, W., Xu, W., Cheng, W., Zhao, Y. and Yan, P. 2017. The Influence of Different Constraints and Pretightening Force on Vibration and Stiffness in Railgun. *IEEE Transactions on Magnetics*, 45(7): 1154–1160.
- Daneshjoo, K., Rahimzadeh, M., Ahmadi, R. and Ghassemi, M. 2007. Dynamic response and armature critical velocity studies in an electromagnetic railgun. *IEEE Transactions on Magnetics*, 43(1): 126–131.
- Domin, J. 2016. Hybrid electromagnetic launcher with pneumatic assist – influence of coil - gun “switch on” and “switch off” time upon missile velocity . *Selected Issues of Electrical Engineering and Electronics (WZEE), 2016 13<sup>th</sup>*: 0–3.
- Engel, T. G. 2017. Scientific Classification Method for Electromagnetic Launchers. *IEEE Transactions on Plasma Science*, 45(7): 1333–1338.
- Engel, T. G., Neri, J. M. and Veracka, M. J. 2008. Characterization of the velocity skin effect in the surface layer of a railgun sliding contact. *IEEE Transactions on Magnetics*, 44(7): 1837–1844.
- Fahrenthold, E. P., Price, J. H. and Peterson, D.R. 1989. Structural design of cylindrical railguns. *IEEE Transactions on Magnetics*, 25(1): 180–185.
- Feng, D., He, J., Xia, S., Chen, L. and Tang, L. 2015. Investigations of the Armature – Rail Contact Pressure Distribution in a Railgun. *IEEE Transactions on Plasma Science*, 43(5): 1657–1662.
- Galanin, M. P., Khalimullin, Y. A., Lototsky, A. P., Milyayev, K. K. 2003. 3-D Modeling of Electromagnetic Fields in Application To Electromagnetic Launchers. *IEEE Transactions on Magnetics*, 39(1): 134–138.
- Gavrilov, A. V. 2003. Use Of The Lorentz Transformations In Noninertial Reference Frames. *Russian Physics Journal*, 46(1): 29–32.
- Gildutis, P., Kačianauskas, R., Schneider, M., Stupak, E. and Stonkus, R. 2012. Deformation Analysis of Railgun Cross –Section. *Mechanika*, 18(3): 259–265.
- Gros, L., Reyne, G., Body, C. and Meunier, G. 1998. Strong Ccoupling Magneto Mechanical Methods Applied to Model Heavy agnetostrictive Actuators. *IEEE Transactions on Magnetics*, 34(5): 3150–3153.
- Hasirci, U., Balikci, A., Zabar, Z. and Birenbaum, L. 2015. 3D FEM Analysis of a Novel Magnetic Levitation System. *IEEE Transactions on Plasma Science*, 43(5): 1261–1265.
- Hively, L. M. and Condit, W. C. 1991. Electromechanical railgun model. *IEEE Transactions on Magnetics*, 27(4): 3731–3734.

- Hsieh, K. T. 2007. Hybrid FE / BE Implementation on Electromechanical. *IEEE Transactions on Magnetics*, 43(3): 1131–1133.
- Hsieh, K. T. 1995. A Lagrangian Formulation for Mechanically, Thermally Coupled Electromagnetic Diffusive Processes with Moving Conductors. *IEEE Transactions on Magnetics*, 31(1): 604–609.
- Hundertmark, S., Schneider, M. and Vincent, G. 2013. Payload Acceleration Using a 10-MJ DES Railgun. *IEEE Transactions on Plasma Science*, 41(5): 1455–1459.
- Jarnieux, M., Reyne, G. and Meunier, G. 1994. FEM Modelling of the Magnetic, Thermal, Electrical and Mechanical Transient Phenomena in Linear Induction Launchers. *IEEE Transactions on Magnetics*, 30(5): 3312–3315.
- Johnson, A.J. and Moon, F.C. 2006. Elastic waves and solid armature contact pressure in electromagnetic launchers. *IEEE Transactions on Magnetics*, 42(3): 422–429.
- Johnson, A.J. and Moon, F.C. 2007. Elastic waves in electromagnetic launchers. *IEEE Transactions on Magnetics*, 43(1): 141–144.
- Kahya, V. and Turan, M. 2018. Vibration and stability analysis of functionally graded sandwich beams by a multi-layer finite element. *Composites Part B: Engineering*, 146(1): 198–212.
- Keshtkar, A. 2005. Effect of rail dimension on current distribution and inductance gradient. *IEEE Transactions on Magnetics*, 41(1):383–386.
- Keshtkar, A., Bayati, S. and Keshtkar, A. 2008. Effect of rail's material on railgun inductance gradient and losses. *2008 14th Symposium on Electromagnetic Launch Technology, EML, Proceedings*: 130–133.
- Knoepfel, H.E. 2000. *Magnetic Fields*, John Wiley & Sons, Inc.
- Koczka, G., Außerhofer, S., Bíró, O. and Preis, K. 2009. Optimal fixed-point method for solving 3D nonlinear periodic eddy current problems. *COMPEL—The international journal for computation and mathematics in electrical and electronic engineering*, 28(4): 1059–1067.
- Kolm, H. Mongeau, P. and Williams, F. 2017. Electromagnetic launchers. (1980). *IEEE Transactions on Magnetics*, M(1980): 719–725.
- Lee, Y., Kim, S., An, S., Bae, Y., and Lee, B. 2017. Dynamic Response of an Electromagnetic Launcher Accelerating a C-Shaped Armature. *IEEE Transactions on Plasma Science*, 45(7): 1639–1643.
- Leferink, F. B. J. 1995. Inductance calculations; methods and equations. *Electromagnetic Compatibility, 1995. Symposium Record., 1995 IEEE International Symposium on*, (1938): 16–22.
- Li, M., Wang, G., Wang, L., Pan, R., Sun, D. and Yan, P. 2013. Numerical simulation and experiment on the sliding electrical contact of the solid armature and rails interface. *IEEE Transactions on Plasma Science*, 41(12): 3645–3650.

- Liebfried, O., Brommer, V., Scharnholz, S. and Spahn, E. 2013a. Refurbishment of a 30-MJ-Pulsed Power Supply for Pulsed Power Applications. *IEEE Transactions on Plasma Science*, 41(5): 1285–1289.
- Liebfried, O. 2011. *The Investigation of Electromagnetic Processes in Electromagnetic Launchers Using Colossal*, Doctoral dissertation.
- Liebfried, O., Schneider, M., Stankevic, T., Balevicius, S. and Zurauskiene, N. 2013b. Velocity-induced current profiles inside the rails of an electric launcher. *IEEE Transactions on Plasma Science*, 41(5): 1520–1525.
- Liebfried, O., Schneider, M. and Balevicius, S. 2011. Current distribution and contact mechanisms in static railgun experiments with brush armatures. *IEEE Transactions on Plasma Science*, 39(1): 431–436.
- Logan, D. L., Veitch, E., Carson, C., Burrell, K. R., Gould, V. and Wagner, E. 2007. *A First Course in the Finite Element Method Fourth Edition*. 147(4): 1-836.
- Marshall, R. A. and Ying, W. 2004. *Railguns: their science and technology*, China Machine Press.
- McNab, I. R. 2013. Reduce Space Launch Costs. *IEEE Transactions on Plasma Science*, 41(5), pp.1047–1054.
- McNab, I. R., Stefani, F., Crawford, M., Erengil, M., Persad, C., Satapathy, S., Vanicek, H., Watt, T. and Dampier, C. 2005. Development of a naval railgun. *IEEE Transactions on Magnetics*, 41(1): 206–210.
- McNab, I. R., 1999. Early electric gun research. *IEEE Transactions on Magnetics*, 35(1): 250–261.
- McNab, I. R., Crawford, M. T., Satapathy, S. S., Stefani, F. and Watt, T. J. 2011. IAT armature development. *IEEE Transactions on Plasma Science*, 39(1): 442–451.
- McNab, I. R. 2009. Progress on hypervelocity railgun research for launch to space. *IEEE Transactions on Magnetics*, 45(1): 381–388.
- McNab, I. R. 2015. Pulsed power options for large em launchers. *IEEE Transactions on Plasma Science*, 43(5): 1352–1357.
- McNab, I. R. and Beach, F. C. 2007. Naval railguns. *IEEE Transactions on Magnetics*, 43(1): 463–468.
- Metwally, I. 2013. Coaxial-cable wound rogowski coils for measuring large-magnitude short-duration current pulses. *IEEE Transactions on Instrumentation and Measurement*, 62(1): 119-128.
- Murugan, R. and Udayakumar, K. 2005. Effect of Rail Dimensions on Rail Gun Design Parameters. *IEEE Indicon 2005 Conference*, (9): 1–4.
- Musulino, A. 2001. Electromagnetic analysis in devices with sliding contacts. *COMPEL: The International Journal for Computation and Mathematics in Electrical and Electronic Engineering*, 20(2): 463–472.

- Musulino, A. and Rizzo, R. 2011. Numerical analysis of brush commutation in helical coil electromagnetic launchers. *IET Science, Measurement & Technology*, 5(4): 147–154.
- Newill, J. F., Powell, J. D. and Zielinski, A. E. 2003. Coupled finite-element codes for armature design. *IEEE Transactions on Magnetics*, 39(1): 148–152.
- Özakın, M. B. and Aksoy, S. 2016. Application of Magneto–Quasi-Static Approximation in the Finite Difference Time Domain Method. *IEEE Transactions on Magnetics*, 52(8): 7209809.
- Parker, J. 1998. Experiments to Measure Armature Wear Part 1: Wear Measurements on the KJ202 Armature. Doctoral dissertation: 1–90.
- Perotoni, M. B., Mergl, M. and Bernardes, V. A. 2017. Coilgun Velocity Optimization With Current Switch Circuit. *IEEE Transactions on Plasma Science*, 45(6): 1015–1019.
- Peterson, D. R. 1993. Magnetic design for structural stiffness: The tailored railgun. *IEEE Transactions on Magnetics*, 29(1): 1201–1206.
- Pitman, R. K., Ellis, R. L. and Bernardes, J. S. 2004. Iterative transient model for railgun electromechanical performance optimization. *2004 12th Symposium on Electromagnetic Launch Technology*: 96–99.
- Ren, Z., Ionescu, B., Besbes, M., Razek, A. 1995. Calculation of Mechanical Deformation of Magnetic Materials in Electromagnetic Devices. *IEEE Transactions on Magnetics*, 31(3): 1873–1876.
- Roch, M., Hundertmark, S., Löffler, M., Zacharias, P. 2014. First Experiment With the Modular Augmented Staged Electromagnetic Launcher. *IEEE Transactions on Plasma Science*, 42(10): 3239–3244.
- Rodger, D. and Lai, H. C. 2001. A comparison of formulations for 3D finite element modeling of nelectromagnetic launchers. *IEEE Transactions on Magnetics*, 37(1): 135–138.
- Rodger, D. and Leonard, P.J. 1993. Modelling the Electromagnetic Performance of Moving Rail Gun Launchers Using Finite Elements. *IEEE Transactions on Magnetics*, 29(1): 496–498.
- Schneider, M., Eckenfels, D. and Hatterer, F. 2003. Transition in brush armatures. *IEEE Transactions on Magnetics*, 39(1): 76–81.
- Schneider, M. and Schneider, R. 2007. Advanced Rail-Sabot Configurations for Brush Armatures. *IEEE Transactions on Magnetics*, 43(1): 186–189.
- Schneider, M., Woetzel, M. and Wenning, W. 2009. The ISL rapid fire railgun project RAFIRA - Part II: First results. *IEEE Transactions on Magnetics*, 45(1): 448–452.
- Schuppler, C., Tumonis, L., Kačianauskas, R., Schneider, M. 2013a. Experimental and numerical investigations of vibrations at a railgun with discrete supports. *IEEE Transactions on Plasma Science*, 41(5): 1508–1513.

Schuppler, C., Alouahabi, F. and Schneider, M. 2013b. Electromechanical aspects of reliable loading procedures for multishot railguns. *IEEE Transactions on Plasma Science*, 41(5): 1387–1391.

Siaenen, T., Schneider, M. and Hogan, J. 2015. Block diagram model for the simulation of an electromagnetic rail accelerator system. *IEEE Transactions on Plasma Science*, 43(5): 1580–1584.

Stankevic, T., Schneider, M. and Balevičius, S. 2013. Magnetic diffusion inside the rails of an electromagnetic launcher: Experimental and numerical studies. *IEEE Transactions on Plasma Science*, 41(10): 2790–2795.

Stefani, F. and Parker, J.V. 1999. Experiments to measure gouging threshold velocity for various metals against copper. *IEEE Transactions on Magnetics*, 35(1): 312–316.

Tan, S. Lu, J., Li, B., Zhang, Y., Jiang, Y. 2017. A New Finite-Element Method to Deal With Motion Problem of Electromagnetic Rail Launcher. *IEEE Transactions on Plasma Science*, 45(7): 1374–1379.

Thomas, A. M. 2014. National security research in plasma physics and pulsed power: Past, present, and future. *IEEE Transactions on Plasma Science*, 42(5): 1088–1117.

Tompkins, M. W., Anderson, M. A., Kim, K., Feng, Q., Zhang, J., King, T. L. 1995. Development of advanced compact railguns for injection of hypervelocity hydrogen pellets into magnetic fusion plasmas. *SOFE '95. "Seeking a New Energy Era". 16th IEEE/NPSS Symposium Fusion Engineering*, 2: 1582–1585 vol.2.

Tumonis, L. Schneider, M., Kačianauskas, R., Vadluga, V. 2011. The structural mechanics of rail guns with discrete supports showing the influence of des. *IEEE Transactions on Plasma Science*, 39(1): 144–148.

Tzeng, J. T. 2005. Structural mechanics for electromagnetic railguns. *IEEE Transactions on Magnetics*, 41(1): 246–250.

Tzeng, J. T. and Schmidt, E. M. 2011. Comparison of electromagnetic and conventional launchers based on mauser 30-mm MK 30-2 barrels. *IEEE Transactions on Plasma Science*, 39(1): 149–152.

Upshaw, J. L. and Kajs, J. 1991. Micrometeoroid Impact Simulations Using A Railgun Electromagnetic Accelerator. *IEEE Transactions on Magnetics*, 27(1): 607–610.

Vincent, G. and Hundertmark, S. 2012. Using the hexagonal segmented railgun in multishot mode with 3 projectiles. *Electromagnetic Launch Technology (EML), 2012 16th International Symposium*: 1–4.

Wagg, D. and Neild, S. 2010. *Nonlinear Vibration with Control: For Flexible and Adaptive Structures*. Springer.

Wey, J., Spahn, E. and Lichtenberger, M. 1997. Railgun Modeling with the P-Spice Code. *IEEE Transactions on Magnetics*, 33(1): 619–624.

Wikipedia, 2017. No Title. *Rogowski coil*. Available at: [https://en.wikipedia.org/wiki/Rogowski\\_coil](https://en.wikipedia.org/wiki/Rogowski_coil).

- Wild, B., Alouahabi, F., Simicic, D., Schneider, M., Hoffman, R. 2017. A Comparison of C-Shaped and Brush Armature Performance. *IEEE Transactions on Plasma Science*, 45(7): 1227–1233.
- Wild, B., Schuppler, C., Alouahabi, F., Schneider, M., Hoffman, R. 2015. The Influence of the Rail Material on the Multishot Performance of the Rapid Fire Railgun. *IEEE Transactions on Plasma Science*, 43(6): 2095–2099.
- Xu, L. & Geng, Y. 2012. Forces of rails for electromagnetic railguns. *International Journal of Applied Electromagnetics and Mechanics*, 38(4): 47–64.
- Xue, X. Shu, T., Yang, Z., Feng, G. 2017. A New Electromagnetic Launcher by Sextupole Rails: Electromagnetic Propulsion and Shielding Numerical Validation. *IEEE Transactions on Plasma Science*, 45(9): 2541–2545.
- Yang, F., Zhao, Z., Liu, Y., Wu, Y., Chen, Z., Sun, H., and Rong, M. 2016. Electromagnetic-Mechanical Characteristics Study of a High-Speed Electromagnetic Launcher. *IEEE Transactions on Plasma Science*, 44(10): 2218–2225.
- Yang, L., Nie, J., Liu, R., Jiao, Q. and Li, J. 2017. Simulation Study on Mechanical Response of Cambered Surface Armature and Rail Under Electromagnetic and Thermal Loads. *IEEE Transactions on Plasma Science*, 45(7): 1579–1584.
- Zielinski, A. E., Newill, J. F. and Powell, J. D., 2003. Experiments to Assess Structural Loads During Solid Armature Contact Transition. *IEEE Transactions on Magnetics*, 39(1): 92–96.
- Zienkiewicz, O. 1977. Three-dimensional magnetic field determination using a scalar potential—A finite element solution. *IEEE Transactions on Magnetics*, MAG-13(5): 1649–1656.





---

# List of Scientific Publications by the Author on the Topic of the Dissertation

## Papers in the Reviewed Scientific Journals

Schneider, M., Račkauskas, J., Loffler, M. J. 2013. Electromechanical Modeling of Components of a Linear Electromagnetic Accelerator. *IEEE Transactions On Plasma Science*, 41(10): 2796–2799. DOI: 10.1109/TPS.2013.2255626 (Clarivate Analytics Web of Science).

Stonkus, R., Račkauskas, J., Schneider, M., Kačianauskas, R. 2015. Structural mechanics of railguns with open barrels and elastic supports: the influence of multishot operation. *IEEE Transactions On Plasma Science*, 43(5): 1510–1515. DOI: 10.1109/TPS.2014.2387791 (Clarivate Analytics Web of Science).

Račkauskas, J., Kačianauskas, R., Schneider, M. 2018. Investigation of armature-rail interaction in linear electromagnetic launcher. *Journal of Vibroengineering*, 20(2): 1234–1239 (Clarivate Analytics Web of Science).

Račkauskas, J., Schneider, M., Kačianauskas, R. 2018. Refining FE Structural Mechanics Simulations of a Railgun by Taking Into Account Electromagnetic Effects. *IEEE Transactions On Plasma Science*, PP(99): 1–6. DOI: 10.1109/TPS.2018.2845892 (Clarivate Analytics Web of Science).

## Papers in Other Editions

Stonkus, R., Račkauskas, J., Schneider, M., Kačianauskas, R. 2014. Structural mechanics of railguns with open barrels and elastic supports: the influence of multishot operation. *The 17th International Symposium on Electromagnetic Launch Technology, Conference Proceedings, San Diego, California, July 7–11, 2014*. Washington: IEEE. ISBN 9781479927333. p. 1–6. DOI: 10.1109/EML.2014.6920657.

Račkauskas, J., Kačianauskas, R., Schneider, M. 2015. FEM simulation of electromagnetic forces in the rails of electromagnetic launcher. *PCM-CMM 2015: 3rd Polish Congress of Mechanics and 21st Computer Methods in Mechanics, September 8th–11th, 2015, Gdansk, Poland: short papers*. Vol. 2. Gdansk: Gdansk University of Technology, 2015. ISBN 9788393210763. p. 131–132.

Rackauskas J., Schneider M., Kačianauskas R. 2016. Refining FE Structural Mechanics Simulations of a Railgun by Taking into Account Electromagnetic. *18th International Symposium on Electromagnetic Launch Technology (EML), Conference Proceedings, Wuhan, China 24–28 October 2016*. Washington: IEEE. Vol. 1. p. 444–446.

---

# Summary in Lithuanian

## Įvadas

### Problemos formulavimas

Elektromagnetinės svaityklės gali būti naudojamos tiek leidžiant objektus į kosmosą, tiek kaip ginklas, tiek kaip medžiagų tyrimo įrankis pramonėje ir moksle. Šis prietaisas, gali sviesti objektus kilometrų per sekundę greičio ribose. Vienas labiausiai akcentuojamų elektromagnetinės svaityklės privalumų yra lengvai kontroliuojamas sviedinio sviedimo greitis, nes užtenka keisti impulsinės srovės šaltinio energijos kiekį. Sviedinio sviedimo greitis yra sudėtingai kontroliuojamas įrenginiuose naudojančiuose sprogstamas chemines medžiagas (kurą).

Elektromagnetinės svaityklės konstrukcija yra paprasta. Tačiau įrenginiu tekančios didelės galios elektros impulsinės srovės įtakoja konstrukcijos stabilumą, kuris trukdo sklandžiam elektromagnetinės svaityklės darbui. Veikiant išorinėms ir vidinėms jėgoms konstrukcija yra deformuojama, ko pasekoje atsiranda trukdžiai sklandžiam elektromagnetinės svaityklės darbui. Taikant baigtinių elementų metodą analizuojama elektromagnetinės svaityklės konstrukcijos elgsena, veikiant elektromagnetinėms jėgoms.

Disertacinis darbas skirtas tirti dviejų bėgių tipo atvirojo kanalo elektromagnetines svaityklės konstrukcijos elgseną naudojant susieto elektromagnetinio ir mechaninio uždavinio sprendimą nuosekliai.

## Darbo aktualumas

Elektromagnetinės svaidyklės mechaninė elgsena, sviedinio judėjimo šaunamajame kanale metu, jos konstrukcijos elementuose susidaranti jėgos ir jos veikimo formos pokyčiai priklauso nuo konstrukcinio rėmo sandaros ir į konstrukciją veikiančių elektromagnetinių jėgų. Mechaninės savybės yra mažai ištirta sudėtingų daugiafizikinių procesų sritis. Elektromagnetinės svaidyklės konstrukcijos elgsenos dinamika ir lokalus elektromagnetinių jėgų poveikis į konstrukciją yra aktuali mokslinė ir technologinė problema, kuri sprendžiama tiriant ir projektuojant tokio tipo prietaisą ir gerinant jo eksploatacines savybes. Esminis energijos perdavimo trikdys yra deformuotas bėgio paviršius, atsirandantis dėl elektromagnetinių jėgų skečiamojo poveikio. Elektromagnetinės svaidyklės veikimo technologijai tirti išskiriami elektromagnetinio, mechaninio ir terminio modeliavimo metodai. Tačiau, bendro skaičiuojamojo metodo ir susiejimo į vieną matematinį modelį nėra. Skaičiavimo įrangos nepakankamumas riboja didelės apimties trimačio elektromagnetinio uždavinio sprendimą, todėl susietieji uždaviniai yra aprašomi tik analiziškai, o bendro sprendimo ir rezultato nėra.

Disertacijoje pritaikytas dviejų metodų – elektromagnetinio ir mechaninio uždavinių sprendimas, kuris leidžia ištirti elektromagnetinės svaidyklės konstrukcijos elgseną lokaliai. Nuoseklus skaičiavimo algoritmas apima elektromagnetinio uždavinio sprendimą, apskaičiuotų elektromagnetinių jėgų integravimą į atitinkamus tūrius ir mechaninio uždavinio sprendimą, naudojant integruotas tūrines jėgas. Tokia susietojo uždavinio sprendimo seka leidžia išspręsti didelio masto uždavinius neskaiciuojant elektromagnetinės dalies visai elektromagnetinės svaidyklės konstrukcijai. Greičiau ir su mažesniais skaičiavimo resursais yra pasiekiamas tokio pat tikslumo rezultatas, kaip ir sprendžiant visos konstrukcijos uždavinį.

Trimačiu modeliavimu paremtas elektromagnetinės ir mechaninės elgsenos uždavinys yra sudėtingas, tačiau leidžia nustatyti problematiškiausias elektromagnetinės svaidyklės konstrukcijos vietas ir jas tobulinti.

## Tyrimo objektas

Darbo tyrimų objektas yra dviejų bėgių atvirojo kanalo elektromagnetinė svaidyklė ir erdvinio magnetinio lauko poveikio įtaka mechaninei svaidyklės elgsenai.

## Darbo tikslas

Ištirti elektromagnetinės svaidyklės trimatinį magnetinių jėgų poveikį mechaninei svaidyklės konstrukcijos elgsenai.

## Darbo uždaviniai

Darbo tikslui pasiekti reikia spręsti šiuos uždavinius:

1. Apžvelgti literatūroje esamus tyrimus elektromagnetinių svaidyklių tematika, išanalizuoti atvirojo kanalo esamus elektromagnetinės ir mechaninės analizės metodus.
2. Sudaryti dviejų bėgių atvirojo kanalo elektromagnetinės svaidyklės RAFIRA trimačius elektromagnetinės ir mechaninės analizės baigtinių elementų modelius.
3. Taikant sukurtą elektromagnetinių modelių seką, nustatyti ir įvertinti erdvinį elektromagnetinį lauką aplink judantį sviedinį ir jo sukeltas magnetines jėgas.

4. Ištirti ir palyginti tūrinių ir paviršinių magnetinių jėgų įtaką bėgio konstrukcijos mechaniniam deformavimui.
5. Ištirti elektromagnetinės apkrovos poveikį elektromagnetinės svaidyklės konstrukcijos mechaniniai elgsenai.

### **Tyrimų metodika**

Darbe taikomi silpnai susieti elektromagnetikos ir klasikinės mechanikos sprendimo metodai naudojant baigtinių elementų metodus.

### **Darbo mokslinis naujumas**

Rengiant disertaciją buvo gauti šie atvirojo kanalo elektromagnetinės svaidyklės rezultatai:

1. Elektromagnetiniam laukui tirti sviedinio aplinkoje sukurta seka, kuri buvo pritaikyta elektromagnetiniam laukui ir jo sukeltoms jėgoms apskaičiuoti. Šių modelių sprendiniai leidžia įvertinti konstrukcinių elementų ir sviedinio geometrinių parametrų įtaką.
2. Apskaičiuotos tūrinės magnetinės jėgos, buvo pritaikytos skaičiuojant bėgio paviršiaus deformavimą
3. Nustatyta magnetinių jėgų įtaka atvirojo kanalo elektromagnetinei svaidyklei būdingų konstrukcinių elementų mechaniniam darbui: jungiamųjų varžtų jėgai ir bėgio paviršiaus deformavimui.

### **Darbo rezultatų praktinė reikšmė**

Sukurtas elektromagnetinės svaidyklės elektromagnetinio ir mechaninio modelio sujungimo algoritmas, kuris gali būti pritaikytas kiekvienam elektromagnetinės svaidyklės veikimo režimui. Pritaikytas skaičiavimo metodas leido ištirti elektromagnetinių ir mechaninių gradientų pasiskirstymą elektromagnetinės svaidyklės konstrukcijos tūryje, dėl to galima nustatyti konstrukcijos silpniausias vietas ir pagerinti elektromagnetinės svaidyklės veikimo efektyvumą. Sukurtas susieto uždavinio algoritmas gali būti naudojamas ir kitų elektromagnetinių svaidyklių formų tyrimui.

### **Ginamieji teiginiai**

1. Pasiskirsčiusių tūrinių jėgų įvertinimas sumažina lokalias deformacijas į elektromagnetinės svaidyklės bėgį.
2. Tūrinės magnetinės jėgos veikiančios bėgio tūryje sukelia bėgio paviršiaus nevienodą deformavimą.
3. Sviedinio aplinkoje elektromagnetinė jėga sumažėja ties elektromagnetinės svaidyklės konstrukciniais varžtais.

### **Darbo rezultatų aprobavimas**

Disertacijos tema paskelbti 7 straipsniai: 4 – mokslo žurnaluose, įtrauktuose į Clarivate Analytics Web of Science sąrašą (Schneider *et al.* 2013), (Stonkus *et al.* 2015), (Račkauskas *et al.* 2018), (Račkauskas *et al.* 2018), 1 – konferencijos medžiagoje, referuotoje Clarivate Analytics Web of Science Proceedings duomenų bazėje (Stonkus *et al.* 2015), 2 –

recenzuojamose tarptautinių konferencijų medžiagose (Račkauskas *et al.* 2015), (Račkauskas *et al.* 2016).

Disertacijoje atliktų tyrimų rezultatai buvo paskelbti keturiuose mokslinėse konferencijose Lietuvoje ir užsienyje:

- Tarptautinėje konferencijoje „The 17<sup>th</sup> Electromagnetic Launch Technology Symposium (EML)“, 2014 m. liepos 7–11 d., San Diego, Kalifornijoje;
- Tarptautinėje konferencijoje „3<sup>rd</sup> Polish Congress of Mechanics and 21<sup>st</sup> Computer Methods in Mechanics (PCM-CMM 2015)“, 2015 m. rugsėjo 8–11 d., Gdanske, Lenkijoje;
- Tarptautinėje konferencijoje „The 18<sup>th</sup> Electromagnetic Launch Technology Symposium (EML)“, 2016 m. spalio 24–28 d., Wuhan, Kinijoje.
- 13<sup>-o</sup> tarptautinėje konferencijoje „Mechatronics Systems and Materials“, 2017 m. liepos 3–5 d., Vilniuje, Lietuvoje.

### **Disertacijos struktūra**

Disertaciją sudaro įvadas, keturi skyriai ir bendrosios išvados. Taip pat yra penki priedai. Darbo apimtis yra 100 puslapių, neskaitant priedų, tekste panaudotos 31 numeruotos formulės, 41 paveikslas ir 4 lentelės. Rašant disertaciją buvo panaudoti 92 literatūros šaltiniai.

### **Padėka**

Pirma noriu padėkoti savo darbo vadovui Rimantui Kačianauskui, kuris buvo mokytojas ir padėjėjas studijų metais.

Taip pat noriu padėkoti straipsnių bendra autoriui ir konsultantui Markus Schneider iš Saint-Louisio Prancūzijos-Vokietijos tyrimo instituto. Jis pasiūlė mokslinio tyrimo kryptį, kuri yra aktuali elektromagnetinių svaidyklių srityje. Taip pat priėmė stažuotis ir sudarė galimybes atlikti eksperimentinius bandymus.

Dėkoju Martin Roch, kuris bendravo ir diskutavo elektromagnetinių svaidyklių klausimais ir pasiūlė idėjų, leidžiančių kitaip pažvelgti į tyrinjamą problemą.

Už palaikymą tariau ačiū savo žmonai Ievai ir sūnui Izidorui, kurie mane palaikė visapusiškai dalyvavo mano studijų procese. Dėkoju savo tėvams Danguolei ir Gintautui, kurie išugdė ryžtą ir palaikė mane visuose mano pasirinkimuose.

## **1. Elektromagnetinių svaidyklių tyrimams taikomų skaitinių analizės metodų apžvalga**

Elektromagnetinės svaidyklės idėja pirmą kartą buvo pademonstruota dar XIX amžiaus pradžioje, Norvegijoje. Didžiausią idėjos tobulinimą atliko Prancūzijos mokslininkai Pirmojo pasaulinio karo metais. Antrojo pasaulinio karo metais šią technologiją intensyviai pradėjo plėtoti Vokietija ir Japonija (McNab 1999). Pastaraisiais metais elektromagnetinių svaidyklių tyrimai yra plačiau plėtojami Vakarų Europos šalyse, Kinijoje bei Jungtinėse Amerikos valstijose.

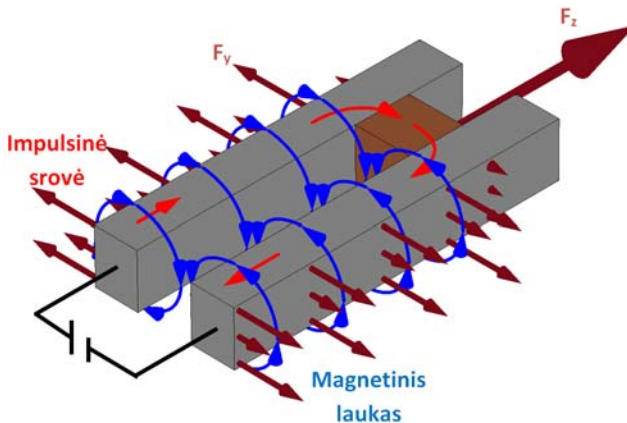
Elektromagnetinės svaidyklės apimą didelę tyrimų sritį. Pirmą elektromagnetinės svaidyklės yra kaip tiriamasis objektas, kuris gali atlikti kūno sviedimo darbą. Antra, elektromagnetinės svaidyklės yra įrenginys, kuris leidžia nagrinėti didelės galios impulsines sroves, medžiagas ir jų atsparumą didelės galios elektriniam ir magnetiniam laukams, taip pat svaidyklės naudojamos kaip prietaisas medžiagų smūginiam tūsumui tirti ir t. t. Pagal literatūros šaltinius matyti, jog mokslininkų, tiriančių elektromagnetines svaidykles, darbai yra pasiskirstę į dvi sritis. Viena mokslininkų grupė tyrinėja fizikines savybes, siekdami kuo tikslesnio sviedimo proceso algoritmo su kuo didesniu efektyvumu. Viena grupė mokslininkų dirba su fizikinėmis savybėmis, siekdami kuo tikslesnio sviedimo proceso algoritmo su kuo didesniu efektyvumu. Skaitinis elektromagnetinių svaidyklių sviedimo proceso valdymo sistemos tyrimas leidžia nustatyti optimalų impulso generavimo algoritmą, siekiant gauti kuo naudingesnę sviedimo procesą. Tokio tipo uždaviniams spręsti naudojamos MATLAB Simulink arba PSPICE programos, kurios turi blokinius analitinės analizės metodus. Antra mokslininkų grupė mokslininkų grupė nagrinėja atskiras ir bendras elektromagnetinės svaidyklės konstrukcijos dalis bei konstrukcijos elgseną: kaip elektromagnetinėje svaidyklėje yra pasiskirsčiusios impulsinės srovės, magnetiniai laukai ir kokia jų įtaka mechaninei konstrukcijai. Taip pat yra nagrinėjamas sviedinio kontaktas su elektromagnetinės svaidyklės bėgiu. Nagrinėjami dvimačiai ir erdviniai uždaviniai leidžia suprasti fizikinių gradientų išsidėstymą elektromagnetinės svaidyklės konstrukcijoje. Tyrimų sritis apima baigtinių elementų metodo taikymą, nagrinėjant elektromagnetinės svaidyklės konstrukciją bendrai arba lokaliai. Skaitinis konstrukcijos tyrimas apima elektromagnetinius, mechaninius ir termodinamikos uždavinius. Eksperimentiniai tyrimai rodo, jog bėgis lydosi ir dega, todėl yra svarbūs ir temperatūros reiškiniai, atsirandantys elektromagnetinės svaidyklės sviedimo metu.

Literatūros šaltiniuose aprašomi dvimačiai uždaviniai, apimantys impulsinės srovės pasiskirstymą elektromagnetinės svaidyklės bėgyje ir magnetinio lauko pasiskirstymą bėgyje ir aplink jį (Bayati & Keshkar 2015). Plėtojant dvimačių uždavinių modelius, keičiant tyrimų objektus ir metodikas buvo plėtojami skaitiniai skaičiavimai, sviedinio sukeliams fizikiniams reiškiniams tirti. Išsprendus dvimatį elektros impulsinės srovės ir magnetinio lauko pasiskirstymo uždavinius laike, pastebėti fizikiniai reiškiniai buvo patikrinti magnetinio lauko matuokliu eksperimentiškai, ir gauti matavimai pagrindė skaitiškai gautus rezultatus (Stankevic *et al.* 2013). Tokio pobūdžio tyrimai validuoja sprendimo skaitinį algoritmą ir leidžia ištirti elektromagnetinės svaidyklės elgseną, sviedimo proceso metu, atitinkamu laiko momentu. Pagal literatūros šaltinius matyti, jog dvimačius modelius tyrinėja nemažai mokslininkų grupių, kurie savo laiku dirbo su dvimačiais elektromagnetinių svaidyklių modeliais, nagrinėdami srovės paviršinį efektą ir magnetinio lauko pasiskirstymą aplink elektromagnetinės svaidyklės konstrukciją (Keshkar *et al.* 2008). Nuo dvimačių uždavinių yra pereinama prie trimačių uždavinių, kurie gali pateikti rezultatus ne tik plokštuminių atžvilgiu, tačiau ir paskirstymą erdvėje, todėl yra mokslininkų grupės, kurios tiria skaitinius metodus dvimačiuose ir trimačiuose uždaviniuose ir fiksuoja skaičiavimų rezultatų skirtumus (Tan *et al.* 2017). Toks skaičiavimų skirtumų tyrimas ir eksperimentais paremti matavimai leidžia sudaryti tiriamųjų objektų bazę, kurioje pateikiami rezultatai apie skaitinių metodų galimybę naudoti vieną ar kitą metodą atskiroms konstrukcijų dalims ar fizikiniams parametrams nagrinėti.

Tyrimai neapsiriboja vien tik elektromagnetinės svaidyklės bėgio tyrimais, yra tyrėjų grupės, kurios apima elektromagnetinės svaidyklės sviedinio tyrimus. Dažniausiai tiriant sviedinį yra naudojami trimačiai modeliai, kurie pateikia skaitinį ir vizualų vaizdą (Liebfried, Schneider, *et al.* 2013). Trimatis uždavinys leidžia pamatyti tiriamo parametro pasiskirstymą bendrai ir lokaliai. Išplitus trimačiams skaitiniams metodams atsirado galimybė lokaliai tirti elektromagnetinės svaidyklės konstrukcinius mazgus. Viena iš tokių svarbių sričių yra sviedinio ir bėgio kontakto vieta, kuri reikšminga sklandžiam elektromagnetinės svaidyklės darbui. Nemažai kontaktų tyrimo modelių ir metodų galima rasti literatūros šaltiniuose (Feng *et al.* 2015; Li *et al.* 2013).

## 2. Duomenys apie RAFIRA elektromagnetinę svaidyklę

Elektromagnetinę svaidyklę sudaro du lygiagrečiai esantys bėgiai, sujungti laidžia dalimi (S2.1 paveikslas). Elektros srovė tekėdama vienu bėgiu ir pereidama bėgių jungiamąja dalimi, grįždama atgal uždarame kontūre sukuria didelės galios magnetinį lauką. Magnetinis laukas savo ruožtu priverčia judėti laisvąją konstrukcijos dalį (armatūrą-sviedinį).



S2.1. pav. Elektromagnetinės svaidyklės veikimo schema

Tekant didelės galios impulsinei srovei susidaro didelės galios magnetinis laukas, kuris kartu su tekančia elektros srove sudaro Lorencio jėgą (apskaičiuojama pagal (S2.1) formulę) ir priverčia sviedinį judėti. Lorencio jėga veikia ne tik sviedinį bet ir elektromagnetinės svaidyklės konstrukcijos elektrai laidžiąją dalį (bėgius). Toks magnetinių jėgų veikimas priverčia sviedinį judėti ir tuo pačiu metu deformuoja elektromagnetinės svaidyklės laikančiąją konstrukciją. Magnetinė jėga veikdama priešingomis kryptimis didina tarpą tarp bėgių. Sviedinio sviedimo metu būtina, jog elektromagnetinės svaidyklės konstrukcija būtų stabili ir būtų užtikrinamas elektrinis kontaktas tarp elektromagnetinės svaidyklės bėgių ir sviedinio.

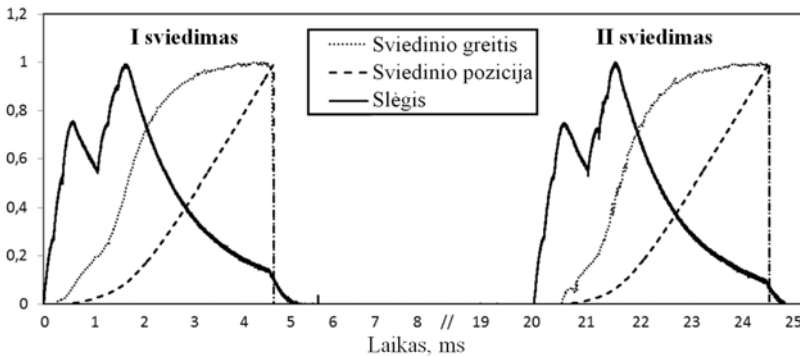


$$F = \int_V \vec{j} \times \vec{B} dV. \quad (\text{S2.1})$$

Remiantis literatūros duomenimis, mechaninės jėgos apskaičiuojamos vertinant impulsinės srovės stiprį ir konstrukcijos dimensijas. Taikant (S2.2) formulę apskaičiuojamas slėgis į bėgio paviršių atitinkamu laiko momentu (Schuppler, Tumonis, *et al.* 2013).

$$p(t) = \frac{L'}{2wh} I(t)^2, \quad (\text{S2.2})$$

čia  $w$  yra bėgių plotis, o  $h$  yra atstumas tarp bėgių. Ši formulė parodo, kaip kinta mechaninis spaudimas kintant laikui. Skaičiuojant slėgį į bėgius, reikia įvertinti kaip kinta srovės stipris ir induktyvumo gradientas, kintant laikui. Daugumos mokslininkų darbuose matyti, jog vertindami bėgio apkrovos slėgį neįvertina kintančio induktyvumo ir srovės stiprio pokyčio, t. y. naudoja apkrovos slėgį kaip konstantą, kuri būna arba pamatuota momentiška, arba paskaičiuota tik atitinkamam elektromagnetinės svaityklės veikimo momentui. Elektromagnetinės svaityklės RAFIRA atveju induktyvumo gradiento dydis yra lygus  $0,467 \mu\text{H/m}$ .

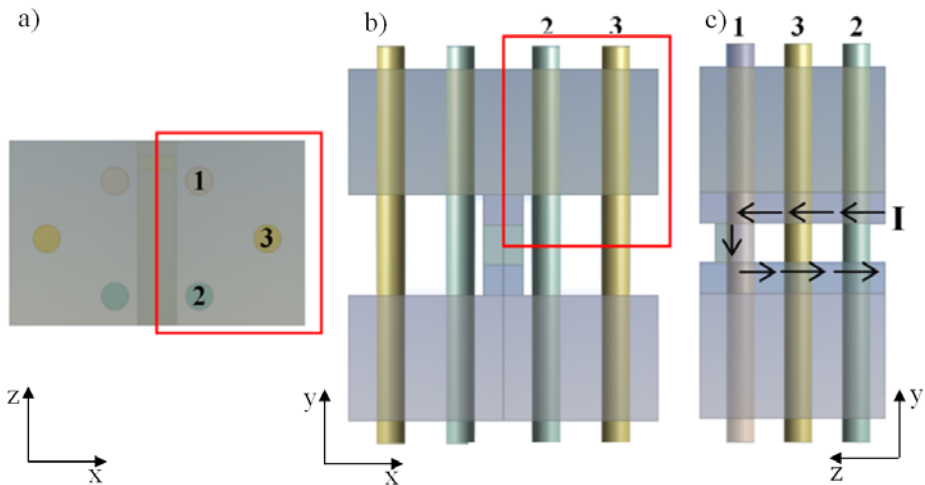


**S2.2. pav.** Eksperimentiškai pamatuotos santykinės parametų vertės atitinkamu laiko momentu

Eksperimentinio bandymo metu per elektromagnetinę svaityklę buvo leista 726 kA stiprio impulsinė elektros srovė, kuri apskaičiavus pagal (S2.2) formulę, sugeneruoja 185 MPa slėgį į bėgio paviršių. Esant tokiam elektros impulsui, sviedinys iš elektromagnetinės svaityklės buvo išsviestas per 4,65 ms ir pasiekė 1136 m/s greitį. S2.2 paveiksle pateikti eksperimentiškai gauti trijų fizikinių dydžių (sviedimo greitis, sviedimo pozicija, slėgis į bėgio paviršių) rezultatai, kurie atvaizduojami kaip santykis nuo fizikinio parametro maksimalios reikšmės, kintant laikui.

### 3. Elektromagnetinės svaidyklės elektromagnetinė analizė

Skaičiuojamieji tyrimai pradami elektromagnetinio uždavinio sprendimu, kuris sudaromas pagal RAFIRA elektromagnetinės svaidyklės geometrinius duomenis ir eksperimentiškai gautus matavimus, kraštinių sąlygų aprašymui. Siekiant iširti kuo tikslesnį elektromagnetinės svaidyklės elgsenos būvį tam tikrais laiko momentais, buvo nuspręsta sudaryti elektromagnetinių modelių seką, kuri apimtų įvairius elektromagnetinės svaidyklės darbo režimus sviedinio sviedimo metu. Seką sudaro 6 modeliai, kurie yra 14 cm ilgio: bėgis be sviedinio; bėgis su sviediniu, kurio forma yra kubas; bėgis su paskirstytu sviediniu (apibūdinantis šepetėlių tipo sviedinį); bėgis su C formos sviediniu; bėgis su konstrukciniais varžtais, be sviedinio; bėgis su konstrukciniais varžtais ir su kubo formos sviediniu. Visi uždaviniai buvo sprendžiami, naudojant dažnių aproksimaciją, siekiant imituoti sviedinio sviedimo greitį bei naudojant laiko grafiką, aprašant judančio sviedinio uždavinį. Visa 12 uždavinių seka įvertina lokalius elektromagnetinio lauko pasiskirstymus kiekvienu elektromagnetinės svaidyklės veikimo atveju, bei konstrukcinių dalių įtaką magnetiniam laukui. S3.1 paveiksle pavaizduotas pilnas modelis, kuris apima konstrukcinius varžtus ir kubo formos sviedinį.



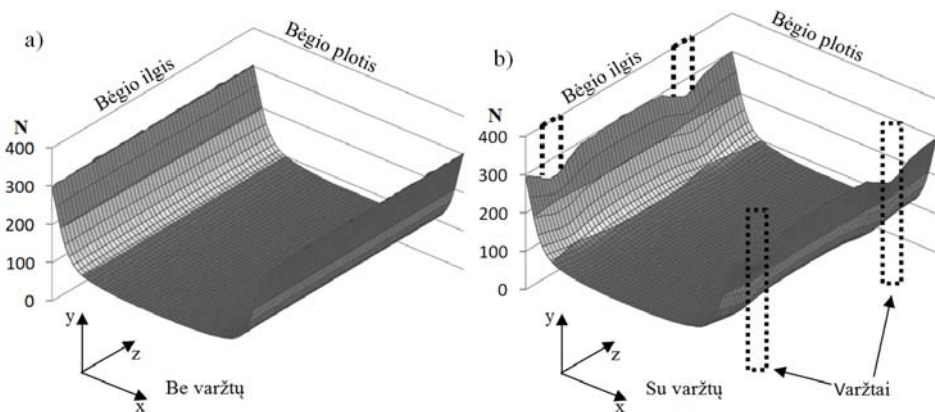
**S3.1. pav.** Elektromagnetinio uždavinio skaitinis modelis: a) projekcinis vaizdas iš viršaus; b) projekcinis vaizdas iš priekio; c) projekcinis vaizdas iš šono

Skaičiuojamasis konstrukcijos ilgis yra 14 cm, tai sudaro 4,5% visos konstrukcijos ilgio. Tokio ilgio pakanka, kad būtų tenkinama keturių kalibrų taisyklė, kuri nusako, kad pilnam jėgos suveikimui, reikia keturis kartus ilgesnio atstumo, negu yra tarp bėgių (Marshall, Ying 2004). Vertinat konstrukcijos simetrijos plokštumas buvo nagrinėjama tik  $\frac{1}{4}$  elektromagnetinės svaidyklės skerspjūvio. Į tai patenka ketvirtadalis sviedinio ir pusė elektromagnetinės svaidyklės bėgio. S3.1 paveiksle nagrinėjama konstrukcijos dalis yra pažymėta raudonu kvadratu. Norint apskaičiuoti Lorencio jėgą, reikia įvertinti magnetinio

lauko pasiskirstymą erdvėje, o tam turi būti apskaičiuotas aplinkos oro, kuris yra aplink elektromagnetinę svaidyklę, poveikis (tai nėra atvaizduota S3.1 paveiksle).

Išsprendus varžtų ir tuščio bėgio elektromagnetinį uždavinį matyti, jog jėga elektromagnetinio bėgio tūryje yra pasiskirsčiusi atitinkamai ties bėgio kraštais. Magnetinė jėga, veikianti elektromagnetinės svaidyklės bėgį, skersine kryptimi (x-y) yra mažiausia ties bėgio viduriu, o išilgine kryptimi (x-z) yra vienoda (S3.2a paveikslas). Kitas elektromagnetinis uždavinys, apimantis elektromagnetinės svaidyklės bėgį ir konstrukcinius varžtus, parodo, jog esant konstrukciniams varžtams pasikeičia el-ktromagnetinės jėgos pasiskirstymas bėgio tūryje. Magnetinė jėga, veikianti elektro-magnetinės svaidyklės bėgį, skersine kryptimi (x-y) yra mažiausia ties bėgio viduriu, o išilgine kryptimi (x-z) yra didžiausia tarp konstrukcinių varžtų (S3.2b paveikslas).

Esant tokiam magnetinių jėgų pasiskirstymui matyti, jog konstrukciniai varžtai suteikia neigiamą efektą elektromagnetinio lauko pasiskirstymui. S3.2 paveiksle pateikti bėgių paviršių žemėlapiai, integruoti visame bėgio skerspjūvyje, ir atvaizduojantys elektromagnetinių jėgų pasiskirstymą z-x ašių kryptimi (išilgai bėgio).



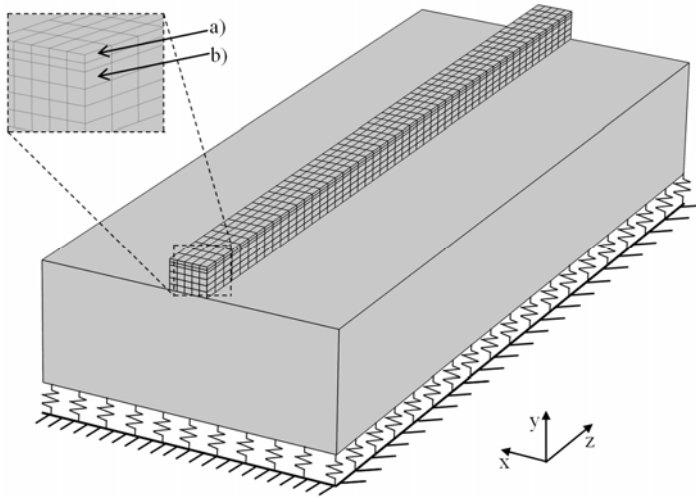
**S3.2. pav.** Elektromagnetinės svaidyklės bėgių skėtimo jėgos tūrio integralo pasiskirstymas išilgai bėgio plokštumos: a) be konstrukcinių varžtų; b) su konstrukciniais varžtais

Varžtų įtaka paviršiaus deformacijai ir varžtų įtakos skirtumas mechaninei konstrukcijai yra aprašomas 4-ame skyriuje.

## 4. Elektromagnetinės svaidyklės mechaninė analizė

Išsprendus elektromagnetinės svaidyklės elektromagnetinių uždavinių seką, toliau tiriama mechaninės konstrukcijos dalis. Mechanškai konstrukcija tiriama dviem etapais. Pirmasis etapas nagrinėja konstrukcijos lokalias deformacijas, naudojant naują skaičiavimo metodą, pagal kurį mechaninis konstrukcijos bėgis yra suskaidomas į tam tikro dydžio stačiakampius gretasienius:  $5 \times 2 \times 10$  mm (S4.1a paveikslas) ir  $5 \times 4 \times 10$  mm (S4.1b paveikslas). Tai leidžia nagrinėti mechaninę konstrukciją, apkraunant bėgį tūryje

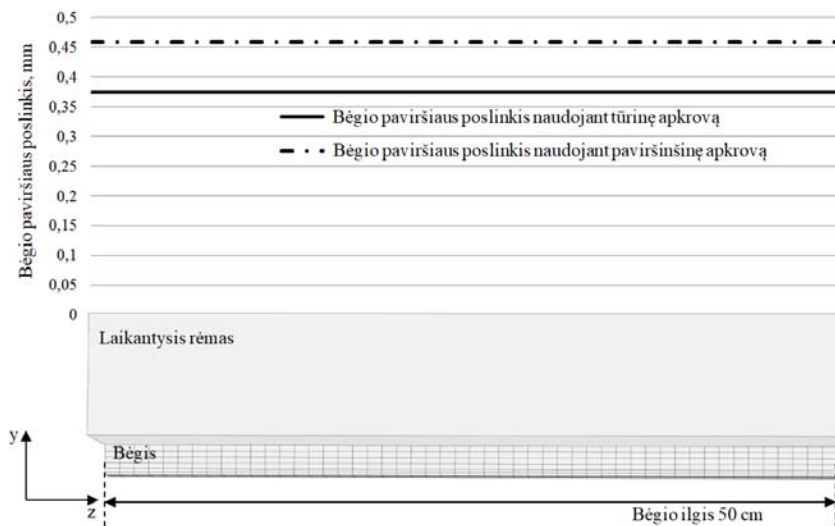
pasiskirsčiosiomis magnetinėmis jėgomis, kurios buvo apskaičiuotos pagal elektromagnetinių modelių seką. Skirtingas elektromagnetinio uždavinio sprendinys skirtingai veikia mechaninę elektromagnetinės svaidyklės konstrukcijos elgseną. Tai buvo vertinama, naudojant apskaičiuotų magnetinių jėgų pasiskirstymą, ir integruojant į tūrius, kurių dydis yra būtent minėti stačiakampiai gretasieniai. Elektromagnetinio modelio uždavinys ir mechaninio modelio uždavinys skiriasi tuo, jog elektromagnetiniame uždavinyje yra sprendžiamas uždavinys apimantis 14 cm konstrukcijos ilgio, o mechaninio modelio uždavinys apima 50 cm konstrukcijos ilgio, todėl tūrinių stačiakampių gretasienių skaičius skiriasi. Integruotų tūrinių jėgų stačiakampių gretasienių skaičius elektromagnetiniame uždavinyje yra mažesnis, todėl formuojant kaštines sąlygas tūrinių stačiakampių gretasienių skaičius padidinamas kopijuojant pasikartojančius elektromagnetinius efektus arba paliekant tokias pat tūrines apkrovas homogeninėse zonose (toli nuo sviedinio, elektromagnetinių jėgų pasiskirstymas yra homogeniškas). Toks tūrinių stačiakampių gretasienių dauginimo metodas leidžia išplėsti mechaninio uždavinio apimtį analizuojant ilgesnę elektromagnetinės svaidyklės konstrukciją.



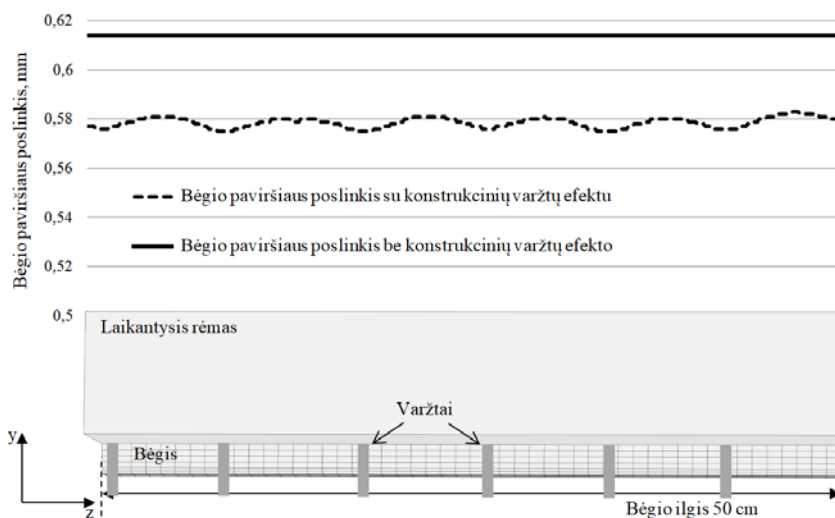
S4.1. pav. Mechaninio uždavinio skaitinis modelis

Visi elektromagnetinės sekos modeliai buvo spęsti naudojant magnetines jėgas į mechaninės sistemos bėgio tūrį. Pradėta nuo paprasčiausio modelio, kuris aprašo tik bėgius. Šio modelio sprendinys imituoja elektromagnetinės svaidyklės darbinį režimą, kai nėra konstrukcinių varžtų, o sviedinys yra toli nuo tiriamos vietos. Tūrinių jėgų apkrova bėgio tūryje 0,1 mm mažiau deformavo bėgio paviršių, nei apkrova į elektromagnetinės svaidyklės bėgio paviršių. Iš rezultatų matyti, jog tūrinių jėgų apkrova mažiau deformuoja elektromagnetinės svaidyklės bėgio paviršių, nei apkrova į bėgio paviršių (S4.2 paveikslas). Kitas sekos uždavinys aprašo konstrukcinių varžtų poveikį elektromagnetinės svaidyklės bėgio deformacijai. S4.3 paveikslas pavaizduoja bėgio paviršiaus deformaciją, kai naudojama magnetinė apkrova į bėgio tūrį, gauta sprendžiant elektromagnetinį bėgio uždavinį be konstrukcinių varžtų, ir apkrova į bėgio tūrį, gauta sprendžiant elektromagnetinį

uždavinį su konstrukciniais varžtais. Šie rezultatai rodo, kad apkrovos jėgų nevienodas išsidėstymas, duoda skirtingus rezultatus ir mechaninėje konstrukcijoje. Gautas 0,037 mm skirtumas nėra reikšmingas ir vertinant eksperimentinius rezultatus gali būti eliminuojamas, nes elektromagnetinės svaityklės konstrukcijos geometrijos tolerancija yra gerokai didesnė nei skaitiškai gautas rezultatų skirtumas.



S4.2. pav. Elektromagnetinės svaityklės bėgio paviršiaus poslinkis tiriant apkrovas į tūrį ir apkrovas į bėgio paviršių

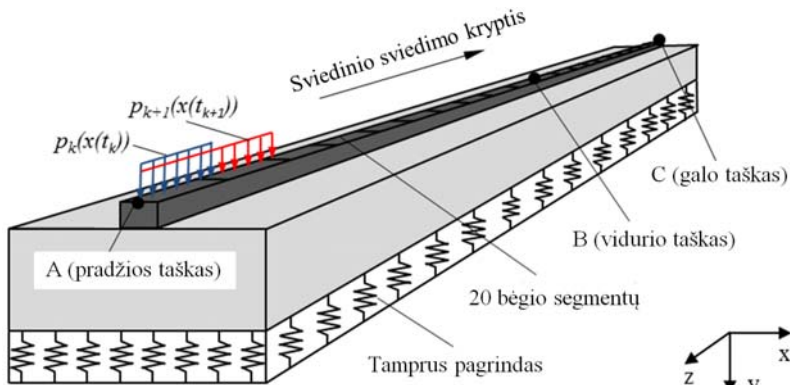


S4.3. pav. Varžtų poveikis mechaninei konstrukcijai

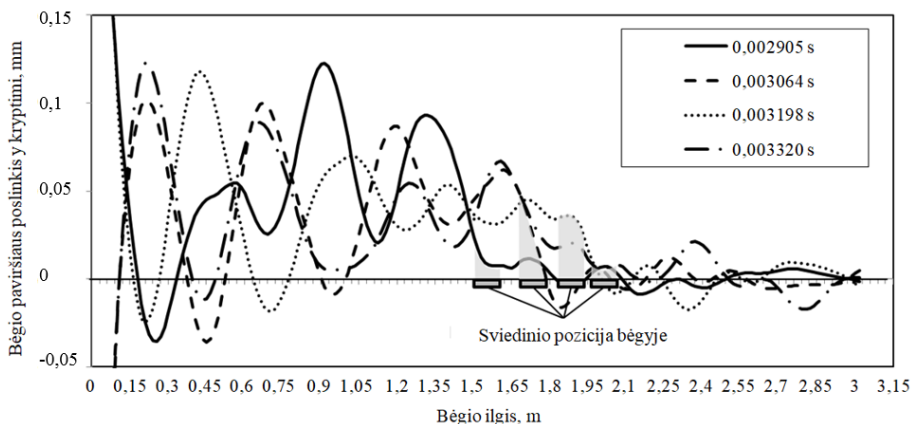
Antro mechaninio tyrimo modelio uždavinys apima visą (3,15 m ilgio) elektromagnetinės svaidyklės ir leidžia analizuoti elektromagnetinės svaidyklės mechaninės konstrukcijos elgsena dinamiškai. Šiame uždavinyje sprendžiama lygčių sistema (S4.1), kurioje slopinimas nebuvo įvertintas.

$$[M]\ddot{u}(t) + [C]\dot{u}(t) + [K]u(t) = F_N(t). \quad (\text{S4.1})$$

Sprendžiant pilnos konstrukcijos elgsenos uždavinį naudota jėgos apkrova į bėgio paviršių. Jėgos dydis apskaičiuotas remiantis slėgio skaičiavimo formule (S2.2). Slėgis proporcingas impulsinės srovės stiprio kvadratui, todėl slėgio į bėgio paviršių profilis sutampa su eksperimentiškai išmatuotos impulsinės srovės pulso forma. Remiantis eksperimentiškai išmatuotu sviedinio skriejimo greičiu, buvo nustatyta, kaip kintant laikui, kinta sviedinio pozicija elektromagnetinės svaidyklės bėgyje. Turimi duomenys leidžia atkurti sviedinio slydimo kelią kiekvienu laiko momentu.



S4.4. pav. Skaitinio uždavinio dinaminis modelis



S4.5. pav. Elektromagnetinės svaidyklės sviedinio ir bėgio santykis kiekvienu laiko momentu

Pirmojo sviedinio sviedimo metu atsiranda bėgio paviršiaus svyravimai, kurie išlieka iki antrojo sviedimo. Šie svyravimai vyksta tiek teigiama bėgio paviršiaus y-kryptimi, tiek neigiama. Konstrukcijos virpėjimas apsunkina naujo sviedinio užkrovimą į elektromagnetinės svaityklės pagrindinį kanalą bei lemia naujai užkrauto sviedinio slydimo procesą (S4.5 paveikslas). Toks bėgio paviršiaus nestabilumas daro neigiamą įtaką elektromagnetinės svaityklės efektyvumui. Tuo metu kai tarpas tarp bėgio yra plečiamas, atsiranda trukdžiai tarp sviedinio ir bėgio elektrinio kontakto, kitu metu, kai tarpas tarp bėgių yra spaudžiamas, sviedinio slydimo takas yra spaudžiamas, dėl to didėja slydimo trintis, kuri taip pat turi įtakos elektromagnetinės svaityklės efektyvumui.

## Bendrosios išvados

1. Apžvelgus elektromagnetinių, atvirojo kanalo, svaityklių tyrimus nustatyta, kad skaičiuojant mechaninį šaudyklės konstrukcijų būvį vyrauja eksperimentiniai magnetinio lauko sukeltų jėgų nustatymo metodai. Susietieji elektromagnetomechaniniai modeliai tokio tipo elektromagnetinėms svaityklėms nebuvo taikyti. Absoliučią skaičiavimo rezultatų tokio pobūdžio elektromagnetinėms svaityklėms nebuvo rasta.
2. Siekiant įvertinti modelio tikslumą buvo vertinamas elektromagnetinės svaityklės induktyvumo parametras skaičiuojant skirtingais metodais ir atlikus eksperimentinius matavimus. Jis parodė pakankamą trimatį elektromagnetinių ir mechaninio baigtinių elementų modelių kokybę, taikant dviejų bėgių atvirojo kanalo RAFIRA elektromagnetinėms svaityklėms. Įvertinimas atliktas naudojant magnetinės energijos vertinimo metodą.
3. Ištirtas lokalus sviedinio ir konstrukcinių varžtų poveikis. Rezultatai rodo, kad magnetinė jėga prie sviedinio padidėja 2,5 karto. Konstrukcinių varžtų vertinimas rodo, kad magnetinių jėgų poveikis ties konstrukciniais varžtais sumažėja 17,5 %. Susieto uždavinio skaičiavimo metodas leidžia įvertinti lokalius pokyčius elektromagnetinės svaityklės konstrukcijoje.
4. Didelės galios elektromagnetinės svaityklės konstrukciniai komponentai turi atitikti elektromagnetinius reikalavimus, nes elektromagnetinės svaityklės veikimo metu vyrauja didelės elektromagnetinės jėgos, veikiančios ne tik laikančiąją konstrukciją, bet ir laidininkus. Jėgos, veikiančios ant bėgių, trukdo išlaikyti gerą kontaktą tarp bėgio ir armatūros. Skaičiavimais nustatyta, kad jėga elektromagnetinės svaityklės tūryje ir bėgio paviršiuje yra pasiskirsčiusi nevienodai: skersine kryptimi didžiausios jėgos yra ties bėgio kraštais, o išilgine kryptimi didžiausios jėgos yra tarp konstrukcinių varžtų.
5. Skaičiavimais parodyta, jog elektromagnetinis poveikis sukelia papildomą bėgio paviršiaus deformavimą, kuris kinta priklausomai nuo simetrijos plokštumos. Taip įvertinamas žalingas poveikis sumažinantis kontakto plotą. Slėgio veikiančio į paviršių apkrovos tipo ir tikslios tūrinės jėgos skaičiavimai naudojant elektromagnetinius modelius apkrovos tipo rezultatai skirtingai paveikia bėgio paviršiaus poslinkį, kuris gali skirtis iki 0,1 mm. Šepetėlių armatūrai tokie skirtumai gali sumažinti bėgio ir armatūros elektrinio kontakto charakteristikas.

6. Lokalus elektromagnetinės svaityklės tyrimas atskleidė, kad elektromagnetinės svaityklės armatūros konstrukcinės formos lemia ne tik kitokį jėgų pasiskirstymą lokaliai, bet ir turi poveikį elektromagnetinės svaityklės konstrukcijos elgsenai. Nustatyta, jog naudojant skirtingas armatūros konstrukcines formas, gaunamas 10 % elektromagnetinės svaityklės bėgio paviršiaus poslinkio skirtumas. Bėgio paviršiaus deformavimas naudojant paskirstytą sviedinį yra 10 % mažesnis negu bėgio paviršiaus poslinkis naudojant C-formos sviedinį.
7. Atlikta trimatė elektromagnetinės svaityklės modelio analizė pateikia bėgių elseną kiekvieno laiko momentu. Dviejų šūvių metu, liekamieji svyravimai po pirmojo šūvio yra pradinių sąlygų būseną antrajam šūviui. Toks svyravimų pasiskirstymas įtakoja antro šūvio efektyvumą ir bendros sistemos virpėjimą.
8. Atlikta šaudyklės mechaninio būvio daugiašūvio proceso metu atskleidė pirmojo šūvio liekamųjų svyravimų įtaką mechaniniam atsakui, gautam po antrojo šūvio. Iki antrojo šūvio impulso piko, bėgio paviršiaus poslinkio amplitudės yra didesnės lyginant su pirmo šūvio metu atsiradusiais bėgio paviršiaus poslinkiais. Antrojo šūvio metu, priešingai nei buvo pirmoje impulso piko pusėje, likutiniai bėgio paviršiaus svyravimai slopina bėgio paviršiaus poslinkio amplitudę.



---

## Annexes<sup>1</sup>

**Annex A.** COMSOL Report of Electromagnetic Model

**Annex B.** COMSOL Report of Mechanical Model

**Annex C.** Declaration of the Dissertation Authority

**Annex D.** The Co-authors Agreements to Present  
Publications for the Dissertation Defense

**Annex E.** Copies of Scientific Publications by the Author  
on the Topic of the Dissertation

---

<sup>1</sup>The annexes are supplied in the enclosed compact disc.

Justinas RAČKAUSKAS

MAGNETOMECHANICAL STUDY OF OPEN-BORE TWO-RAIL  
ELECTROMAGNETIC LAUNCHER

Doctoral Dissertation  
Technological Sciences,  
Mechanical Engineering (09T)

Justinas RAČKAUSKAS

BĖGIŲ TIPO ATVIROJO KANALO ELEKTROMAGNETINĖS  
SVAIDYKLĖS MAGNETOMECHANINIO EFEKTO TYRIMAS

Daktaro disertacija  
Technologijos mokslai,  
Mechanikos inžinerija (09T)

2018 07 13. 9,5 sp. I. Tiražas 20 egz.  
Vilniaus Gedimino technikos universiteto  
leidykla „Technika“,  
Saulėtekio al. 11, 10223 Vilnius,  
<http://leidykla.vgtu.lt>  
Spausdino BĮ UAB „Baltijos kopija“  
Kareivių g. 13B, 09109 Vilnius